PATIENT-SPECIFIC APPROACHES TO BONE REGENERATION

A Dissertation
Presented to
The Academic Faculty

by

Albert Cheng

In Partial Fulfillment
of the Requirements for the Degree
Doctor of Philosophy in Bioengineering

George W. Woodruff School of Mechanical Engineering
Georgia Institute of Technology
August 2018

PATIENT-SPECIFIC APPROACHES TO BONE REGENERATION

Approved by:

Dr. Robert Guldberg, Advisor
School of Mechanical Engineering
Georgia Institute of Technology

Dr. Johnna Temenoff
Department of Biomedical Engineering
Georgia Institute of Technology

Dr. Greg Gibson
School of Biological Sciences
Georgia Institute of Technology

Dr. Steven Stice
Regenerative Bioscience Center
University of Georgia

Dr. Krishnendu Roy
Department of Biomedical Engineering
Georgia Institute of Technology

Date Approved: March 27, 2018

To my future self:

I hope this was all worth it

Also, don’t forget to call Mom

ACKNOWLEDGEMENTS

First and foremost, I'd like to thank my thesis advisor, Bob Guldberg. I'm partly convinced the main reason he agreed to take me was due to my status as a fellow Michigan alum… and I'm totally fine with that. Going to the most expensive public school in the country had to pay off somewhere right? In all seriousness though, I could not have asked for a better scientific mentor to guide me through the arduous journey of a PhD. Very early on, Bob instilled in me the confidence to make informed decisions about my own research and was also patient enough to let me make some of my own mistakes rather than always telling me exactly what to do. I know that I am a better scientist and critical thinker because of these struggles and am grateful for all the experiences afforded to me as one of Bob's students.

I'd also like to thank the wonderful faculty that served on my thesis committee. Johnna Temenoff was one of the first professors I talked to during BME recruitment before I chose to come to Georgia Tech. Her expertise in biomaterials and orthopedic research were instrumental in helping frame some of the results of my work and pushed me to think broader in terms of how they contributed to the field. Greg Gibson is an endless well of knowledge when it comes to genomics and analytical techniques. I fondly remember one of our discussions that went off on a philosophical tangent centered on what is the actual significance of comparing cycle thresholds (I still ponder this question from time to time and slightly fear it will trigger some sort of existential crisis down the road). I got to know Steve Stice from our collaboration where we delivered genetically-modified MSCs to our rat segmental defect, and saw first-hand his great mind and

enthusiasm for science. Krish Roy was extremely generous with his time and resources as he opened up his lab to let me better explore this crazy thing called the immune response, and I always appreciated his perspective as someone who made the switch back from industry to academia.

There are too many people to name from the Guldberg lab (both past and present) that require my thanks, as our work necessitated spending so much time together. Angela Lin is a CT wizard and perhaps an even better ultimate frisbee player. Hazel Stevens is an unparalleled mix of sarcastic wit and biology knowledge, in addition to being the best lab manager ever. The fact that she accomplished all of this in spite of her Tottenham allegiances is all the more commendable. Laxmi Krishnan, a former postdoc in the lab that I worked closely with throughout my PhD, deserves many thanks for enduring long surgery days with me and being my constant sounding board for ideas. Brennan, Giuli, and Olivia, I couldn't imagine a better cohort to join/graduate the lab with. Brett and Marissa, y'all are the next in line and I've enjoyed watching you learn and grow as scientists. Lina, Ryan, Gilad, Casey, and Ramesh are the newest Guldberglars and all are great additions to the lab. I'd also like to acknowledge the two undergrads that I had the opportunity to mentor during my time at Georgia Tech: Boao Xia and Nari Lee. Both were instrumental in helping me with CT evaluations, troubleshooting histology stains, and surgery preparation for my animal studies. I'm excited to see what you both accomplish in the future. In the end, I can say with absolute confidence that there is (was) no better lab to join at Georgia Tech.

Other mentors/collaborators/colleagues that deserve thanks are Nick Willett, Lisa Tran, Dalia Arafat, Seth Andrews, Pallab Pradhan, Levi Wood, and Laura Weinstock. Andrés García and Laura Paige are the fearless leaders of the BioE program and were invaluable resources throughout my time in grad school. Despite not serving on my thesis committee, Andrés had a huge influence on my growth as a researcher, as well as my perspective outside of science. Side note, I'll never forget the intensity and "gamesmanship" he displayed during the Lair Olympics basketball game. I'd also like to thank everyone on the Georgia Tech PRL team. In particular, Altair, Ogeda, Brittany, Josh, Andrea, Kim, Dr. Noel, and Dr. O'Farrell, always made sure my animals had the best possible care and were very accommodating to my needs on hectic surgery days. Without you guys I could not have accomplished all the *in vivo* work involved in my thesis.

Outside of lab and school, I had an amazing group of friends that I was able to explore Atlanta with and distract myself from failed experiments. Besides some of the Guldberglars already mentioned, Ted, Amy, Cam, Apoorva, Sonny, Devon, Jose, Efrain, Chris, Daniela, Alex, Dwight, Pete, and Kayla, all contributed to my sanity these past few years. Without all the happy hours, beer festivals, road trips, hooch shooting, climbing excursions, and other shenanigans, I may have graduated a little sooner… but definitely would have been a lot more miserable too so I have no regrets about that. Needless to say, I am eternally grateful for the friendships I've made these past few years and hope we continue to stay in touch.

Lastly, I’d like to thank my family for their love and support throughout my entire graduate school career (as well as the 21 years before). I know that I was fortunate enough to pursue a PhD without any additional burdens or financial obligations weighing on my mind because of the sacrifices my parents made, and only made it through to the end because of conversations and constant words of encouragement from my sister. I love you all and this achievement is yours as much as it is mine.

TABLE OF CONTENTS

LIST OF TABLES

LIST OF FIGURES

LIST OF SYMBOLS AND ABBREVIATIONS

2D	Two-dimensional
3D	Three-dimensional
ACS	Absorbable collagen sponge
ALP	Alkaline phosphatase
ANOVA	Analysis of variance
ATP	Adenosine triphosphate
BMD	Bone mineral density
BMP	Bone morphogenetic protein
BV	Bone volume
CARS	Compensatory anti-inflammatory response syndrome
CD	Cluster of differentiation
cDNA	Complementary deoxyribonucleic acid
C_t	Cycle threshold
DNA	Deoxyribonucleic acid
ECM	Extracellular matrix
EGF	Epidermal growth factor
ELISA	Enzyme-linked immunosorbent assay
FBS	Fetal bovine serum

FDA	Food and drug administration
FDR	False discovery rate
GAG	Glycosaminoglycan
G-CSF	Granulocyte colony-stimulating factor
GM-CSF	Granulocyte-macrophage colony-stimulating factor
HA	Hydroxyapatite
H&E	Hematoxylin and eosin
HSC	Hematopoietic stem cell
IACUC	Institutional animal care and use committee
IFNγ	Interferon gamma
IHC	Immunohistochemistry
IL	Interleukin
IP-10	Interferon gamma-induced protein 10
LIX	Lipopolysaccharide-induced CXC chemokine
LV	Latent variable
μCT	Micro-computed tomography
MCP-1	Monocyte chemoattractant protein 1
MEMα	Minimum essential medium alpha
MIP	Macrophage inflammatory protein

MMP	Matrix metalloproteinase
MSC	Mesenchymal stem cell
MODS	Multiple organ dysfunction syndrome
NFM	Nanofiber mesh
NSAID	Nonsteroidal anti-inflammatory drug
OCN	Osteocalcin
OPG	Osteoprotegerin
OPN	Osteopontin
ON	Osteonectin
OSX	Osterix
PBS	Phosphate-buffered saline
PCA	Principal component analysis
PCL	Poly(ε-caprolactone)
PICS	Persistent inflammation/immune suppression catabolism syndrome
PLSDA	Partial least squares discriminant analysis
PLSR	Partial least squares regression
pMOI	Polar moment of inertia
qRT-PCR	Quantitative real-time polymerase chain reaction
RANKL	Receptor activator of nuclear factor kappa-B ligand

RANTES	Regulated on activation, normal T cell expressed and secreted
RGD	Arginine-glycine-aspartic acid (cell adhesion motif)
rhBMP	Recombinant human bone morphogenetic protein
RNA	Ribonucleic acid
ROS	Reactive oxygen species
RSA	Rat serum albumin
RUNX2	Runt-related transcription factor two
Saf-O	Safranin-O
SIRS	Systemic inflammatory response syndrome
SEM	Standard error of the mean
TGFβ	Transforming growth factor beta
TLR	Toll-like receptor
TNFα	Tumor necrosis factor alpha
VEGF	Vascular endothelial growth factor
VOI	Volume of interest

SUMMARY

Bone is the second-most transplanted tissue after blood with more than 1.6 million bone grafting procedures performed annually in the US at a cost of over 5 billion dollars. Treatment of large bone defects in particular remains one of the most challenging problems faced by orthopedic surgeons. Current therapies include bone grafts and/or delivery of osteoinductive proteins such as bone morphogenetic protein 2 (BMP-2). Despite advances in surgical technique and medical care, many of these treatment options still exhibit high variability in healing, suggesting that patient-specific factors, such as age, gender, immune status, and presence of certain co-morbidities may play a much more crucial role in treatment success than previously thought. Thus, the need to account for these patient-specific factors with more sophisticated treatment strategies has become increasingly apparent.

The main objective of this work was to use preclinical animal models to investigate the influence of patient-specific factors on bone regeneration, with a particular focus on long-term immune profile characterization as it relates to the bone healing response after treatment. The impact of age and dose on large bone defect healing was assessed using a well-established bone injury rat model along with delivery of BMP-2 in a collagen sponge, which is the current clinical standard. We found that young rats healed better and were more responsive to increases in BMP-2 dose compared to adult rats, without experiencing greater complications. These results suggest that a more conservative dosing strategy may be the best approach for pediatric patients, for whom BMP-2 use is currently contraindicated and yet still occurs. Additionally, this work

sought to elucidate some of the key mechanisms that lead to impaired healing following nonunion, a significant clinical problem that still affects up to 10% of patients with long bone injuries. To accomplish this, a chronic nonunion model was established by delaying treatment to the bone defect by 8 weeks, after mineralized end-capping has occurred. We showed that delayed treatment after nonunion results in impaired healing compared to acute treatment of fresh defects. This new animal model can potentially serve as a more rigorous and clinically-relevant platform for studying nonunion and testing novel therapeutics. Finally, the issue of trauma-induced immune dysregulation following nonunion was investigated. We demonstrated differences in the local and systemic immune responses between acute and delayed treatment, and further showed that myeloid-derived suppressor cells (MDSCs) are a potential predictor of poor healing outcomes. Collectively, these studies have advanced our understanding of the factors that affect bone regeneration and represent a pivotal step towards improved, more personalized treatment strategies for bone repair.

CHAPTER 1. INTRODUCTION

Large segmental bone defects, often the result of traumatic injury, wound debridement, tumor resection, or congenital deformity, remain one of the most challenging problems faced by orthopedic surgeons today. Current treatments involve bone grafts and/or delivery of osteoinductive proteins such as bone morphogenetic protein 2 (BMP-2). Unfortunately, the use of BMPs has been associated with increased inflammation, heterotopic bone formation, and osteolysis. Despite these risks, BMPs are still commonly used to treat large bone defects because there are currently no better bone graft substitutes. In many of these clinical cases there is high variability in patient outcomes, suggesting that patient-specific factors, including age, treatment timing, and immune status, may play a much more pivotal role in treatment success than previously thought. **The main objective of this work is to use preclinical animal models to better understand how patient-specific factors influence bone regeneration, with a particular focus on exploring systemic immune profiling as a potential metric for monitoring the bone healing response after treatment**. This will be accomplished in the following specific aims:

1.1 Specific Aim I

Investigate the effects of age and dose on gene expression and segmental bone defect repair following BMP-2 delivery

The use of BMP-2 is currently contraindicated by the FDA for children due to concerns about side effects and the fact that very little is known about the appropriate

dosing for pediatric patients. Despite this warning and several documented cases of adverse reactions, off-label use of BMP-2 still occurs. By adapting our established segmental bone defect animal model to young and old rats, we will be able to identify age-related differences and hopefully provide guidance for developing better treatment strategies. Our hypothesis is that young animals will exhibit an increased inflammatory response to BMP-2 treatment but also have a lower BMP-2 dose requirement for healing compared to older animals.

1.2 Specific Aim II

Elucidate differences between healing and non-healing bone defects by assessing bone repair in a model of chronic nonunion

Despite recent improvements to bone grafting procedures, complications such as delayed union and nonunion remain common, up to 10% in long bone injuries and 40% in spinal fusion cases. The pathophysiology of nonunion is poorly understood and the critical events that determine whether bones do or do not heal are not well known. Historically, the vast majority of bone regeneration research in animal models involve delivering treatment acutely, i.e. immediately after creation of the bone defect or other injury. For this aim, we seek to establish a model where the defects are first allowed to progress towards nonunion before any therapeutic intervention is performed. We believe this chronic nonunion model will be more challenging and better recapitulate the clinical scenarios of delayed union and nonunion, thus providing new insight into the mechanisms that lead to nonunion as well as improved treatment strategies. Our hypothesis is that chronic nonunion defects will demonstrate impaired healing compared

to acutely-treated defects due to differences in the inflammatory response after injury and treatment, including systemic inflammatory cytokine expression as well as the immune cell populations mobilized following injury.

1.3 Specific Aim III

Characterize the long-term immune profiles during acute and delayed treatment, and assess whether poor bone healing outcomes correlate with trauma-induced immune dysregulation

Incidence of morbidity and mortality of severely injured trauma patients remains high, even with early treatment and surgical intervention. Recent evidence suggests that one major factor contributing to poor healing in these patients may be long-term immune dysregulation, specifically a persistent, low level inflammatory response that eventually leads to systemic chronic immunosuppression. Others have shown recently that this immunosuppressed state coincides with a rise in systemic myeloid derived suppressor cells (MDSCs) and a reduction in hematopoietic stem cell niches. We will characterize the long-term systemic immune profile of rats following segmental bone injury with acute or delayed treatment, as established in Aim II, using longitudinal blood analyses. As a complementary study, we will also investigate early local differences in inflammation between bone defects that received acute or delayed treatment. Our hypothesis for this aim is that delayed treatment will result in a dysregulated immune response compared to acute treatment, which can be quantified and correlated with long-term bone healing outcomes.

Overall, this work is significant as it addresses several important clinical issues and knowledge gaps with current bone treatment options. The impact of age on large bone defect healing will be elucidated using an established bone injury model along with delivery of rhBMP-2 in a collagen sponge, which is the current clinical standard. These results may provide valuable insight on a controversial subject: the use of rhBMP-2 in pediatric patients. Additionally, this work will seek to identify some of the key mechanisms that lead to nonunion, a significant clinical problem that affects up to 10% of patients with long bone injuries. A novel chronic nonunion model will be established that can potentially serve as a more rigorous and clinically relevant platform for testing new technologies and therapeutics. Finally, the issue of trauma-induced immune dysregulation will be explored in the context of bone healing, which will perhaps motivate future work on immunomodulatory treatment strategies to enhance bone repair. Collectively, these studies will advance our understanding of the complex factors that influence bone regeneration and represent a critical step towards improved, more personalized care and management of patients recovering from orthopedic trauma.

CHAPTER 2. BACKGROUND

2.1 Clinical Significance of Bone Injuries

Bone is one of the unique tissues in the human body, along with liver and certain mucosal sites [1], that has capacity for scar-free repair. For humans, a bone defect is considered critical-size (i.e. one that will not spontaneously heal on its own) when it is approximately 2 cm in length [2]. Despite this fact, treatment of large bone defects often resulting from trauma, tumor resection, infection, or congenital deformity remains one of the most challenging problems faced by orthopedic surgeons. The current gold standard in treatment is autograft, most commonly harvested from the medullary cavity or iliac crest [3]. An estimated 1.6 million bone grafting procedures are performed annually in the US [4] and these procedures have an associated cost of over $5 billion [5]. However, these types of bone grafts have drawbacks such as limited tissue availability, donor site pain and morbidity, and additional healthcare costs associated with multiple surgeries.

Allografts from cadavers are used to a lesser extent but often have poor structural strength and demonstrate decreased osteogenesis compared to autografts [6], as well as carry additional risks of rejection and possible disease transmission. Bone graft substitutes, including demineralized bone matrix, hydroxyapatite composites, and bone morphogenetic proteins (BMPs), offer a promising alternative but are currently only approved for a select few indications [7]. BMPs in particular have been an area of intense research focus as these growth factors are among the most osteoinductive proteins discovered and have demonstrated some commercial success with Medtronic's Infuse (rhBMP-2) and Stryker's OP-1 (rhBMP-7) products. However, there have also been numerous reports of complications following BMP treatment [8-11] and as a result, BMPs have yet to be fully embraced by the orthopedic community. Thus, there seems to

be a great need to optimize BMP dosing and other currently available treatment options for each patient based their particular needs and circumstances in order maximize healing and minimize potential side effects.

2.2 Influence of Aging on Bone Repair

One of the most commonly cited factors that impacts bone healing is age. It has been well established that bone fractures in elderly patients do not heal as quickly and are more prone to complications compared to fractures in younger patients [12, 13]. A number of mechanisms have been implicated for this diminished bone healing capacity with age, including delayed angiogenesis [14], impaired stem cell recruitment and cell differentiation [15], poor callus mineralization [16], and increased presence of co-morbidities like osteoporosis and diabetes mellitus [17, 18]. One group has even demonstrated that the bones of mice slowly lose their adaptive response to mechanical stimuli as they age [19]. Interestingly, others have shown that there are very few gene expression differences between young and old animals during fracture healing despite the latter group exhibiting a delayed healing response [20].

It is worth noting that all of the work referenced above and the majority of work found in literature on age-related differences in bone healing focus solely on fracture repair, and not the more challenging case of large bone defect repair, which may actually involve different endogenous mechanisms. Furthermore, none of the studies have directly investigated the role that age plays in the response to bone healing treatments, such as bone grafts or delivery of biologics. It remains to be seen whether patients of different ages require further considerations to determine the optimal treatment strategy. For example, even though autografts are usually assumed to be the gold standard, would it

actually be better for an older patient with a number of co-morbidities to receive an allograft (from a younger relatively healthy donor) supplemented with BMP instead? On the other end of the age spectrum, rhBMP-2 is currently contraindicated by the FDA for use in pediatric patients, but off-label use still occurs and no one has yet performed a controlled dosing study to determine if age significantly affects the response to rhBMP-2 treatment. Such critical work is still needed to advance the field and improve therapeutic outcomes.

2.3 Nonunion and Treatment Timing

Although there has been significant progress in the treatment of bone injuries, the incidence of delayed union and nonunion remain high, up to 10% in long bone injuries and 40% in spinal fusion cases [21-23]. The clinical diagnosis of nonunion is often made when the injured bone demonstrates no radiographical evidence of union after 6 months and no visible signs of healing progression for 3 consecutive months [24, 25]. Nonunions can be further categorized as hypertrophic or atrophic depending on the level of callus formation. There are several known causes of nonunion including mechanical instability, inadequate vascularization, periosteal disruption, infection, and poor soft tissue coverage [26, 27]. Most hypertrophic nonunion cases are believed to be due to insufficient stabilization [27, 28], and are easily corrected with proper fixation. Atrophic cases are not as simple, and usually require more extensive fixation, resection of nonviable bone and fibrous tissue, and delivery of more grafts/biologics [29]. This process often occurs in a trial-and-error basis over the course of multiple revision surgeries, incurring long recovery times and increasing financial costs for the patient. This problem highlights the

fact that the underlying biological mechanisms of nonunion remain poorly understood and merit further investigation in appropriate preclinical models.

A thorough review of literature revealed that most studies using preclinical animal models to research bone regeneration involve creation of some type of injury followed immediately by treatment. This is contrary to current clinical practice, as large bone defect injuries are often not given reparative treatment immediately (outside of wound stabilization) or even within the first couple weeks after injury. In fact, less than 7% of orthopedic surgeons surveyed support the idea of immediate bone grafting to treat segmental defects [3]. Instead, one of the increasingly used practices in treating large bone defects has been the Masquelet technique [30, 31]. This technique involves use of an antibiotic-doped polymethyl methacrylate (PMMA) cement spacer that remains in place for approximately 6-8 weeks, allowing most of the post-trauma inflammation to subside and a highly vascularized membrane to form around the defect. Subsequently during a revision surgery, the spacer is carefully removed with minimal disruption to the pre-formed membrane, and treatments such as autologous bone grafts are delivered. It has even been demonstrated that this vascularized membrane that forms around the defect secretes potent growth factors such as VEGF, TGFβ1, and BMP-2 and can also prevent resorption of the bone grafts [32, 33]. The recent establishment and increasing adoption of the Masquelet technique suggests a need to improve current preclinical models to be more representative of these clinical scenarios, possibly by incorporating delayed treatment. For critically-sized large bone defect models in particular, there remains a great opportunity to characterize some of the biological changes that occur with delayed

treatment and to provide further insight into some of the mechanisms that can lead to delayed union and nonunion.

2.4 Inflammation and the Immune Response Following Trauma

Immediately following any type of injury, inflammatory cytokines and danger signals called danger-associated molecular patterns (DAMPs) are released from the damaged tissue. Common DAMPs include intracellular molecules that normally are never found outside of the cell, such as many nuclear and cytosolic proteins, DNA, ATP, uric acid, and heat shock proteins [34, 35]. Presence of these DAMPs in the extracellular environment can be detected through binding of receptors, such as those in the Toll-like receptor (TLR) family [34, 36, 37]. Many TLRs and DAMPs are promiscuous and can actually bind to several different ligands and receptors, respectively, which can dictate the magnitude of the immune response generated as well as the specific pathways that are activated. For example, one of the most common DAMPs is the DNA chromatin-associated high mobility group box 1 (HMGB1) protein, which can bind to both TLR2 and TLR4 [38, 39]. Many groups have shown that using antibodies to target HMGB1 can knockdown specific TLR activation and even serve as an effective treatment strategy in animal models of sepsis [40, 41] and rheumatoid arthritis [42].

Many of these TLRs are expressed on the cell or endosomal surface of innate immune cells, including mast cells, monocytes/macrophages, dendritic cells, and natural killer cells [43]. Binding of ligands to the respective TLR activates these immune cells and induces secretion of chemokines that recruit other immune cells to the wound area. Within minutes following trauma, the initial danger signals have been processed and

amplified, resulting in the classical inflammatory response: phagocytosis of cellular debris, neutralization and elimination of potentially harmful pathogens, increased systemic expression of inflammatory cytokines and local release of granular enzymes and reactive oxygen species (ROS), as well as recruitment of fibroblasts and endothelial cells to help stabilize the wound area and initiate revascularization. All of these local and systemic events constitute a normal acute inflammatory response to injury, and can also be referred to as the systemic inflammatory response syndrome (SIRS) [44].

2.5 Chronic Immune Dysregulation and the Cellular Mediators

The most difficult bone injury cases to treat are often the result of severe trauma, which involve substantial injury to bone and multiple soft tissues including vasculature, nerve, and muscle. The Centers for Disease Control estimates that trauma costs over $580 billion annually and accounts for about 30% of all life years lost in the US [45]. While mortality rates following severe trauma have greatly decreased in recent decades, prolonged impairment and disability, both physical and mental, remain high even with acute medical and surgical care. Some have estimated that residual impairments prevail in up to 80% of severe trauma patients even three years after the initial trauma [46].

Recent studies have identified a dysregulated immune response, including chronic immunosuppression and immune paralysis, as an important cause of morbidity following severe trauma [47-49]. Trauma-induced immune dysfunction occurs roughly in two stages. The first stage encompasses the aforementioned SIRS phase, characterized by acute hyper-inflammation with overproduction of pro-inflammatory cytokines (IL-1, IL-6, TNFα), countered by a compensatory anti-inflammatory response syndrome (CARS)

with increased expression of anti-inflammatory cytokines (IL-1Ra, IL-10, TGFβ) [50]. CARS follows almost immediately after SIRS is initiated, as prolonged exposure to the high levels of inflammatory factors and ROS generated during SIRS is damaging to the surrounding tissues and can lead to multiple organ dysfunction syndrome (MODS) if left unchecked [44, 51]. In most cases of uncomplicated healing, the SIRS and CARS responses eventually resolve one another and systemic immune homeostasis is restored within a couple weeks. Failure to achieve this balance can lead to a genomic storm of elevated pro- and anti-inflammatory signals that lasts up to 28 days post-injury [52], and will eventually result in a second stage called persistent inflammation, immunosuppression, and catabolism syndrome (PICS) [53]. PICS is often characterized by chronic low level inflammation combined with long term systemic immune suppression. Patients exhibiting symptoms of PICS are more prone to opportunistic infections, sepsis, MODS, and often require multiple surgical interventions and hospitalizations, which incur greater healthcare costs as well as increase the physical and emotional burden experienced by the patient [53-55].

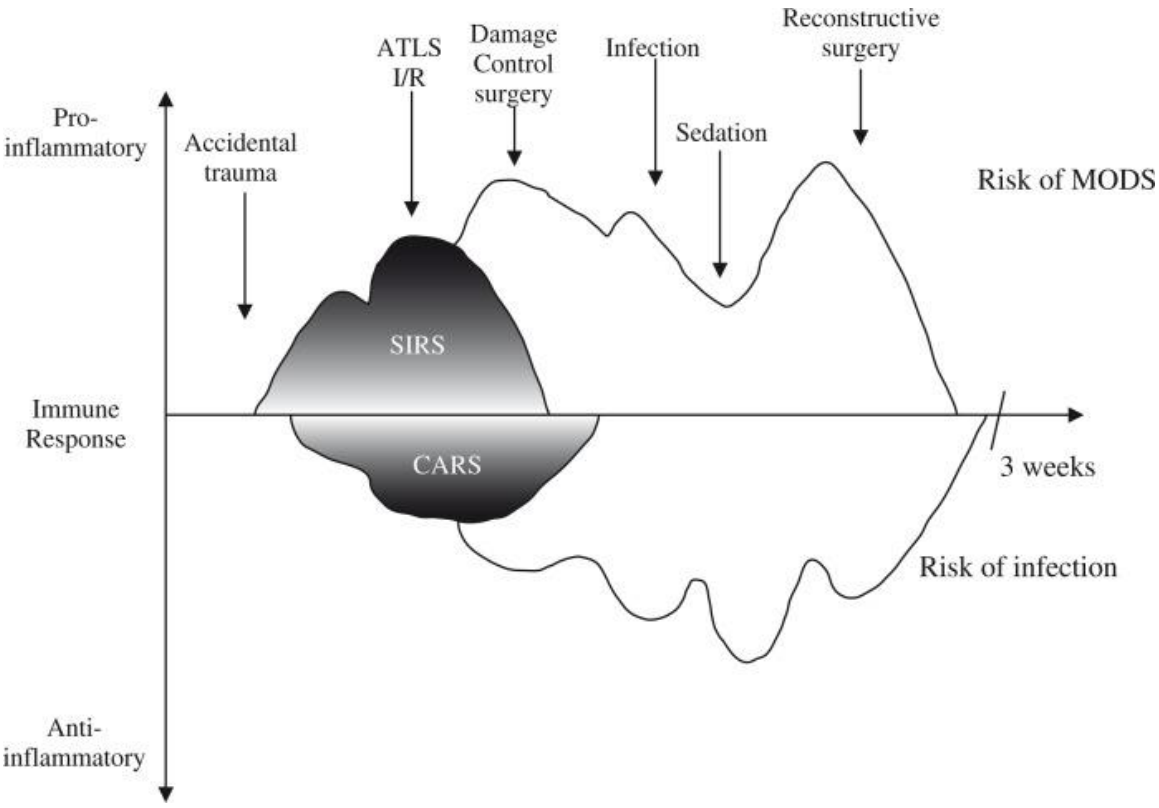

Schematic depiction of the pro- and anti-inflammatory responses after trauma and how subsequent interventions/procedures can prolong immune disruption and increase the risk for MODS. Adapted from Brochner et al. [56].

Some of the primary cellular mediators of long-term immune paralysis observed in PICS are the immune suppressor cell types, including T regulatory cells (Tregs) and myeloid-derived suppressor cells (MDSCs) [48, 49, 54]. These cells suppress immune function by secreting anti-inflammatory factors such as IL-1RA, IL-10, and TGFβ, which can inhibit activation of other immune effector cell types, such as in T cell anergy, or even reduce immune populations over time by promoting premature apoptosis of these cells [54, 57-59]. Tregs are commonly identified as the CD4+FoxP3+CD25+ subset of T

helper cells, and are usually associated with a shift towards the anti-inflammatory Th2 adaptive immune response [60, 61]. These immune suppressive cells have multiple roles in disease progression, and have been directly implicated in many autoimmune disorders [62] as well as in cancer tumor immune evasion [63, 64]. In the context of trauma and sepsis, it has been widely observed that Treg populations increase after injury and at the onset of septic shock [60, 65, 66], and they can induce rapid immune suppression through direct cell-to-cell contact with CD4+ and CD8+ T cells [67] as well as through Fas ligand-mediated apoptosis of monocytes [68]. Not surprisingly, it has been shown that elevated circulating levels of Tregs and their cytokines were associated with higher incidence of sepsis and greater risk of mortality following severe burn injuries [69].

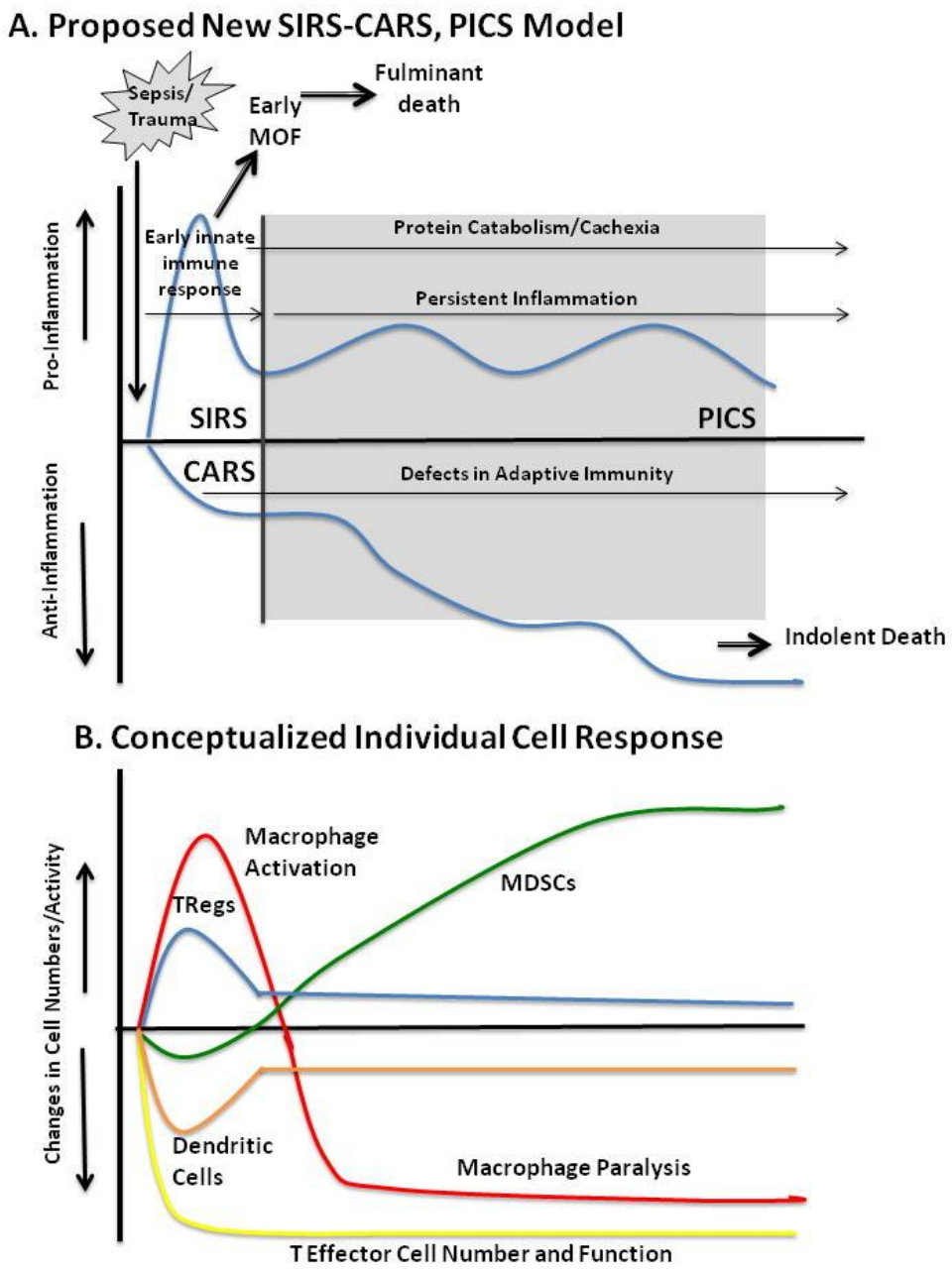

Proposed conceptual model of PICS development after trauma/sepsis (Panel A) and the corresponding changes in immune cell populations (Panel B). This schematic describes a gradual rise of immunosuppressive cell types, particularly MDSCs, which coincides with a rapid decrease in macrophage and T cell numbers/function. Adapted from Gentile et al. [54].

MDSCs are immature myeloid lineage cells originating in the bone marrow, separate from other myeloid immune cells such as macrophages, granulocytes, and dendritic cells [70]. While generally thought to be heterogeneous in nature, MDSCs are most commonly identified in rats as expressing both neutrophil (His48) and monocyte (CD11b) markers [71, 72]. These cells can directly suppress T cell function through depletion of the amino acid L-arginine [73], which is a critical mediator of T cell metabolism and activity [74], as well as through promotion of nitric-oxide-mediated T cell apoptosis [71]. Others have even shown that MDSCs are also involved in TGFβ1-mediated suppression of natural killer cells [75] and can possibly enhance T regulatory cell survival [76]. In humans, circulating MDSCs have been observed to persist at high levels up to 28 days in severely septic patients, and were linked to adverse outcomes and prolonged ICU stays [59]. Similar to recent approaches that target Tregs, treatments that target MDSCs in order to mitigate immune suppression have been of great interest, particularly in the context of enhancing cancer immunotherapies [77].

CHAPTER 3. THE EFFECTS OF AGE AND DOSE ON BMP-2-MEDIATED BONE REPAIR[1]

3.1 Abstract

Age is a well-known influential factor in bone healing, with younger patients generally healing bone fractures more rapidly and suffering fewer complications compared to older patients. Yet, the impact age has on the response to current bone healing treatments, such as delivery of bone morphogenetic protein 2 (BMP-2), remains poorly characterized. It remains unclear how or if therapeutic dosing of BMP-2 should be modified to account for age-related differences, in order to minimize potential adverse effects and consequently improve patient bone healing outcomes. For this study, we sought to address this issue by using a preclinical critically-sized segmental bone defect model in rats to investigate age-related differences in bone repair following delivery of BMP-2 in a collagen sponge, the current clinical standard. Femoral defects were created in young (7-week-old) and adult (8-month-old) rats, and healing was assessed using gene expression analyses, longitudinal radiography, ex vivo micro-computed tomography (μCT), as well as torsional testing. We found that young rats demonstrated elevated expression of genes related to osteogenesis, chondrogenesis, and matrix remodeling at an early 1 week time point compared to adult rats. These early gene expression differences may have impacted long-term healing as the regenerated bones of young rats exhibited higher bone mineral densities compared to those of adult rats after 12 weeks. Furthermore, the young rats demonstrated significantly more bone formation and increased mechanical strength when BMP-2 dose was increased from 1 to 10 μg, a

finding not observed in adult rats. Overall, these results indicate there are age-related differences in BMP-2-mediated bone regeneration, including relative dose sensitivity, suggesting that age is an important consideration when implementing a BMP-2 treatment strategy.

[1]Portions of this chapter were adapted from A. Cheng*, L. Krishnan*, L. Tran, H.Y. Stevens, B. Xia, N. Lee, J.K. Williams, G. Gibson, R.E. Guldberg. The effects of age and dose on gene expression and segmental bone defect repair following BMP-2 delivery. Under review in JBMRPlus (2018).

3.2 Introduction

The repair of large bone defects represents one of the most challenging problems faced by orthopedic and craniofacial surgeons today. The gold standard in treatment is autograft [78], but graft substitutes and/or delivery of osteoinductive proteins such as the bone morphogenetic protein (BMP) family are also common alternatives with demonstrated efficacy in bone regeneration [79-81]. While the effects of age on endogenous bone healing have been well documented, both in preclinical animal models [15, 19, 20, 82-84] and human patients [12, 13, 17], the influence of age on the response to current bone healing treatments is much less informed. It has been demonstrated *in vitro* that age (as well as donor site) influences the responsiveness of bone marrow stromal cells to BMP-2 [85]. Indeed, clinical studies have shown similar trends, as use of BMP-2 and allograft in spine fusion in elderly patients (>65 years) demonstrated lower fusion rate and longer fusion time compared to younger patients (<65 years) receiving the same treatment [86]. Yamaji et al. also showed *in vivo* that the thickness of new bone formed when BMP-2 is injected into a palatal site is much lower in elderly 70-week-old

rats compared to young 10-week-old rats [87]. Importantly, this study also demonstrated an age-related difference in the osteoinductive response to increasing doses of BMP-2. While the elderly animals showed an increase in thickness of new bone over a large range of increasing BMP-2 doses (0 – 16 μg), the younger animals exhibited a much smaller benefit window (0 – 4 μg), beyond which a significant reduction in new bone thickness was actually observed. Additionally, the use of higher BMP-2 doses to enhance bone defect regeneration in mature rats (12-14 weeks of age) has been shown to result in heterotopic ossification and formation of abnormal spongy bone with thin trabecular networks [88, 89].

These results indicate that cells from younger animals are more responsive to BMP-2, which suggests that younger patients may respond better to lower BMP-2 doses, while older patients may not attain comparable responses even with higher BMP-2 exposure [87]. However, the use of higher BMP-2 doses is fraught with risks including heterotopic mineralization, osteolysis, infection, and potentially life-threating inflammation/swelling, as extensively demonstrated in preclinical and clinical studies [8-10]. These complications could potentially be most devastating in the pediatric population, with reports of massive inflammatory reactions and acute pain in some pediatric patients [90-92]. As a result, the use of any BMPs in skeletally immature patients is currently not approved by the U.S. Food and Drug Administration (FDA) [93]. Despite these known risks, off-label use of BMP-2 still occurs due to a lack of better alternatives in many scenarios, as well as documented successful cases without any noticeable complications [92, 94, 95]. In the absence of controlled trials to optimize therapeutic dosing (which remain unfeasible due to ethical considerations and costs), the

use of relevant preclinical animal models represent the best approach to gain insight into how age influences the response to BMP-2 treatment during bone healing.

We have previously established a critically-sized segmental bone defect model in rats [96] to study bone regeneration and furthermore, have shown this model to be robust enough to qualitatively and quantitatively evaluate the efficacy of different treatments, including autograft and the clinical standard BMP-2 in collagen sponge [81, 97, 98]. Here, we adapted this model to 7-week-old young adolescent (young) and 8-month-old middle-aged adult (adult) rats in order to investigate how age impacts BMP-2-mediated bone repair at both a sub-healing low dose (1 μg) and relatively higher dose (10 μg) of BMP-2 [97]. We hypothesized that the osteogenic response would be a function of animal age, with young animals showing greater bone regeneration at the low dose and signs of supraphysiological levels of BMP-2 at the high dose, and the adult animals healing only at the high dose. We further hypothesized that young rats would demonstrate elevated early expression of genes related to bone healing as well as inflammation (particularly at the high BMP-2 dose), and this would correlate to improved long-term bone regeneration compared to the adult rats. Early (1 week post-surgery) gene expression profiles of young and adult animals at the two doses of BMP-2 were assessed by quantitative real-time polymerase chain reaction (qRT-PCR) to identify potential mechanistic differences. To compare bone regeneration, defect mineralization was monitored over time using longitudinal radiographs and end point micro-computed tomography (μCT) scans were analyzed for quantitative measures of new bone formation. Finally, the biomechanical properties of the regenerated femurs were measured by

torsional testing, serving as a functional metric to assess healing, while routine histology of harvested femora provided qualitative assessment of the newly formed bone.

3.3 Materials and Methods

3.3.1 Animals

For these studies, 7-week-old and 8-month-old (retired breeders) male Sprague Dawley rats (Harlan Laboratories/Envigo) were used. Herein age refers to age at the time of surgery. Rats were pair housed in individually ventilated caging (Tecniplast) with a tunnel and gnawing blocks (Bio-Serv) for enrichment. Bedding was a mixture of corn cob and processed paper. Purina Mills International #5001 was fed ad libitum. Filtered tap water treated with ultraviolet light was provided ad libitum in bottles. Sentinel results from Charles River Laboratories International Rat Prevalent PRIA testing were negative for all pathogens in the housing room. All animals were allowed to acclimate for at least 2 weeks before any procedures were performed. Following each procedure, a divider was temporarily placed in the cage for better monitoring of post-operative recovery. Animals were randomly allocated to treatment groups.

3.3.2 Surgical procedure

All surgical procedures were approved by the Georgia Institute of Technology Institutional Animal Care and Use Committee. The surgical procedure has been described previously [96]. Anesthesia was induced and maintained using isoflurane (Henry Schein Animal Health) inhalation. Briefly, an anterolateral skin incision was made in the thigh followed by blunt dissection to separate the overlaying muscles to reach the femur bone.

Limited extension of this muscle window allowed for placement of a radiolucent polysulfone fixation plate for internal stabilization. Critically-sized 8 mm defects were created in the mid-diaphysis of the femur using an oscillating saw. A collagen sponge loaded with BMP-2 was then delivered to the defect site, and finally the muscle and skin were closed using 4-0 vicryl suture and wound clips, respectively. Prior to surgery, all animals were given a subcutaneous injection of sustained-release buprenorphine (ZooPharm) for analgesia.

3.3.3 Collagen sponge preparation

The day before each surgery, BMP-2 (Pfizer) in 0.1% rat serum albumin (Sigma-Aldrich) in 4 mM HCl solution was prepared and stored overnight at 4°C. Collagen sponge cylinders ~5mm in diameter and 10mm in length were created by biopsy punch from a sheet of collagen sponge (Kensey Nash/DSM). All collagen sponges were used directly from the manufacturer's sterile packaging or sterilized by ethylene oxide if previously opened. During the surgery, the collagen sponge cylinders were transferred to a 24-well plate, and then 150 μl of the BMP-2 solution was carefully loaded onto each cylinder. The sponge was left for ~10 minutes to soak up any residual BMP-2 solution in the well before being gently press-fit into the bone defect.

3.3.4 qRT-PCR and analyses

At 1 week post-surgery, all tissue within the bone defect as well as a portion of the surrounding muscle were harvested and stored separately in RNAlater solution (Thermo Fisher Scientific) at 4°C. Bone and muscle tissue were similarly harvested from naïve age-matched animals for both age groups. Within 1 month of harvesting tissues, RNA

was isolated by following the QIAzol extraction method (Qiagen). RNA quality and concentration were assessed using the 2100 Bioanalyzer system (Agilent) and Nanodrop ND-1000 Spectrophotometer (Thermo Fisher Scientific), respectively. Subsequently, 300 ng of RNA from each sample was converted to DNA using the RT2 First Strand cDNA kit (Qiagen) and then stored at -20°C (all remaining RNA was stored at -80°C). Samples and TaqMan primers (Thermo Fisher Scientific; see Table 2 for more detailed primer information) for 46 genes of interest were prepared for loading into 48.48 gene expression IFC chips (Fluidigm) according to the manufacturer's protocols [99]. The chips were then primed, loaded with sample and primer reaction mixes, and then run through the BioMark System (Fluidigm). AccuRef rat universal cDNA (Gene Scientific) and distilled water were used as positive and negative controls, respectively, to ensure run fidelity.

Table 1 - Summary of gene targets for qRT-PCR

Group	Genes
Osteogenic	*Runx2, Bmp2, Osx, Opg, Col1a1, On, Rankl, Opn, Ocn*
Myogenic	*Pax7, Myf5, Myod1, Myog, Myh2, Ckm*
Angiogenic	*Vegfa, Epas1*
Chondrogenic	*Col2a1, Acan, Sox9, Tgfb1, Frzb*
Inflammatory	*Ifng, Tnf, Il1a, Il1b, Il6, Mcp1, Ccl3, Ccr7, Csf1*
Anti-inflammatory	*Il1rn, Il10, Tgfb1*
Matrix remodeling	*Mmp2, Mmp3, Mmp9, Mmp13, Timp1, Adamts4, Adamts5*
Housekeeping	*Hprt1, Rplp1, Rpl13a Gapdh, Ppia*

Table 2 - TaqMan probe information for all primers

Gene	TaqMan ID	Amplicon Length	NCBI Ref Seq
Acan	Rn00573424_m1	74	NM_022190.1
Adamts4	Rn02103282_s1	105	NM_023959.1
Adamts5	Rn01458486_m1	77	NM_198761.1
Bmp2	Rn00567818_m1	126	NM_017178.1
Ccl3	Rn01464736_g1	63	NM_013025.2
Ccr7	Rn02758813_s1	65	NM_199489.4
Ckm	Rn01644605_m1	61	NM_012530.2
Col1a1	Rn01463848_m1	115	NM_053304.1
Col2a1	Rn01637087_m1	97	NM_012929.1
Csf1	Rn00696122_m1	79	NM_023981.4
Epas1	Rn00576515_m1	70	NM_023090.1
Frzb	Rn01746979_m1	63	NM_001100527.1
Gapdh	Rn01775763_g1	174	NM_017008.4
Hprt1	Rn01527840_m1	64	NM_012583.2
Ifng	Rn00594078_m1	91	NM_138880.2
Il1a	Rn00566700_m1	73	NM_017019.1
Il1b	Rn00580432_m1	74	NM_031512.2
Il1ra	Rn00573488_m1	76	NM_022194.2
Il6	Rn01410330_m1	121	NM_012589.2
Il10	Rn00563409_m1	70	NM_012854.2
Mcp1/Ccl2	Rn00580555_m1	95	NM_031530.1
Mmp2	Rn01538170_m1	63	NM_031054.2
Mmp3	Rn00591740_m1	67	NM_133523.3
Mmp9	Rn00579162_m1	72	NM_031055.1
Mmp13	Rn01448194_m1	65	NM_133530.1
Myf5	Rn01502779_g1	135	NM_001106783.1
Myh2	Rn01470656_m1	82	NM_001135157.1
Myod1	Rn01457527_g1	143	NM_176079.1
Myog	Rn01490689_g1	94	NM_017115.2
Ocn/Bglap	Rn00566386_g1	104	NM_013414.1
On/Sparc	Rn01470624_m1	107	NM_012656.1
Opg/Tnfrsf11b	Rn00563499_m1	75	NM_012870.2
Opn/Spp1	Rn01449972_m1	124	NM_012881.2
Osx/Sp7	Rn02769744_s1	76	NM_001037632.1
Pax7	Rn01518732_m1	60	NM_001191984.1
Ppia	Rn00690933_m1	149	NM_017101.1
Rankl/Tnfsf11	Rn00589289_m1	69	NM_057149.1
Rp113a	Rn00821946_g1	66	NM_173340.2
Rplp1	Rn03467157_gH	96	NM_001007604.2
Runx2	Rn01512298_m1	86	NM_001278483.1
Sdf1/Cxcl12	Rn00573260_m1	60	NM_022177.3
Sox9	Rn01751069_mH	60	NM_080403.1
Tgfb1	Rn00572010_m1	65	NM_021578.2
Timp1	Rn01430873_g1	118	NM_053819.1
Tnf	Rn01525859_g1	92	NM_012675.3
Vegfa	Rn01511601_m1	69	NM_031836.3

Auto-estimation of threshold cycle (Ct) was performed within the native Fluidigm software and the data exported for further processing. Variances of 5 housekeeping genes (*Hprt1, Rplp1, Rpl13a, Gapdh, and Ppia*) were examined and the three housekeeping genes with the lowest variance over all the runs were chosen for normalization (*Gapdh* and *Ppia* were excluded). Relative expression of genes of interest was determined by normalizing to the average of the three chosen housekeeping genes (Ct^{Gene} - $Ct^{Arithmetic\ Mean\ of\ 3\ HK}$) for each sample [100]. Finally, the normalized expression values were inverted by subtracting from 31 (1 greater than the highest observed cycle number), which allowed for more straightforward analysis – higher adjusted Ct numbers represent higher relative expression levels. These data were then imported into JMP Genomics 8 software (SAS Institute Inc.) and analyzed using the basic expression workflow module. Principal variance component analysis (PVCA) was performed to determine the proportion of variance for each of the major principal components explained by age, BMP-2 dose, and their interaction components, and the principal components were examined visually to assess the degree of sample clustering on scatter plots. Hierarchical clustering analysis allowed grouping of samples according to similarity in expression profiles. Subsequently, significant differences in gene expression for this data set of 75 samples and 46 genes in our array were assessed using ANOVA and gene-specific linear modeling [101], controlling for multiple comparisons with a 5% Benjamini-Hochberg false discovery rate (FDR). The sample sizes for each group were: Young, unoperated (n = 7), Young, 1 μg BMP-2 (n = 8), Young, 10 μg BMP-2 (n = 7), Adult, unoperated (n = 6), Adult, 1 μg BMP-2 (n = 5), Adult, 10 μg BMP-2 (n = 5).

3.3.5 Radiography and micro-computed tomography

To qualitatively assess longitudinal bone regeneration, 2D *in vivo* digital radiographs were acquired with an MX-20 digital machine (Faxitron X-ray Corp) at 2, 4, 8, and 12 weeks post-surgery. Bridging scores were assigned to each radiograph by two blinded investigators where bridging was defined as continuous bone spanning the entire defect space (from bone end to bone end). In instances of disagreement, a third blinded investigator served as tiebreaker. New bone formation was quantitatively evaluated using 3D micro-computed tomography (μCT) at 12 weeks post-surgery. *Ex vivo* scans of the harvested femora were performed before mechanical testing using the vivaCT40 (Scanco Medical) at a 21 μm voxel size, 55 kVp voltage, and a 145 μA current. A threshold corresponding to 50% of native cortical bone density was applied to segment bone mineral and identify newly regenerated bone, as established previously [96]; these thresholds were determined to be ~315.7 and 406.6 mg hydroxyapatite/cm^3 for the young and adult animals, respectively. The volume of interest (VOI) consisted of the central 5.54 mm (264 slices) of the 8 mm defect. Mineralization was further defined as orthotopic (defect bone volume), within a 6 mm circular contour which corresponded to the diameter of intact bone, or heterotopic (ectopic bone volume), which formed outside of the 6 mm circular contour, as established previously [88, 102]. All μCT and biomechanical test data were normalized to native bone values (unoperated contralateral femur) to account for normal growth-related changes with age and animal-to-animal variability. The sample sizes for each group were: Young, 1 μg BMP-2 (n = 9), Young, 10 μg BMP-2 (n = 12), Adult, 1 μg BMP-2 (n = 10), Adult, 10 μg BMP-2 (n = 6).

3.3.6 Biomechanical testing

Torsional testing to failure was performed as previously described [96]. Femurs were excised at 12 weeks post-surgery, wrapped in PBS-soaked gauze, and stored at -20°C until testing could be performed. On the day of testing, samples were thawed, the surrounding soft tissues were excised, and the femora were first μCT-scanned, as described above. Subsequently, the fixation plate was removed so that the native bone ends could be potted in Wood's metal (Alfa Aesar). The potted femurs were tested to failure in torsion at a rotation rate of 3° per second using the EnduraTEC ELF3200 axial/torsion testing system (Bose). Failure strength was determined by locating the peak torque within the first 60° of rotation. Torsional stiffness was calculated by finding the slope of the linear region before failure in the torque-rotation plot. The sample sizes for each group were: Young, 1 μg BMP-2 (n = 9), Young, 10 μg BMP-2 (n = 12), Adult, 1 μg BMP-2 (n = 10), Adult, 10 μg BMP-2 (n = 6).

3.3.7 Histological characterization

Two representative samples from each treatment group were harvested post-mechanical testing and fixed in 10% neutral buffered formalin at room temperature for 48 hours. Samples were then switched to PBS and sent to HistoTox Labs (Boulder, CO) for decalcification, processing, and Hematoxylin and Eosin (H&E) and Safranin-O staining. Picrosirius red staining was performed in-house according to established protocols.

3.3.8 Statistical analyses and power calculation

All data are reported as mean ± standard error of the mean. Unless otherwise noted, significance was determined using 1-way analysis of variance (ANOVA) with multiple comparisons made by Tukey's post-hoc test. In cases of unequal variances (according to the Brown-Forsythe test), the nonparametric equivalent Kruskal-Wallis test with Dunn's post-hoc test was used instead. Significance was determined by a p-value < 0.05. All statistical calculations were performed using GraphPad Prism 7 software. Sample sizes were determined by performing a power analysis in G*Power software based on bone volume and maximum torque results obtained from previous studies. These power calculations, along with historical data using this segmental bone defect rat model, suggest a sample size of 7-8 is sufficient to give statistical differences between groups.

3.4 Results

3.4.1 Early gene expression characterization in regenerating bone

Local gene expression of the regenerating bone defect tissue at 1 week post-surgery was assessed across a panel of 46 genes (Table 1). Pairwise scatter plots of the first 3 principal components (Figure 1) demonstrated clear separation of unoperated controls from operated/treated groups along the principal component 1 (PC1) axis. Interestingly within the treated groups, the majority of samples clustered according to age rather than BMP-2 dose, as can be observed in PC2. There was slight separation along PC3 according to BMP-2 dose, but this split was not as obvious as in PC1 and 2.

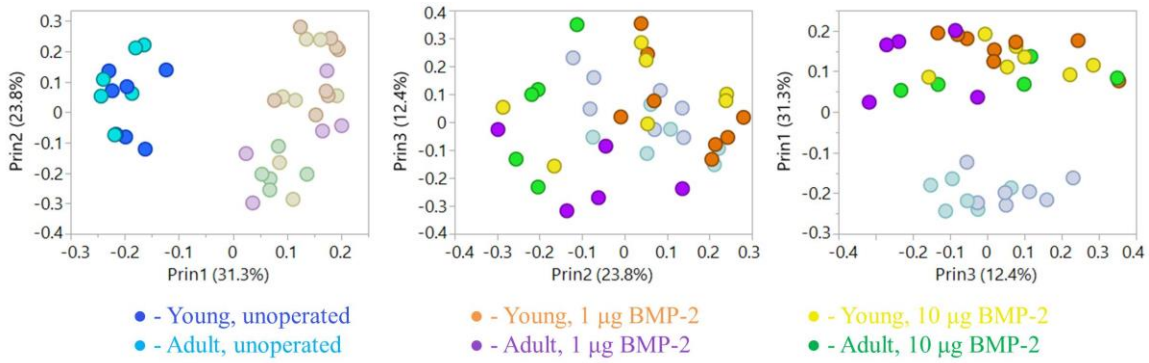

Figure 1 - Principal component analysis of bone defect gene expression at 1 week. PCA scatter plots revealed sample segregation across multiple principal components. The PC1 axis exhibited distinct separation between unoperated controls (which are highlighted in the left panel) from treated samples. Furthermore, among the treated samples, there was separation based on age along PC2 (irrespective of BMP-2 dose), as can be seen in the middle panel with the adult (purple and green) and young (orange and yellow) samples highlighted. Finally, the panel on the right indicates slight separation based on dose along PC3 between the 1 µg (orange and purple) and 10 µg (yellow and green) BMP-2 samples.

These observations were verified by hierarchical clustering analysis (Figure 2), which also showed overall clustering of treated samples based on age rather than BMP-2 dose.

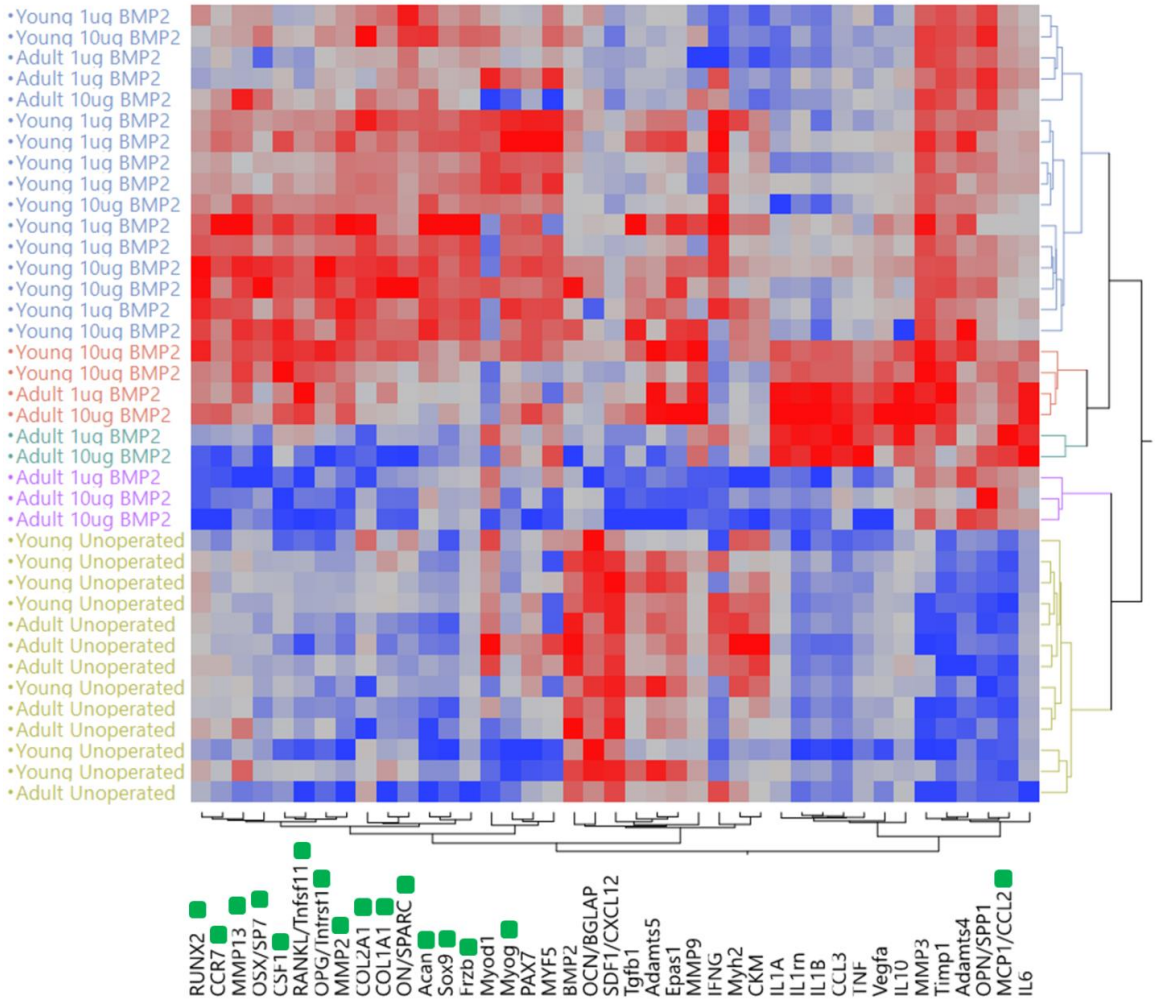

Figure 2 - Hierarchical clustering of bone defect samples at 1 week. Heatmap revealed gene expression clustering primarily according to age, rather than BMP-2 dose, as well as clear separation of unoperated controls. Expression levels are represented on a scale of lower (blue) to higher (red) relative expression. Green squares denote significant difference ($p<0.05$) in expression of corresponding gene between young and adult animals at one or both BMP-2 doses (excluding unoperated controls).

After removing the unoperated samples from the analyses, we used ANOVA to further evaluate the contributions of age and BMP-2 dosage to the expression of each gene. Overall, the young animals demonstrated elevated expression of genes related to osteogenesis (Figure 3A) compared to adult animals, including *Runx2, Osx/Sp7, Col1a1, Opg,* and *On/Sparc* and the osteoclastogenesis gene, *Rankl*. Similarly, the young rats also

had higher expression of chondrogenic genes *Sox9, Col2a1*, *Acan,* and *Frzb*, as well as matrix remodeling genes *Mmp2* and *Mmp13* (Figures 3B and 3C, respectively) compared to adults.

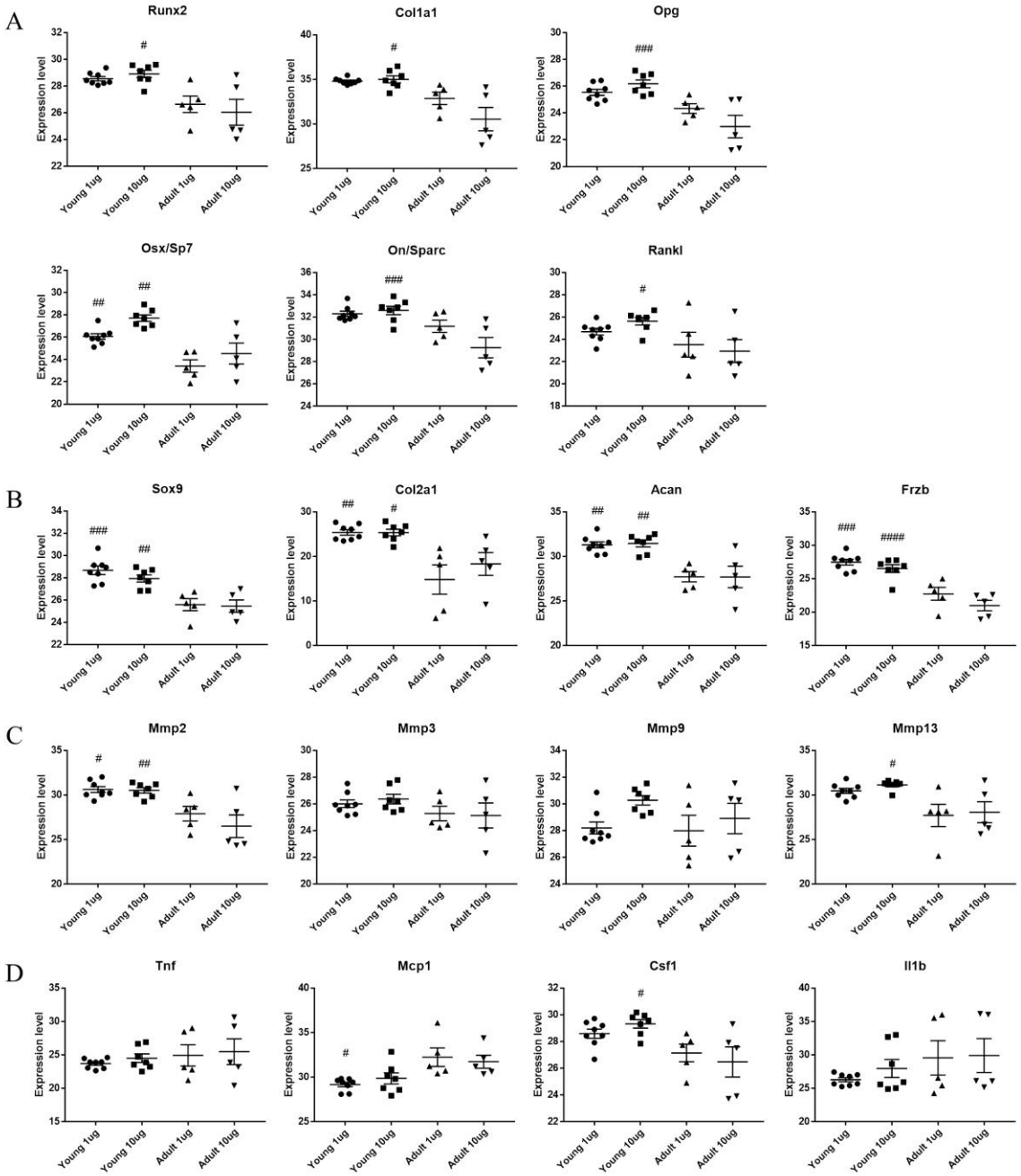

Figure 3 - Expression differences for select genes in bone defect tissue at 1 week. Overall, young rats demonstrated elevated expression of genes relating to osteogenesis

(A), chondrogenesis (B), and matrix remodeling (C) at 1 week, particularly at the higher 10 μg BMP-2 dose. There were relatively few inflammatory gene differences (D), as the young rats exhibited lower expression of Mcp1 but higher expression of Csf1. There was no significant effect of BMP-2 dose on gene expression for either age group. #p<0.05, ##p<0.01, ###p<0.001, ####p<0.0001 vs. adult of same dose, n=5-8/group.

There were relatively few inflammatory (Figure 3D) or myogenic (Figure 4) gene expression differences: expression of *Csf1* and *Myog* were increased while *Mcp1* expression was decreased in young rats.

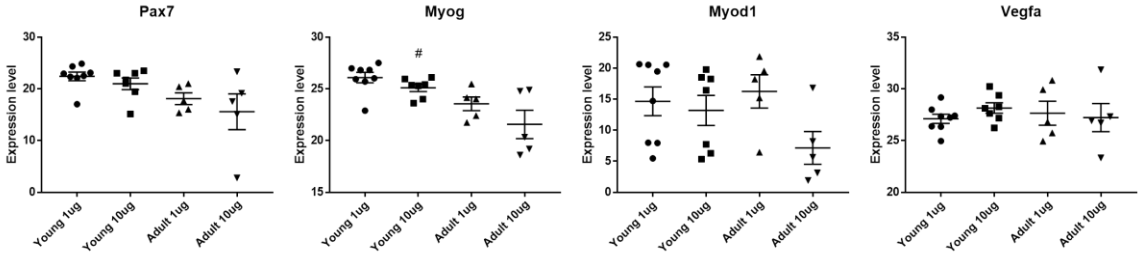

Figure 4 - Myogenic and angiogenic gene expression in bone defect tissue at 1 week. Young rats showed elevated expression of Myog compared to adult rats at the 10 μg BMP-2 dose. #p<0.05 vs. adult of same dose, n=5-8/group.

Surprisingly, differential gene expression with respect to BMP-2 dosing was much reduced relative to the effect of age. Many of these gene expression differences were validated with a linear model approach controlling for multiple comparisons using a 5% FDR criterion (Figure 5). This analysis revealed 21 significant gene expression differences between young and adult rats (Figure 5A), of which only 1 or 2 are expected to be false positives. Similar to what was observed with ANOVA, there were very few BMP-2 dose-related differences (Figure 5B). Only *Osx* exhibited decreased expression at the low 1 μg dose. Although very few significant differences were attributed to BMP-2 dose, the PCA results (separation observed in PC3) suggest that a larger sample size may have increased power sufficiently to enable detection of more dose-dependent effects.

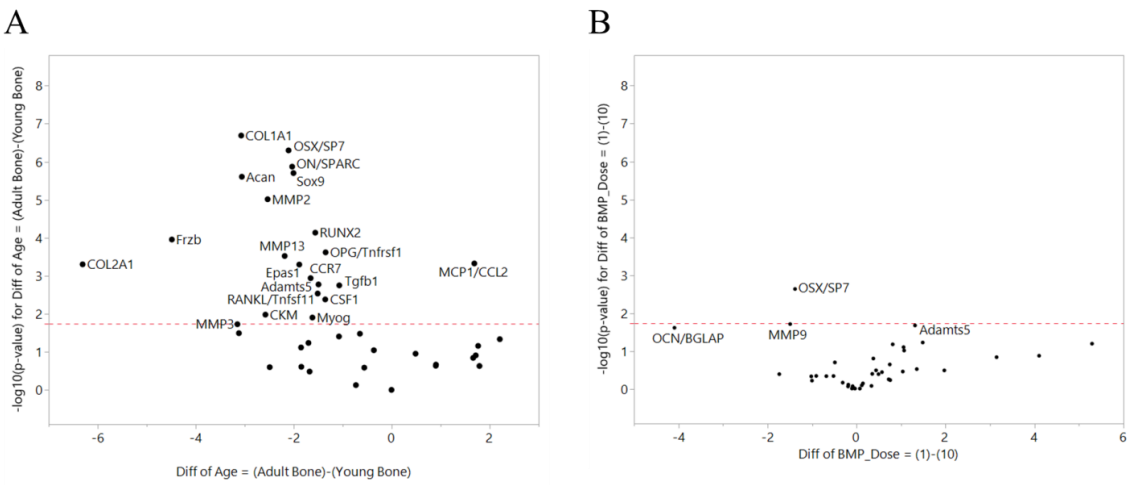

Figure 5 - Significant gene expression differences at 1 week using linear model approach with FDR. There were 21 differentially expressed genes between young and adult animals (A), many of these overlap with those identified by ANOVA in Figure 2. In contrast, there was only 1 differentially expressed gene between the two BMP-2 doses (B): Osx expression was significantly lower in the samples that received 1 μg BMP-2 compared to 10 μg. All genes that are above the dashed red line are significant at a false discovery rate (FDR) of 0.05.

3.4.2 Evaluation of new bone formation

Radiographical assessment at 12 weeks (Figure 6A) demonstrated that both the young and adult rats had qualitatively lower bone mineral formation at the low 1 μg BMP-2 dose; less than 50 percent of defects bridged in both groups (3/9 for Young 1 μg, 4/10 for Adult 1 μg). In contrast, at the higher 10 μg BMP-2 dose, both groups had more robust bone formation and all defects were bridged by 12 weeks (12/12 for Young 10 μg, 7/7 for Adult 10 μg). Micro-computed tomography (μCT) reconstructions (Figure 6B) supported these observations and showed a clear BMP-2 dose effect on bone formation for both age groups.

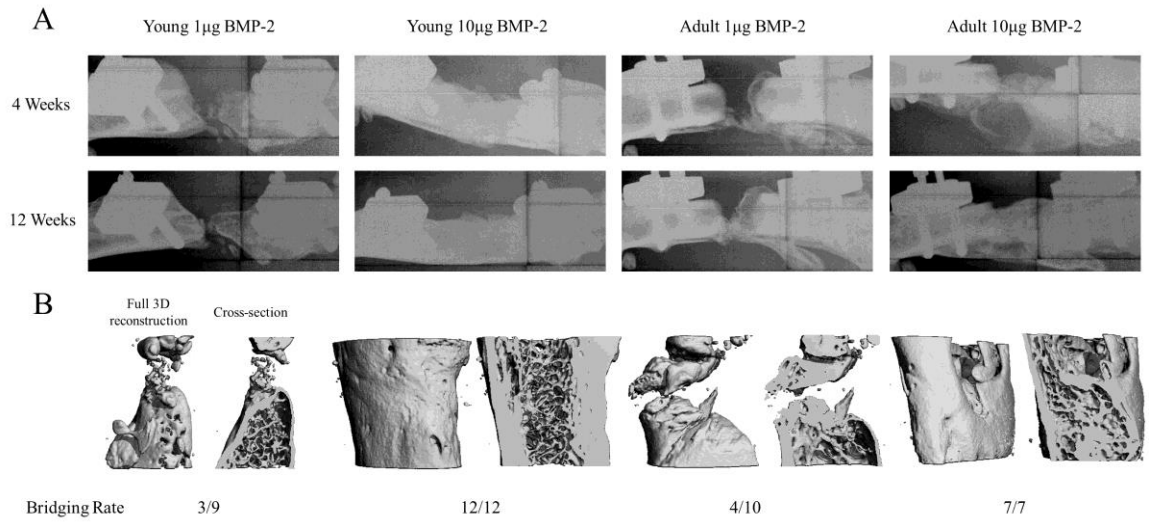

Figure 6 - Representative radiographs and 3D microCT reconstructions of femoral bone defects. 4 and 12-week radiographs (A) and 12-week μCT reconstructions (B) demonstrated a clear effect of BMP-2 dose on new bone formation for both age groups. The low 1 μg BMP-2 dose resulted in poor bone regeneration with impaired defect bridging (<50% for both ages) while the higher 10 μg BMP-2 dose resulted in much more robust bone formation and 100% bridging for both age groups. In addition, the morphology of the newly formed bone at the 10 μg BMP-2 dose appeared more mature and organized from the μCT cross-sectional view, particularly in the young rats.

Quantitative μCT analysis did not yield any differences in defect bone volume between age groups at either of the BMP-2 doses, but the young rats demonstrated a clear BMP-2 dosing effect in forming significantly more defect bone at the higher BMP-2 dose while the adult rats did not (Figure 7A). Furthermore, the newly formed bone in the young rats exhibited significantly higher bone mineral density at both doses compared to that of the adult rats (Figure 7B).

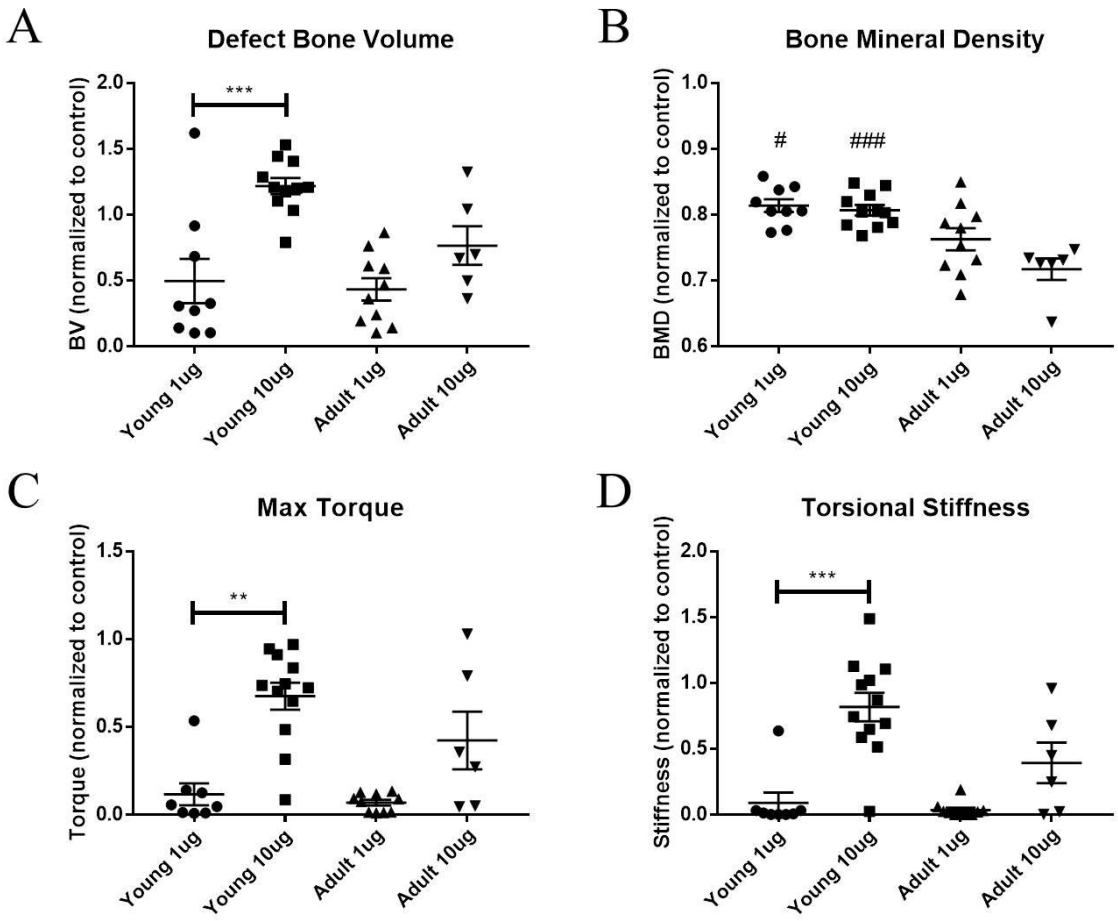

Figure 7 - Quantitative microCT and biomechanics analysis of regenerated bone at 12 weeks. μCT analysis of defect bone volume (A) revealed young rats regenerated significantly more bone in the defect when BMP-2 dose was increased from 1 to 10 μg. In contrast, the adult rats exhibited no significant increase in defect bone formation with increasing BMP-2 dose. The regenerated bone in young rats also exhibited higher bone mineral densities (B) at both BMP-2 doses compared to adult rats. Finally, torsional testing of the regenerated femurs revealed a significant dose-dependent increase in maximum torque (C) and torsional stiffness (D) for the regenerated defects of young rats only. There were no significant differences in mechanical properties between the age groups at either dose level. *$p<0.05$, **$p<0.01$, ***$p<0.001$ as indicated. #$p<0.05$, ##$p<0.01$, ###$p<0.001$ vs. adult of same dose, n=6-12/group.

3.4.3 Biomechanical properties of regenerated bone

Torsional testing of the harvested femurs revealed functional differences in the strengths of the regenerated bones. The maximum torque to failure (Figure 7C) and

torsional stiffness (Figure 7D) were significantly increased with BMP-2 dose only for the young animals, while the adult animals demonstrated no significant BMP-2 dosing effect. Within each dose level, these mechanical parameters were not significantly different between young and adult animals. Thus, as seen with the μCT results, the young animals demonstrated a significant improvement overall, with increased BMP-2 dosing resulting in better functional biomechanical properties.

3.4.4 Histological characterization

Representative samples from each treatment group were sectioned and stained with Hematoxylin and Eosin (H&E), Safranin-O and Fast Green (Saf-O), and Picrosirius red. H&E staining (Figure 8A-D) revealed clear morphologic differences in the tissues formed within the bone defect, particularly between the low and high BMP-2 dose samples. Areas of new bone formation were observed in all samples, but these areas were much larger and more widespread throughout the defect in the high dose BMP-2 samples of both age cohorts. Furthermore, the high dose BMP-2 samples exhibited formation of marrow-like structures directly adjacent to these areas of new bone formation. In contrast, the low dose BMP-2 samples demonstrated only small sparse islands of new bone formation surrounded by mostly fibrous tissue with cellular infiltrate (as indicated by the many nuclei).

Saf-O staining (Figure 8E-H) revealed negligible cartilage present in the defect at 12 weeks post-surgery for all groups. Finally, Picrosirius red staining (Figure 8I-L) and visualization under polarized light demonstrated that the 10 μg treated samples in each age group had more areas of collagen fiber alignment in the areas of new bone formation,

indicative of mature lamellar bone. Conversely, the 1 μg treated samples exhibited a much more disorganized collagen structure, typical of woven bone deposition.

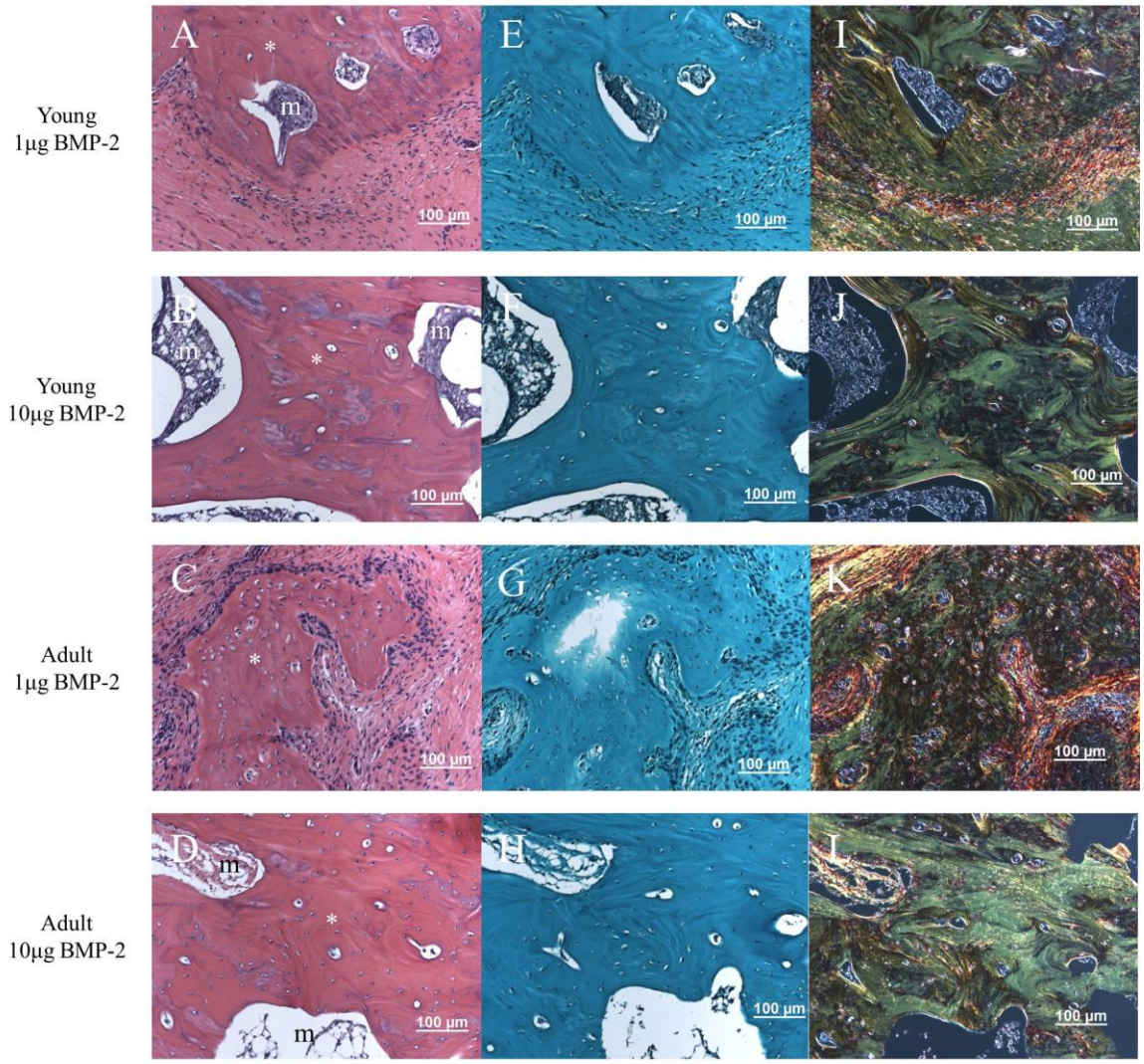

Figure 8 - Histological staining of bone defects at 12 weeks. H&E staining (A-D) of representative sections from each group revealed interesting morphological differences. For both age groups, the 10 µg BMP-2 dose samples demonstrated many large islands of new bone formation (denoted by the asterisk symbol) and more prevalent marrow-like structures (denoted by the letter m) directly adjacent to these areas of new bone. This is in contrast to the 1 µg BMP-2 dose samples, which demonstrated much fewer and smaller areas of new bone formation that were primarily surrounded by soft, fibrous tissue. No positive Safranin-O staining (E-H) was observed within the defect space for any of the samples. Picrosirius red staining (I-L) of collagen fibers demonstrated that much of the new bone formed, particularly in the 10 µg BMP-2 samples of both ages, were more mature and lamellar-like in structure (green).

3.5 Discussion

The use of BMP-2 clinically, both for on-label and off-label indications, remains a highly contentious topic due to its potential for detrimental side effects. In July 2008, six years after the initial approval of BMP-2 use in humans, the FDA issued a black box warning for BMP-2 in cervical spine applications due to potential life-threatening complications [103]. Furthermore, a recent study noted that many of the original industry-sponsored clinical trial publications concerning BMP-2 safety and efficacy had under-reported adverse events [104]. To date, BMP-2 is only approved for three indications: lumbar spine fusion, open tibial fractures, and sinus/alveolar ridge augmentations [105]. And yet, off-label use remains prevalent. This is despite two recent reports describing unapproved use in 66% and 79% of cases reporting adverse events to the FDA, respectively [106, 107]. The continued use of BMP-2 by clinicians in this manner suggests the lack of potential alternatives as well as the recognized benefits of BMP-2 therapy. However, it also highlights the insufficient guidelines currently in place on how to best implement BMP-2 therapies, and further underscores our poor fundamental understanding of the biological factors that influence BMP-2-mediated bone repair.

One patient population who could benefit most from improved BMP-2 treatment strategies are pediatric (skeletally immature) patients, for whom all BMP use is currently contraindicated and yet still occurs [93]. Presently, very little is known about the influence of age on the efficacy of BMP-2 treatment and whether dosing should be adjusted to mitigate potential adverse events. In this work, we sought to address this important problem by studying BMP-2-mediated healing in a preclinical large segmental

bone defect model in rats. To the best of our knowledge, this work represents the first study to directly assess how young and adult rats respond to a clinically-approved bone healing therapy: BMP-2 delivered in a collagen sponge.

Early gene expression analysis revealed that young rats have an elevated expression of many critical genes involved in the normal bone healing response. This partially contradicts findings from another group [20, 108], which showed that young, adult, and elderly rats all had similar overall levels of increased skeletal gene expression following femoral fracture, despite delayed union in the older cohorts. The main difference found in their study was in the temporal expression patterns: young rats had higher levels of mRNA expression that peaked and then returned to baseline levels after 4 weeks, whereas many genes in the older animals remained upregulated up to 6 weeks after fracture [108], including markers of osteoblastic and osteoclastic activity [20]. It is worth noting that these studies utilized a different bone injury rat model, as a simple closed femoral fracture with limited stabilization represents a major change in injury severity and mechanical healing environment compared to large segmental defect repair with BMP-2 treatment, and consequently may involve different signaling pathways and cellular processes.

Interestingly, in the present study, there were very few early differences in inflammatory gene expression. Only *Mcp1* and *Csf1* were differentially expressed between young and adult rats. Both factors are involved in macrophage recruitment and function, which suggests an altered macrophage response and supports recent work highlighting the importance of tissue resident macrophages in bone homeostasis and repair [109]. The relative lack of inflammatory gene expression differences is more

surprising considering the obvious differences observed in the physical condition of the animals. The young rats seemed to tolerate the surgery relatively well: a few demonstrated some swelling that resolved without intervention within the first 2 weeks post-injury but most seemed to recover with no complications. In contrast, the vast majority of adult rats exhibited many more signs of prolonged distress (porphyrin staining, poor grooming, hunched posture, and weight loss) and several had to be euthanized early and excluded from the study due to declining health. Perhaps the chosen 1 week time point was not early enough to detect the changes in local gene expression common to the acute inflammatory phase of bone healing, which has been suggested to peak within the first 72 hours post-injury [110, 111]. It is also possible that inflammatory gene biomarkers alone, despite our panel including many influential cytokines such as tumor necrosis factor, interferon gamma, and a range of interleukins, were insufficient to discern differences in inflammation. Instead, analysis of local immune cell populations or systemic immune profile characterization of serum and/or circulating cells might have been more informative for the time point chosen.

Despite our long-term results indicating higher BMP-2 dose sensitivity with young rats, these did not result in more complications compared to adult rats, contrary to what one might expect, bearing in mind all the concerns with BMP-2 use in pediatric patients. Beyond massive inflammation, another common adverse effect of high dose BMP-2 treatment is ectopic mineralization. However, in this study, the levels of ectopic mineralization were comparable between young and adult rats (Figure 9), if not marginally less in the young rats: 6/12 young and 5/7 adult rats had appreciable amounts of ectopic mineralization ($> 5mm^3$) at the high 10 μg BMP-2 dose. Overall, the degree of

ectopic bone was much lower than that observed in a previous study, involving a higher dose of BMP-2 [88]. Taken together, the relatively low levels of inflammation and minimal amounts of ectopic mineralization in the young rats suggest that these potential complications can be mitigated in pediatric patients, particularly if a conservative approach is taken that utilizes lower doses of BMP-2.

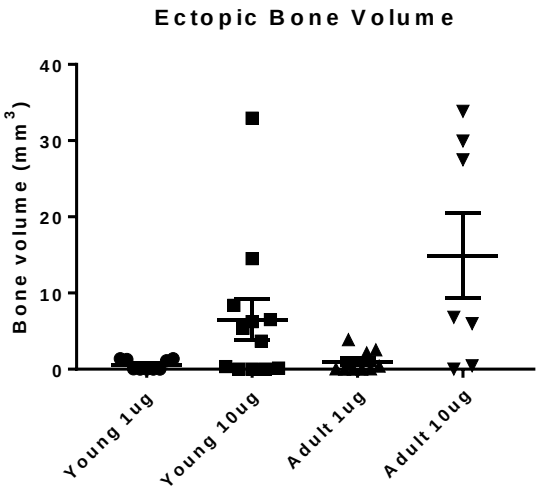

Figure 9 - Quantification of ectopic mineralization at 12 weeks. μCT analysis revealed an increase in the number of samples demonstrating appreciable amounts of ectopic bone formation (>5mm3) in both young and adult animals, although this increase was not statistically significant. There were no differences in amount of ectopic bone between young and adult animals at either of the BMP-2 doses tested.

An intriguing observation from this study was that early gene expression differences (or lack thereof) was not predictive of long-term healing outcomes. Most of the early gene expression differences were age-dependent whereas the long-term functional differences in bone formation and mechanical properties were primarily dose-dependent, particularly in the young animals. This disconnect between early and late differences is not completely unexpected as this study only characterized gene expression at a single time point (1 week post-surgery), providing a snapshot of a highly complex

and dynamic early healing environment. Moreover, quantification of mRNA transcripts can be an imperfect analog for protein levels, and this technique does not account for subsequent modulation of translational or post-translational regulators, all of which could influence protein synthesis and activity. It is thus likely that changes to these complicated and interdependent mechanisms may have influenced the healing and inflammation response with age, and were not completely captured here.

One potential limitation of this work is the absence of a negative control group such as an untreated bone defect or treatment with collagen sponge only (no BMP-2). However, the main focus of this study was to investigate how age and BMP-2 dose impact the response to BMP-2 treatment, not how BMP-2 impacts healing compared to no treatment. Our group has also previously shown that empty bone defects or those receiving carrier alone with no BMP-2 exhibit little to no bone formation and never achieve functional bridging [97, 98, 112]. Furthermore, others have demonstrated that delivery of collagen sponge loaded with saline to critical size defects results in minimal bone formation and very low expression of osteogenic and angiogenic genes compared to BMP-2 treatment [113]. Consequently, we excluded untreated or collagen sponge only control groups given that they would provide limited new insight and prioritized assessment of the interactive effects of age and dose on BMP-2 treatment response.

More extensive studies are needed to better understand the less robust bone healing response exhibited by older animals. Other groups have demonstrated that aging reduces fracture callus vascularization [14], decreases callus volume and cartilage/bone content [114], impairs osteogenic differentiation of bone marrow cells [115], and diminishes periosteal stem cell populations [116]. Further investigations into these aging-related

deficits and how they are impacted by treatments such as BMP-2 may reveal alternative approaches for optimizing current therapeutics as well as uncover potential targets for new therapies.

In summary, the work presented here represents the first investigation into the role of age on BMP-2-mediated segmental bone defect repair using the current clinical standard, BMP-2 delivered in collagen sponge. We found that young rats exhibited elevated early expression of genes involved in bone healing, and were able to form better quality bone long-term. Of clinical significance, our results revealed a clear effect of age on BMP-2 dose sensitivity as young rats appeared more responsive to increases in dosing than adult rats, without experiencing a higher complication rate. These results suggest that adjusting BMP-2 dose based on age may be an advantageous strategy to help minimize the potential risks associated with BMP therapy.

3.6 Acknowledgements

This work was supported by a research partnership between Children's Healthcare of Atlanta and the Georgia Institute of Technology, as well as the Oral and Maxillofacial Surgery Foundation (OMSF). This work was also supported under the AFIRM II (U.S. Armed Forces Institute of Regenerative Medicine) effort, Award No. W81XWH-14-2-0003. The U.S. Army Medical Research Acquisition Activity is the awarding and administering acquisition office. Opinions, interpretations, conclusions, and recommendations are those of the authors and are not necessarily endorsed by the Department of Defense. The authors would like to thank all members of the Guldberg lab for assistance with surgeries and Dalia Arafat for help running the Fluidigm microarrays.

The collagen sponges and BMP-2 used in this study were provided by Kensey Nash (now DSM) and Pfizer Inc., respectively.

Authors' roles: Conception and study design: AC, LK, LT, JW, GG, and REG. Study conduct: AC, LK, LT, and HYS. Data collection: AC, LK, HYS, BX, and NL. Data analysis: AC, LK, and GG. Data interpretation: AC, LK, LT, HYS, GG, and REG. Drafting manuscript: AC. Revising manuscript content: AC, LK, HYS, GG, and REG. Approving final version of manuscript: All authors. AC and LK take responsibility for the integrity of the data analysis.

CHAPTER 4. DELAYED TREATMENT OF BONE DEFECT NONUNION RESULTS IN IMPAIRED HEALING

4.1 Abstract

Delayed union and nonunion are a significant concern for many orthopedic procedures, including long bone fractures and spinal fusions. Treatment of nonunion often entails multiple revision surgeries that further increase the financial, physical, and emotional burden on patients. Unfortunately, the optimal treatment strategy for nonunions remains unclear in many cases, and the risk of complications even after revision procedures remains high. This is in part due to the fact that many of the biological mechanisms that inhibit proper bone healing and lead to nonunion are still not fully understood. And yet, few preclinical models directly investigate how healing is impacted after establishment of nonunion, with most instead primarily focusing on treatment immediately after a fresh bone injury. Here, we utilized a critical size femoral defect model in rats where treatment was delayed 8 weeks post-injury, after capping of the bone ends has been observed previously in this model. In this study, acute and delayed treatments with bone morphogenetic protein-2 (BMP-2) were assessed. We found that delayed treatment results in decreased bone formation and reduced mechanical strength compared to acute treatment, even if BMP-2 dose is increased from 2 to 5 μg. Interestingly, serum cytokine analysis at 20 weeks revealed potential chronic immune dysregulation after delayed treatment, with the non-responders (samples that did not exhibit bridging of the defect) demonstrating higher overall expression of inflammatory cytokines, including TNFα and IL-1β, compared to responders. These findings suggest

that re-establishing long-term immune homeostasis may be critical for successful bone healing, particularly after nonunion.

4.2 Introduction

Although there has been significant progress in the treatment of bone injuries, the incidence of delayed union and nonunion remain high, up to 10% in long bone injuries and 40% in spinal fusion cases [21-23]. The clinical diagnosis of nonunion is often made when the injured bone demonstrates no radiographical evidence of union after 6 months and no visible signs of healing progression for 3 consecutive months [24, 25]. Nonunions can be further categorized as hypertrophic or atrophic depending on the level of callus formation. There are several known causes of nonunion including mechanical instability, inadequate vascularization, periosteal disruption, infection, and poor soft tissue coverage [26, 27]. Most hypertrophic nonunion cases are believed to be due to insufficient stabilization [27, 28], and are readily corrected with proper fixation. Atrophic cases are not as simple, and usually require more extensive fixation, resection of nonviable bone and fibrous tissue, and delivery of more grafts/biologics [29]. This process often occurs in a trial-and-error basis over the course of multiple revision surgeries, incurring long recovery times and increasing financial costs for the patient. This problem highlights the fact that the underlying biological mechanisms of nonunion remain poorly understood and merit further investigation in appropriate preclinical models.

The vast majority of studies using preclinical animal models to investigate bone healing involve creation of some type of injury followed immediately by treatment. This is contrary to current clinical practice, as large bone defect injuries are often not given

reparative treatment immediately (outside of wound stabilization) or even within the first couple weeks after injury. In fact, less than 7% of orthopedic surgeons surveyed support the idea of immediate bone grafting to treat segmental defects [3]. Instead, one of the increasingly used practices in treating large bone defects has been the Masquelet technique [30, 31]. This technique involves use of an antibiotic-doped polymethyl methacrylate (PMMA) cement spacer that remains in place for approximately 6-8 weeks, allowing most of the post-trauma inflammation to subside and a highly vascularized membrane to form around the defect. Subsequently during a revision surgery, the spacer is carefully removed with minimal disruption to the pre-formed membrane, and treatments such as autologous bone grafts are delivered. It has even been demonstrated that this vascularized membrane that forms around the defect secretes potent growth factors such as VEGF, TGFβ1, and BMP-2 and can also prevent resorption of the bone grafts [32, 33]. The recent establishment and increasing adoption of the Masquelet technique suggests a need to improve current preclinical models to be more representative of these clinical scenarios, possibly by incorporating delayed treatment. For critically-sized large bone defect models in particular, there remains a great opportunity to characterize some of the biological changes that occur with delayed treatment and to provide further insight into some of the mechanisms that can lead to delayed union and nonunion.

In this study, we sought to establish a model of chronic nonunion using a critically-sized femoral bone defect in rats, wherein treatment was delayed until 8 weeks following the initial injury. This time point was chosen because we have historically seen mineralized capping of the bone ends by 8 weeks in this model for defects that don’t heal,

which is analogous to one of the hallmarks of long bone nonunion seen clinically. We hypothesized that delayed treatment would result in impaired bone healing compared to acute treatment. Moreover, we also hypothesized that poor healing in this chronic nonunion model could be attributed to a dysregulated long-term immune response. Bone regeneration was evaluated through longitudinal radiographs and quantitative micro-computed tomography (μCT). The biomechanical strengths of the regenerated bones were assessed by torsional testing to failure. Bone histomorphometry was used to further elucidate differences in the newly formed bone between acute and delayed treatment. Finally, end point characterization of immune cells and inflammatory cytokines were performed on isolated spleens and sera, respectively, for the delayed treatment samples.

4.3 Materials and Methods

4.3.1 Animals

For these studies, 13-week-old female SASCO Sprague Dawley rats (Charles River Laboratories, Inc.) were used. Rats were pair housed in individually ventilated caging (Tecniplast) with a tunnel and gnawing blocks (Bio-Serv) for enrichment. Bedding was a mixture of corn cob and processed paper. Purina Mills International #5001 was fed ad libitum. Filtered tap water treated with ultraviolet light was provided ad libitum in bottles. Sentinel results from Charles River Laboratories International Rat Prevalent PRIA testing were negative for all pathogens in the housing room. All animals were allowed to acclimate for at least 2 weeks before any procedures were performed. Following each procedure, a divider was temporarily placed in the cage for better

monitoring of post-operative recovery. Animals were randomly allocated to treatment groups.

4.3.2 Alginate BMP-2 preparation

RGD-functionalized alginate (FMC BioPolymer) was reconstituted in MEM alpha (Thermo Fisher Scientific) to create a 2% w/v solution, as described previously [98]. Recombinant human bone morphogenetic protein 2 (BMP-2, Pfizer Inc.) was reconstituted in a solution of 0.1% rat serum albumin (Sigma Aldrich) in 4 mM hydrochloric acid and mixed with the alginate solution to yield 2 or 5 μg BMP-2 per 150 μl of final solution. This alginate/BMP-2 solution was gelled with the addition of calcium sulfate (Sigma Aldrich) at a 1:25 volume ratio. Hydrogels were prepared under sterile conditions inside a laminar flow hood and stored overnight at 4°C before use in surgery the next day.

4.3.3 Surgical procedures

All surgical procedures were approved by the Georgia Institute of Technology Institutional Animal Care and Use Committee. Anesthesia was induced and maintained using isoflurane (Henry Schein Animal Health) inhalation. Prior to each procedure, all animals were given a subcutaneous injection of sustained-release buprenorphine (ZooPharm) for analgesia. Briefly, an anterolateral skin incision was made in the thigh followed by blunt dissection to separate the overlaying muscles to reach the femur bone. Limited extension of this muscle window allowed for placement of a radiolucent polysulfone fixation plate for internal stabilization. Critically-sized 8 mm defects were created in the mid-diaphysis of the femur using an oscillating saw. For the acutely-treated

animals, a poly-caprolactone (PCL, Sigma Aldrich) nanofiber mesh was carefully placed around the newly exposed bone ends and alginate loaded with BMP-2 was delivered via syringe injection through the mesh perforations. Subsequently the muscle and skin were closed using 4-0 vicryl suture and wound clips, respectively. In contrast, for the animals receiving delayed treatment, the bone defects were initially left empty (no treatment) and the muscle and skin were closed. At 8 weeks, a second procedure was performed on these animals where the original incision was re-opened to expose the fixation plate and femur. An oscillating saw was used to remove any mineralized end capping of the defects and any soft tissue ingrowth within the defect space was cleared to allow for placement of the PCL nanofiber mesh. Finally, alginate/BMP-2 was delivered and the muscle and skin were closed as before.

4.3.4 Radiography and micro-computed tomography

To qualitatively assess longitudinal bone regeneration, 2D in vivo digital radiographs were acquired with an MX-20 digital machine (Faxitron X-ray Corp) at 2, 4, 8, and 12 weeks post-treatment. Bridging scores were assigned to each radiograph by two blinded investigators where bridging was defined as continuous bone spanning the entire defect space (from bone end to bone end). In instances of disagreement, a third blinded investigator served as tiebreaker. Longitudinal bone formation was quantitatively evaluated using 3D micro-computed tomography (μCT) at 4, 8, and12 weeks post-treatment. In vivo scans of the harvested femora were performed before mechanical testing using the vivaCT40 (Scanco Medical) at a 38 μm voxel size, 55 kVp voltage, and a 145 μA current. A threshold corresponding to 50% of native cortical bone density was applied to segment bone mineral and identify newly regenerated bone, as established

previously [96]. The volume of interest (VOI) consisted of the central 5.89 mm (155 slices) of the 8 mm defect.

4.3.5 Biomechanical testing

Torsional testing to failure was performed as previously described [96]. Femurs were excised at 12 weeks post-surgery, wrapped in PBS-soaked gauze, and stored at -20°C until testing could be performed. On the day of testing, samples were thawed, the surrounding soft tissues were excised, and the femora were first μCT-scanned, as described above. Subsequently, the fixation plate was removed so that the native bone ends could be potted in Wood's metal (Alfa Aesar). The potted femurs were tested to failure in torsion at a rotation rate of 3° per second using the EnduraTEC ELF3200 axial/torsion testing system (Bose). Failure strength was determined by locating the peak torque within the first 60° of rotation. Torsional stiffness was calculated by finding the slope of the linear region before failure in the torque-rotation plot.

4.3.6 Histological analyses

A representative sample from each treatment group was harvested post-mechanical testing and fixed in 10% neutral buffered formalin at room temperature for 48 hours. Samples were then switched to PBS and sent to HistoTox Labs (Boulder, CO) for decalcification, processing, and Hematoxylin and Eosin (H&E) and Safranin-O staining.

4.3.7 Serum and spleen collection

Blood was collected by cardiac stick (~3ml per sample) at 20 weeks and into serum collection tubes (Thermo Fisher Scientific) and allowed to clot at room

temperature for 30 minutes before storage at 4°C overnight. The following day, all tubes were centrifuged at 1500g for 10 min and the yellow (straw) serum was collected and stored at -20°C. Spleens harvested at 20 weeks were minced and frozen in cryopreservation media (80% FBS, 20% DMSO) at -80°C overnight before being transferred to a liquid nitrogen dewar for storage.

4.3.8 Multivariate analysis of serum cytokines

Serum collected at 20 weeks were analyzed for cytokines via Luminex multiplex array (Millipore). Partial least squares discriminant analysis (PLSDA) was conducted in MATLAB (Mathworks) using the partial least squares algorithm by Cleiton Nunes (available on the Mathworks File Exchange). All multiplexed signaling data were z-scored, and then used as the independent inputs to the algorithm. An orthogonal rotation in the LV1-LV2 plane was used to choose a new LV1 that best separated responders and non-responders.

4.3.9 Characterization of immune cells by flow cytometry

Cryopreserved spleens were thawed and digested in 2 ml Opti-MEM I reduced serum medium (Thermo Fisher Scientific) with 2 mg/ml collagenase B (Sigma Aldrich) for an hour at room temperature. The digested tissues were then passed through 40 μm cell strainers (Thermo Fisher Scientific) and centrifuged at 500g for 5 minutes. Red blood cells were removed by brief incubation in RBC lysis buffer (eBioscience) and the remaining cells were resuspended in RPMI-1640 media (Sigma Aldrich) for antibody staining. Cells were stained for CD3, CD4, CD8, FoxP3, His48, CD11b, His36, and B220 using manufacturer's recommended protocols, and all samples were then run through an

Accuri C6 flow cytometer (BD Biosciences). All data were exported for analysis in FlowJo software.

4.3.10 Statistical analyses and power calculation

All data are reported as mean ± standard error of the mean. Significance was determined by t-test or analysis of variance (ANOVA) as appropriate, with multiple comparisons made by Tukey's post-hoc test. Significance was determined by a p-value < 0.05. All statistical calculations were performed using GraphPad Prism 7 software. Sample sizes were determined by performing a power analysis in G*Power software based on bone volume and maximum torque results obtained from previous studies. These power calculations, along with historical data using this segmental bone defect rat model, suggest a sample size of 7-8 is sufficient to give statistical differences between groups.

4.4 Results

4.4.1 Qualitative and quantitative evaluation of new bone formation

Radiographs at 12 weeks post-treatment demonstrated clear differences between acute and delayed treatment (Figure 10). All acute 2μg treated defects achieved radiographic bridging while only 50% of delayed 2μg and 75% of delayed 5μg treated defects did so.

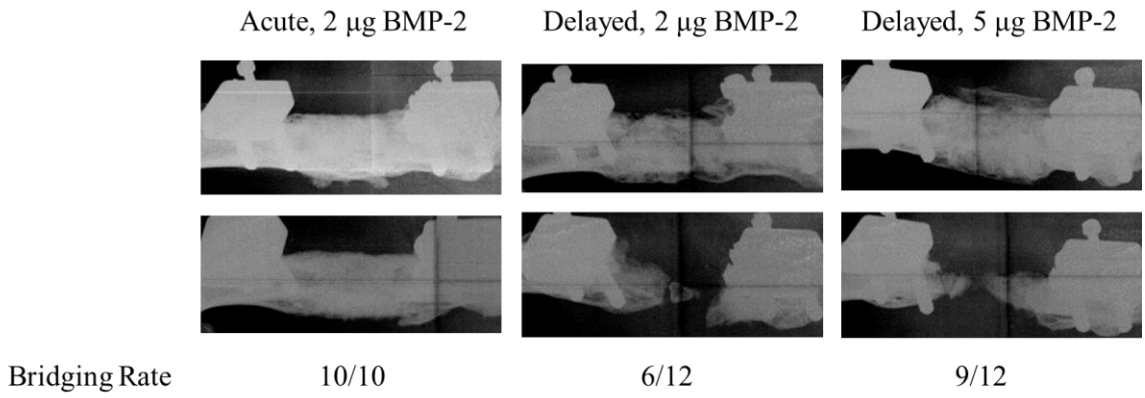

Figure 10 - Radiographic evaluation of regenerated femurs at 12 weeks post-treatment. Two representative radiographs from each treatment group demonstrate much more variability in bone formation with delayed treatment. This is reflected in the bridging scores for each group as 100%, 50%, and 75% of defects were bridged by 12 weeks post-treatment for acute 2 μg, delayed 2 μg, and delayed 5 μg treatment groups, respectively.

These qualitative observations were supported by μCT quantification of new bone formation. The acutely-treated defects had significantly more bone formation at weeks 4, 8, and 12 compared to both delayed treatment groups (Figure 11A). There were no observed differences in bone mineral density between any treatment groups (Figure 11B).

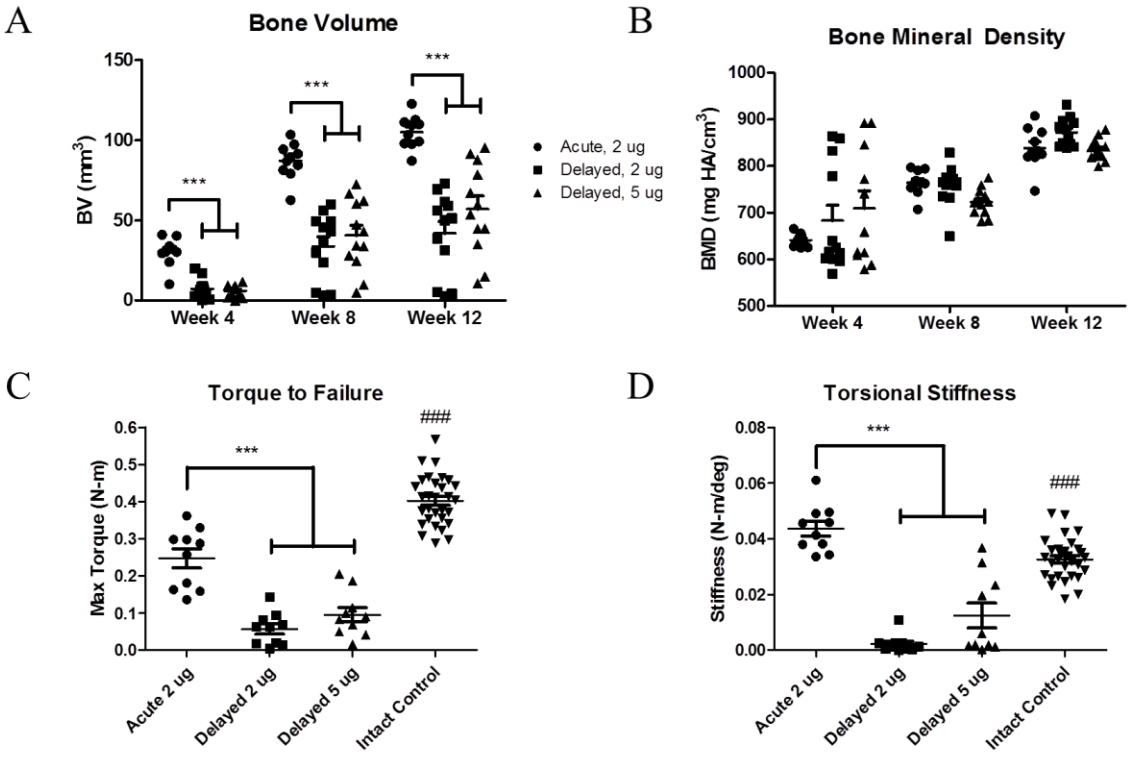

Figure 11 - Quantitative microCT and biomechanical assessment of regenerated bone defects. Acute treatment with 2 μg BMP-2 yielded more bone formation at all time points compared to delayed treatment, at both 2 and 5 μg (A). There were no observed differences in bone mineral densities (B). Acutely-treated defects also demonstrated higher max torque (C) and torsional stiffness (D) compared to both delayed treatment groups at week 12 post-treatment. However, acute treatment resulted in decreased max torque and increased torsional stiffness compared to intact control femurs. ***$p<0.001$ as indicated, ###$p<0.001$ vs. all other treatment groups, n=10-12/ treatment groups, n=30 for intact control group.

4.4.2 Measurement of bone biomechanics

Functional assessment of the newly regenerated bone by mechanical testing revealed similar findings to μCT. The femurs that received acute treatment demonstrated greater torque to failure (Figure 11C) and higher torsional stiffness (Figure 11D) compared to both delayed treatment groups. All treated groups had significantly lower

torque to failure compared to intact control femurs at 12 weeks post-treatment. However, the acutely-treated defects were significantly stiffer than intact controls at this time point.

4.4.3 Histological characterization

H&E staining (Figure 12, top row) revealed several interesting morphological differences. Acute treatment resulted in many larger areas of new bone formation throughout the defect space, while delayed treatment (at both 2 and 5μg BMP-2 doses) resulted in smaller pockets of new bone. Furthermore, H&E also suggested minimal presence of chondrocytes in acutely-treated defects at 12 weeks post-treatment, whereas chondrocytes were more apparent in the delayed treated samples, particularly the delayed 2μg group. These areas of cartilage formation were confirmed by Saf-O staining (Figure 12, bottom row). Interestingly, Saf-O staining also revealed qualitatively more alginate remaining in the defect with acute treatment, and these alginate fragments were primarily adjacent to the large areas of new bone formation.

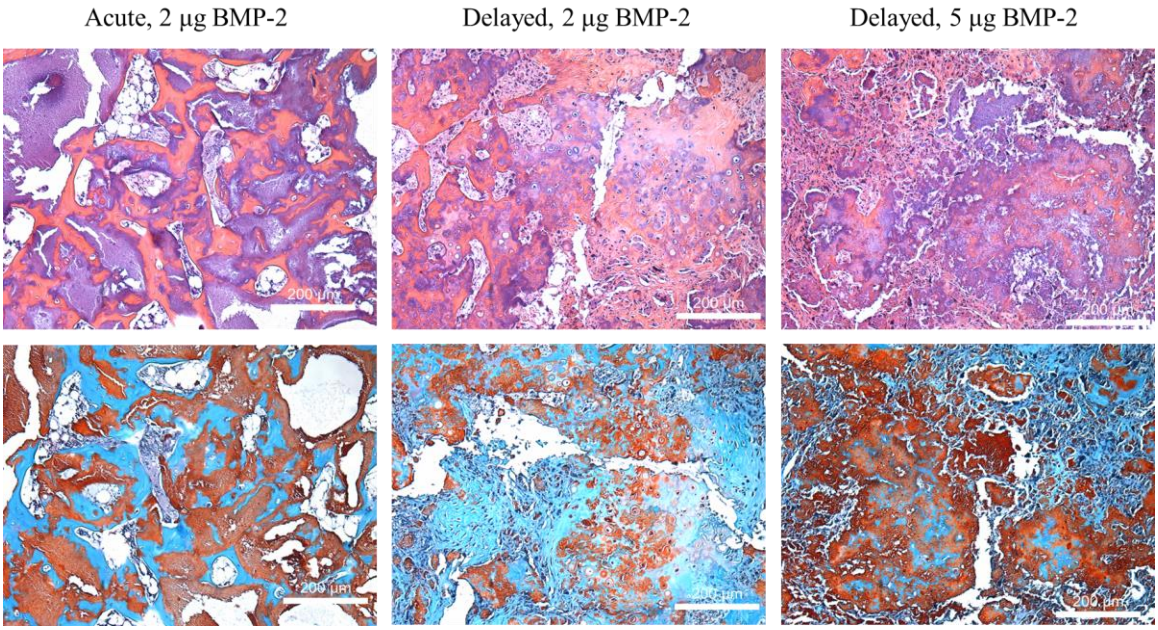

Figure 12 - Bone defect histomorphometry at 12 weeks post-treatment. Representative hematoxylin and eosin staining (top row) revealed more widespread and larger areas of new bone formation with acute treatment compared to either delayed treatment group. Safranin-O staining indicated greater presence of chondrocytes still remaining within the defect space for delayed treatment, particularly at the 2 µg BMP-2 dose.

4.4.4 Serum cytokine analyses

At 12 weeks post-treatment, serum was collected for all samples that received delayed treatment and subsequently analyzed across a panel of inflammatory cytokines (Figure 13).

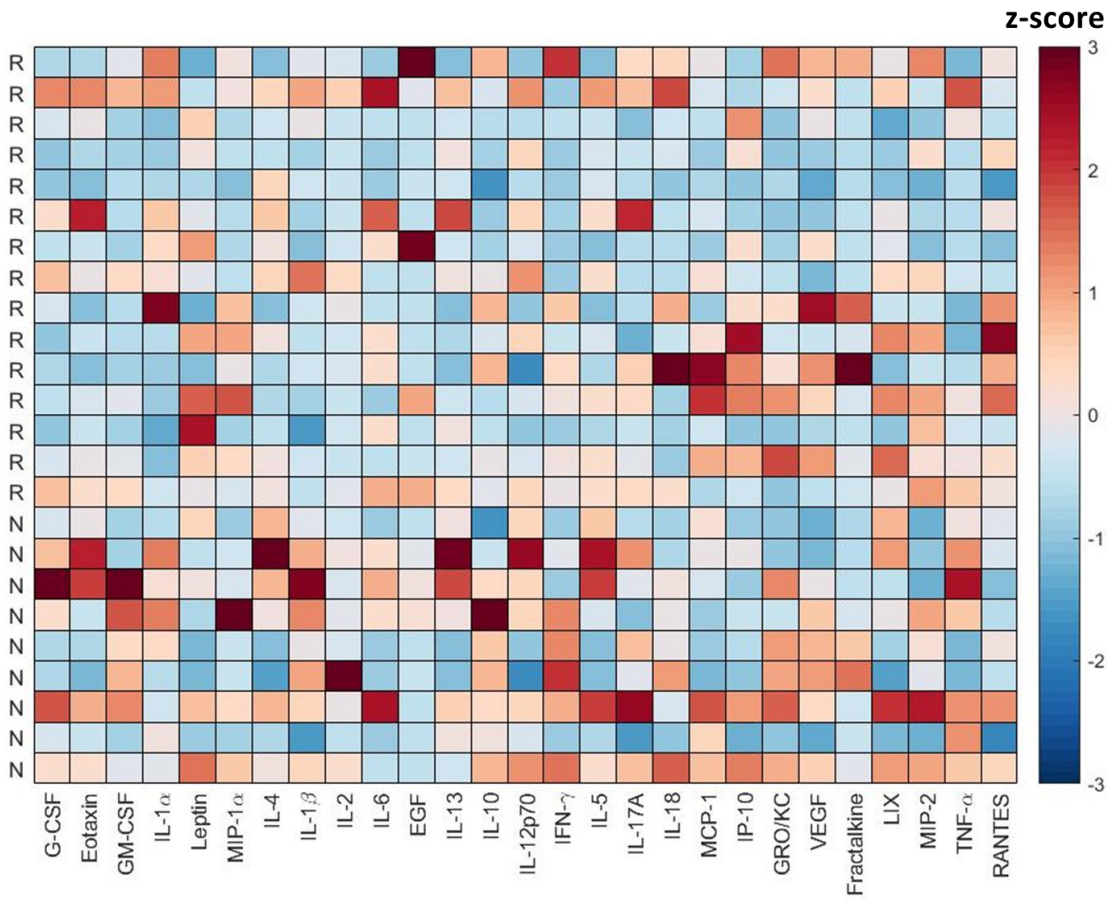

Figure 13 - Heatmap of serum cytokine expression for delayed treatment samples. Serum cytokine expression at 12 weeks post-treatment was quantified via multiplex array. For these analyses, delayed treatment groups were pooled and then separated into responders (R) and non-responders (N) according to whether the defects exhibited bridging by 12 weeks post-treatment.

Partial least squares regression showed distinct separation along LV1 based on responder or non-responder status, i.e. whether or not the defect was successfully bridged, irrespective of BMP-2 dose (Figure 14A). Overall, non-responders were correlated with much higher expression of inflammatory cytokines (IL-1β, GM-CSF, IFNɣ, and TNFα) as well as anti-inflammatory cytokines (IL-2 and IL-10) (Figure 14B).

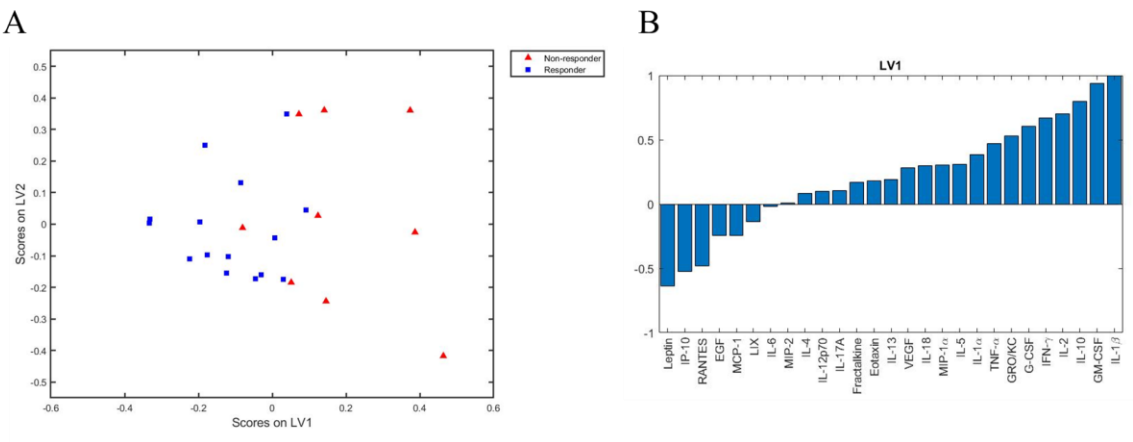

Figure 14 - Partial least squares regression (PLSR) analysis of serum cytokine expression. Regression analysis revealed separation using latent variable 1 (LV1), correlating cytokine profile at 12 weeks post-treatment with responder/non-responder status (A). LV1 composition indicated non-responders were positively correlated with higher expression of many inflammatory and anti-inflammatory cytokines, including IL-1β, GM-CSF, and IL-10 (B).

These computational model results were further supported by direct comparison of responders and non-responders using t-test. These statistical analyses revealed that non-responders had significantly higher levels of TNFα and IL-1β in serum at 12 weeks post-treatment (Figure 15). No significant differences were observed based on BMP-2 dose (not shown).

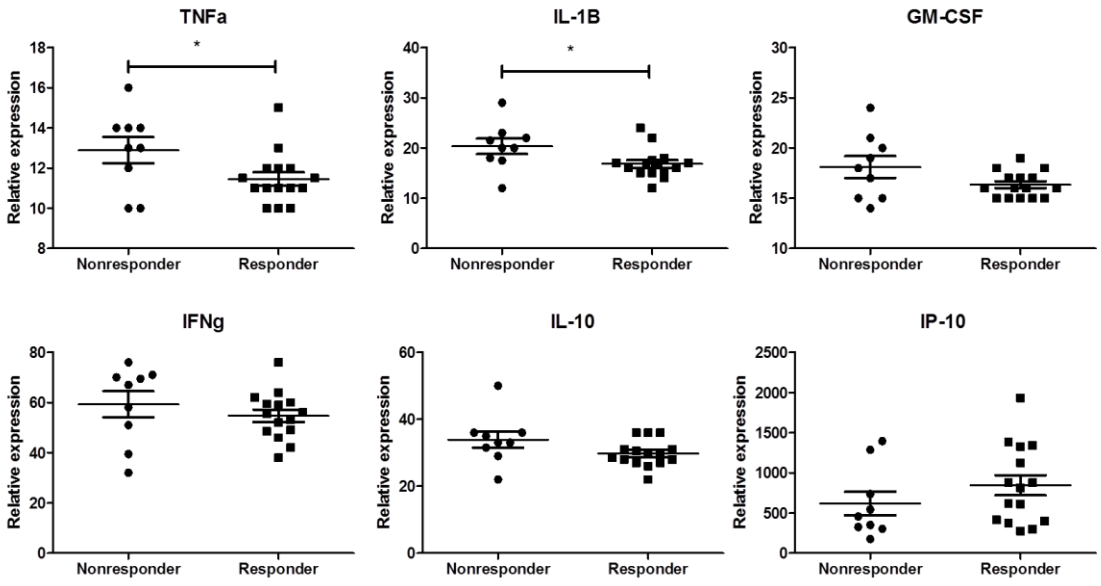

Figure 15 - Select serum cytokine differences between non-responders and responders. Non-responders demonstrated elevated expression of inflammatory cytokines TNFα and IL-1β in serum compared to responders at 12 weeks post-treatment. No significant differences were observed in any other cytokines tested. *$p<0.05$ as indicated, n=9-15/group

4.5 Discussion

The pathophysiology of nonunion remains poorly understood. While some causes have been identified and are fairly easy to identify and correct such as improper mechanical fixation, most others including infection, poor vascularization, and presence of other co-morbidities are much harder to address and the optimal interventions for these cases are unclear [22, 117, 118]. From a basic science perspective, development of reproducible animal models to study impaired bone healing has been difficult, particularly if deliberate mechanical instability is not the main driving force of nonunion [119].

Here, we utilized a critically-sized femoral defect in rats to establish a model of chronic nonunion by delaying treatment with BMP-2 until after nonunion has been established. We found that delayed treatment results in impaired bone regeneration compared to acute treatment. Interestingly, this deficit in healing was not easily overcome with an increase in BMP-2 dose, as the acute 2 μg BMP-2 group still formed significantly more bone and had mechanically stronger regenerated femurs compared to the delayed 5 μg BMP-2 group. These results suggest that the healing environment of a regenerating bone may be substantially altered during the progression and even after nonunion has been established. This has been partially investigated clinically, as recent work analyzing human fracture biopsies demonstrated changes in the local expression of BMP and BMP inhibitors, and the relative proportion of these factors was indicative of subsequent healing outcome [120]. These findings were supported by another group that also investigated fracture callus and nonunion tissues, and observed differences in BMP and BMP inhibitor expression in the chondrocytes present in the tissues [121]. In addition, elevated levels of certain matrix remodeling proteins, specifically MMP-7 and MMP-12, has also been implicated in fracture nonunion in humans and these proteins were shown to actively bind and degrade BMP-2 *in vitro* [122].

While not directly assessed in this study, it is likely that the reparative capacity of local stem and osteoprogenitor cells are greatly diminished after nonunion. Indeed, recent work by Bajada et al. demonstrated that stromal cells isolated from human fracture nonunions exhibited reduced osteogenic and mineral-forming capacity as well as increased senescence compared to control bone marrow mesenchymal stromal cells [123]. Multiple other groups have also shown that proliferation of stem cells as well as

osteoblasts is impaired during nonunion [124, 125]. Taken together, it appears that osteogenesis is impaired during nonunion due to a reduction in the progenitor cells available at the site of injury and diminished ability of these cells that are present to differentiate into osteoblasts and produce new mineral.

The Safranin-O staining showed greater presence of chondrocytes within the defect space for the delayed treatment group at 12 weeks post-treatment compared to the same time point for acutely-treated animals. This indicates perhaps an alteration in the normal endochondral ossification healing process, whereby treatment after nonunion induces a delayed or prolonged period of cartilage deposition that subsequently further delays the onset of mineralization. This could be verified in future studies by histological characterization at multiple time points during healing.

Serum proteomics analysis using partial least squares regression at week 20 for the delayed treatment samples revealed non-responders were correlated with increased expression of many inflammatory factors. These long-term results are suggestive of a chronically dysregulated immune response in the animals that exhibited the worst healing responses. Others have described similar findings clinically in response to trauma [48, 50, 54]. Vanzant et al. observed an increase in inflammatory gene expression with patients that experienced a complicated recovery (>14 days) compared to those that had a relatively uncomplicated recovery (<5 days) from multiple organ injury [55].

A limitation of the immune characterization work performed in this study was that only a single terminal time point (20 weeks) was analyzed. At this late time point, we found no significant differences in the spleen immune cell populations (Figure 16). It is

possible the bone injury alone in this model is not traumatic enough to cause severe immune dysfunction that persists for 20 weeks (12 weeks post-treatment). In fact, recent work in a burn injury model demonstrated that splenic inflammatory monocyte populations were only increased through 8 days postburn [126]. Only in a severe model of sepsis has widespread splenic alterations been observed beyond 14 days [127]. Apart from spleen characterization, immune cell profiling of a more proximal target to the femur, such as the inguinal lymph nodes, bone marrow, and even the surrounding quadriceps muscle may have been more informative.

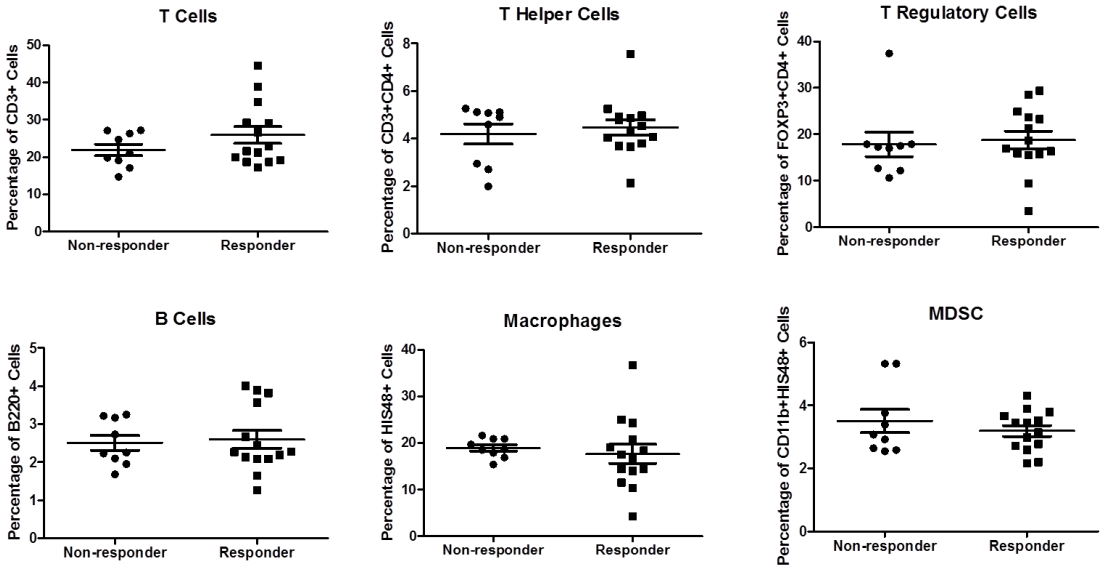

Figure 16 - Flow cytometry analysis of spleen for immune cells. No differences were observed in any spleen immune cell populations between non-responders and responders at 12 weeks post-treatment. n=8-12/group

More work is needed to validate long-term immune dysregulation in this model of chronic nonunion. Longitudinal immune characterization at multiple time points post-treatment would help elucidate the progression of immune dysfunction and perhaps reveal time points for early intervention. Moreover, these results could potentially

motivate new approaches for the clinical treatment of nonunion, such as additional treatment with some type of immunomodulatory therapy prior or in conjunction with a bone-healing therapy to improve patient outcomes.

In conclusion, the study presented here established a chronic nonunion model involving delayed treatment to critical size femoral defects in rats. Our results qualitatively and quantitatively demonstrated impaired healing compared to acute treatment, and this impairment could not be overcome with a modest increase in BMP-2 dose. Interestingly, we found evidence of possible long-term immune dysregulation in the rats that received delayed treatment, as the worst responders in that cohort were associated with higher circulating levels of inflammatory cytokines, including TNFα and IL-1β. These results suggest that the long-term systemic immune response may be indicative of bone healing outcome, which consequently motivates more in-depth investigation into the role of immune homeostasis on bone regeneration.

CHAPTER 5. IMMUNE DYSREGULATION FOLLOWING TREATMENT OF ESTABLISHED NONUNION

5.1 Abstract

Severe traumatic injuries involving extremities are quite prevalent in both military and civilian patients. These types of injuries are often associated with poor outcomes, including greater risk of complications, requiring multiple surgical procedures and longer hospital stays, and can result in long-term functional deficits that severely impact patient quality of life. Recent work has implicated immune dysregulation as an important risk factor following trauma. Failure to fully resolve inflammation following injury can eventually lead to chronic immune suppression that makes the patient much more vulnerable to opportunistic pathogens and even multiple organ dysfunction. Some of the main drivers of systemic immune suppression are immune suppressor cells, such as T regulatory cells and myeloid-derived suppressor cells (MDSCs). However to-date, very little is known about whether long-term immune suppression develops following bone injury, particularly in cases of poor healing such as nonunion, and how immune suppressor cells impact bone formation.

The objective of this study was to elucidate whether long-term immune dysfunction develops during the progression and treatment of nonunion. Using a previously established femoral bone defect model of non-union in rats, we characterized the systemic and local immune profiles of animals through 20 weeks following acute or delayed treatment with BMP-2. We found that delayed treatment results in an altered

early local inflammatory response at 2 weeks post-treatment, and is correlated with lower expression of inflammatory mediators such as IL-4, MIP-1α, and IL-18 in the early defect. Furthermore, longitudinal systemic analyses of blood revealed that bone formation is strongly correlated with cytokines IL-6, LIX, and IL-13 and negatively correlated with IP-10. Interestingly, bone formation was also significantly negatively correlated with circulating MDSCs, as early as 1 and 2 weeks post-treatment. MDSC levels were also elevated in bone marrow at 20 weeks for delayed treatment compared to acute treatment. These results suggest that long-term immune dysregulation does play a role in nonunion, and that increased presence of MDSCs both systemically and locally may be predictive of poor bone healing outcomes.

5.2 Introduction

Musculoskeletal trauma involving extremities is quite common, occurring in up to 71% of battlefield [128] and 59% of civilian injuries [129]. Recent studies have identified a dysregulated immune response, including chronic immunosuppression and immune paralysis, as an important cause of morbidity following severe trauma [47-49]. It has been hypothesized that trauma-induced immune dysfunction occurs roughly in two stages. The first stage encompasses a systemic inflammatory response syndrome (SIRS), characterized by acute hyper-inflammation with overproduction of pro-inflammatory cytokines (IL-1, IL-6, TNFα), countered by a compensatory anti-inflammatory response syndrome (CARS) with increased expression of anti-inflammatory cytokines (IL-1Ra, IL-10, TGFβ) [50]. CARS follows almost immediately after SIRS is initiated, as prolonged exposure to the high levels of inflammatory factors and reactive oxygen species (ROS) generated during SIRS is damaging to the surrounding tissues and can lead to multiple

organ dysfunction syndrome (MODS) if left unchecked [44, 51]. In most cases of uncomplicated healing, the SIRS and CARS responses eventually resolve one another and systemic immune homeostasis is restored within a couple weeks. Failure to achieve this balance can lead to a genomic storm of elevated pro- and anti-inflammatory signals that lasts up to 28 days post-injury [52], and will eventually result in a second stage called persistent inflammation, immunosuppression, and catabolism syndrome (PICS) [53]. PICS is often characterized by chronic low level inflammation combined with long term systemic immune suppression. Patients exhibiting symptoms of PICS are more prone to opportunistic infections, sepsis, MODS, and often require multiple surgical interventions and hospitalizations, which incur greater long-term healthcare costs for the patient [53-55].

Some of the primary cellular mediators of long-term immune paralysis observed in PICS are the immune suppressor cell types, including T regulatory cells (Tregs) and myeloid-derived suppressor cells (MDSCs) [48, 49, 54]. These cells suppress immune function by secreting anti-inflammatory factors such as IL-1RA, IL-10, and TGFβ, which can inhibit activation of other immune effector cell types, such as in T cell anergy, or even reduce immune populations over time by promoting premature apoptosis of these cells [54, 57-59]. MDSCs are immature myeloid lineage cells that originate in the bone marrow, separate from other myeloid immune cells such as macrophages, granulocytes, and dendritic cells [70]. While generally thought to be heterogeneous in nature, MDSCs are most commonly identified in rats as expressing both neutrophil (His48) and monocyte (CD11b) markers [71, 72]. These cells can directly suppress T cell function through depletion of the amino acid L-arginine [73], which is a critical mediator of T cell

metabolism and activity [74], as well as through promotion of nitric-oxide-mediated T cell apoptosis [71]. Others have shown that MDSCs are also involved in TGFβ1-mediated suppression of natural killer cells [75] and can possibly enhance T regulatory cell survival [76]. In humans, circulating MDSCs have been observed to persist at high levels up to 28 days in severely septic patients, and were linked to adverse outcomes and prolonged ICU stays [59]. However, the influence of MDSCs following bone injuries, particularly in cases of poor healing such as nonunion, remains unclear.

Herein, we utilized a previously established femoral bone defect model of chronic nonunion in rats to investigate potential immune dysregulation. In this model, treatment with BMP-2 is delivered 8 weeks after initial creation of the bone defect (delayed treatment), which is the time needed historically to see obvious radiographic evidence of nonunion establishment (mineralized capping of bone ends). Acute treatment (i.e. treatment delivered immediately following defect creation) was also investigated and represented an example of a relatively uncomplicated bone healing scenario. We hypothesized that delayed treatment would result in poor bone healing compared to acute treatment and furthermore, this impairment could be linked to chronic immune dysregulation involving MDSCs. First, the early healing environment was assessed through cytokine analysis of local bone defect tissue at 10 weeks, 2 weeks post-treatment. Next, a longitudinal study involving blood collection at weeks 0, 1, 2, 4, 8, 10, 12, 16, and 20 was performed to assess the systemic immune response over time. Blood collected at each time point was analyzed for multiple immune cell populations by flow cytometry as well for serum cytokines through multiplex array. These results were evaluated with

respect to bone healing, which was quantified by micro-computed tomography (μCT) at weeks 14 and 20 and biomechanical testing at week 20.

5.3 Materials and Methods

5.3.1 Animals

For these studies, 13-week-old female SASCO Sprague Dawley rats (Charles River Laboratories, Inc.) were used. Rats were pair housed in individually ventilated caging (Tecniplast) with a tunnel and gnawing blocks (Bio-Serv) for enrichment. Bedding was a mixture of corn cob and processed paper. Purina Mills International #5001 was fed ad libitum. Filtered tap water treated with ultraviolet light was provided ad libitum in bottles. Sentinel results from Charles River Laboratories International Rat Prevalent PRIA testing were negative for all pathogens in the housing room. All animals were allowed to acclimate for at least 2 weeks before any procedures were performed. Following each procedure, a divider was temporarily placed in the cage for better monitoring of post-operative recovery. Animals were randomly allocated to treatment groups.

5.3.2 Alginate BMP-2 preparation

RGD-functionalized alginate (FMC BioPolymer) was reconstituted in MEM alpha (Thermo Fisher Scientific) to create a 2% w/v solution, as described previously [98]. Recombinant human bone morphogenetic protein 2 (BMP-2, Pfizer Inc.) was reconstituted in a solution of 0.1% rat serum albumin (Sigma Aldrich) in 4 mM hydrochloric acid and mixed with the alginate solution to yield 2 μg BMP-2 per 150 μl of

final solution. This alginate/BMP-2 solution was gelled with the addition of calcium sulfate (Sigma Aldrich) at a 1:25 volume ratio. Hydrogels were prepared under sterile conditions inside a laminar flow hood and stored overnight at 4°C before use in surgery the next day.

5.3.3 Surgical procedures

All surgical procedures were approved by the Georgia Institute of Technology Institutional Animal Care and Use Committee. Anesthesia was induced and maintained using isoflurane (Henry Schein Animal Health) inhalation. Prior to each procedure, all animals were given a subcutaneous injection of sustained-release buprenorphine (ZooPharm) for analgesia. Briefly, an anterolateral skin incision was made in the thigh followed by blunt dissection to separate the overlaying muscles to reach the femur bone. Limited extension of this muscle window allowed for placement of a radiolucent polysulfone fixation plate for internal stabilization. Critically-sized 8 mm defects were created in the mid-diaphysis of the femur using an oscillating saw. For the acutely-treated animals, a poly-caprolactone (PCL, Sigma Aldrich) nanofiber mesh was carefully placed around the newly exposed bone ends and alginate loaded with BMP-2 was delivered via syringe injection through the mesh perforations. Subsequently the muscle and skin were closed using 4-0 vicryl suture and wound clips, respectively. In contrast, for the animals receiving delayed treatment, the bone defects were initially left empty (no treatment) and the muscle and skin were closed. At 8 weeks, a second procedure was performed on these animals where the original incision was re-opened to expose the fixation plate and femur. An oscillating saw was used to remove any mineralized end capping of the defects and any soft tissue ingrowth within the defect space was cleared to allow for placement of the

PCL nanofiber mesh. Finally, alginate/BMP-2 was delivered and the muscle and skin were closed as before.

5.3.4 Radiography and micro-computed tomography

To qualitatively assess longitudinal bone regeneration, 2D in vivo digital radiographs were acquired with an MX-20 digital machine (Faxitron X-ray Corp) at 2, 4, 8, and 12 weeks post-treatment. Bridging scores were assigned to each radiograph by two blinded investigators where bridging was defined as continuous bone spanning the entire defect space (from bone end to bone end). In instances of disagreement, a third blinded investigator served as tiebreaker. Longitudinal bone formation was quantitatively evaluated using 3D micro-computed tomography (μCT) at 4, 8, and12 weeks post-treatment. In vivo scans of the harvested femora were performed before mechanical testing using the vivaCT40 (Scanco Medical) at a 38 μm voxel size, 55 kVp voltage, and a 145 μA current. A threshold corresponding to 50% of native cortical bone density was applied to segment bone mineral and identify newly regenerated bone, as established previously [96]. The volume of interest (VOI) consisted of the central 6.46 mm (170 slices) of the 8 mm defect.

5.3.5 Biomechanical testing

Torsional testing to failure was performed as previously described [96]. Femurs were excised at week 20 (12 weeks post-treatment), wrapped in PBS-soaked gauze, and stored at -20°C until testing could be performed. On the day of testing, samples were thawed, the surrounding soft tissues were excised, and the femora were first μCT-scanned, as described above. Subsequently, the fixation plate was removed so that the

native bone ends could be potted in Wood's metal (Alfa Aesar). The potted femurs were tested to failure in torsion at a rotation rate of 3° per second using the EnduraTEC ELF3200 axial/torsion testing system (Bose). Failure strength was determined by locating the peak torque within the first 60° of rotation. Torsional stiffness was calculated by finding the slope of the linear region before failure in the torque-rotation plot.

5.3.6 Serum and tissue collection

Blood was collected longitudinally via the rat tail vein at 0 (baseline), 1, 2, 4, 8, 9, 10, 12, 16, and 20 weeks into two fractions: one for whole blood and the other for serum in the appropriate microvette collection tubes (Kent Scientific). For serum isolation, tubes were allowed to clot at room temperature for 30 minutes before storage at 4°C overnight. The following day, all serum tubes were centrifuged at 1500g for 10 min and the yellow (straw) serum was collected and stored at -20°C. The spleen, bone marrow from the left tibia, and muscle adjacent to the defect were all harvested at the endpoint (week 20). Red blood cells were lysed in all samples using 1X RBC Lysis Buffer (eBioscience) according to the manufacturer's instructions. Following lysis, cells were fixed using Cytofix fixation buffer (BD), resuspended in FACS buffer containing 1% fetal bovine serum (FBS) in 1X PBS, and stored at 4˚C until staining for flow cytometry.

5.3.7 Protein extraction for local defect tissue

Local defect tissue was harvested at week 10 (2 weeks post-treatment) and immediately snap frozen using liquid nitrogen. These tissue samples were then homogenized in RIPA lysis buffer (Thermo Fisher Scientific) that was supplemented with HALT protease inhibitor cocktail (Thermo Fisher Scientific) based on

manufacturer's recommended concentration. The homogenized samples were subsequently left on ice for at least 15 minutes before centrifugation at 13,000g for 15 minutes. The resulting supernatant was then collected and total protein concentration was determined using a Pierce BCA protein assay kit (Thermo Fisher Scientific). Finally, all protein isolates were snap frozen and stored at -80°C until cytokine analysis by Luminex.

5.3.8 Multivariate analysis of cytokines

Serum isolates collected at all time points and local defect protein extracts collected at 2 weeks post-treatment were analyzed for cytokines via Luminex multiplex array (Millipore). Partial least squares discriminant analysis (PLSDA) and partial least squares regression (PLSR) continuous analysis was conducted in MATLAB (Mathworks) using the partial least squares algorithm by Cleiton Nunes (available on the Mathworks File Exchange). All multiplexed signaling data were z-scored, and then used as the independent inputs to the algorithm. An orthogonal rotation in the LV1-LV2 plane was used to choose a new LV1 that best separated treatment groups.

5.3.9 Flow cytometry

Blood was collected longitudinally via the rat tail vein at weeks 0 (baseline), 1, 2, 4, 8, 9, 10, 12, 16, and 20 for flow cytometry analysis. The spleen, bone marrow from the ipsilateral tibia, and muscle adjacent to the defect were all harvested at the endpoint (week 20) and also analyzed by flow cytometry. Red blood cells were lysed in all samples using 1X RBC Lysis Buffer (eBioscience) according to the manufacturer's instructions. Following lysis, cells were fixed using Cytofix fixation buffer (BD), resuspended in FACS buffer containing 1% fetal bovine serum (FBS) in 1X PBS, and

stored at 4˚C until stained. Prior to staining, cells with Fc receptors were blocked with purified mouse anti-rat CD32 (BD) for 10 minutes at 4˚C to prevent non-specific binding. Cells were then stained for various immune cell populations, including $CD3^+$ T cells, $CD4^+$ T cells ($CD3^+CD4^+$), $CD8^+$ T cells ($CD3^+CD8^+$), T regulatory cells ($CD3^+CD4^+FoxP3^+$), myeloid-derived suppressor cells ($His48^+CD11b^+$), B cells ($B220^+$), mature tissue macrophages ($His36^+$), and monocytes ($CD68^+$, Bio-Rad) with specific anti-rat antibodies (eBioscience, unless otherwise noted). Sample data was collected using a BD Accuri C6 flow cytometer and analyzed using FlowJo software. Gates were positioned based on fluorescent minus one (FMO) controls with less than 1% noise allowed.

5.3.10 Statistical analyses and power calculation

All data are reported as mean ± standard error of the mean. Significance was determined by t-test or analysis of variance (ANOVA) as appropriate, with multiple comparisons made by Tukey's post-hoc test. Significance was determined by a p-value < 0.05. All statistical calculations were performed using GraphPad Prism 7 software. Sample sizes were determined by performing a power analysis in G*Power software based on bone volume and maximum torque results obtained from previous studies. These power calculations, along with historical data using this segmental bone defect rat model, suggest a sample size of 7-8 is sufficient to give statistical differences between groups.

5.4 Results

5.4.1 Early local bone defect characterization

Cytokine expression profiles were quantified using Luminex multiplex arrays. A heatmap overview of cytokine expression suggested distinct profiles between groups, particularly for intact control femurs compared to the other groups (Figure 17A). Direct comparison of expression levels by 1-way ANOVA revealed differences in several cytokines (Figure 17B). Most notably, untreated empty defects exhibited lower expression of epidermal growth factor (EGF) compared to delayed and acute treatment, while delayed treatment demonstrated lower expression of the anti-inflammatory cytokine IL-4 compared to both acute treatment and empty groups.

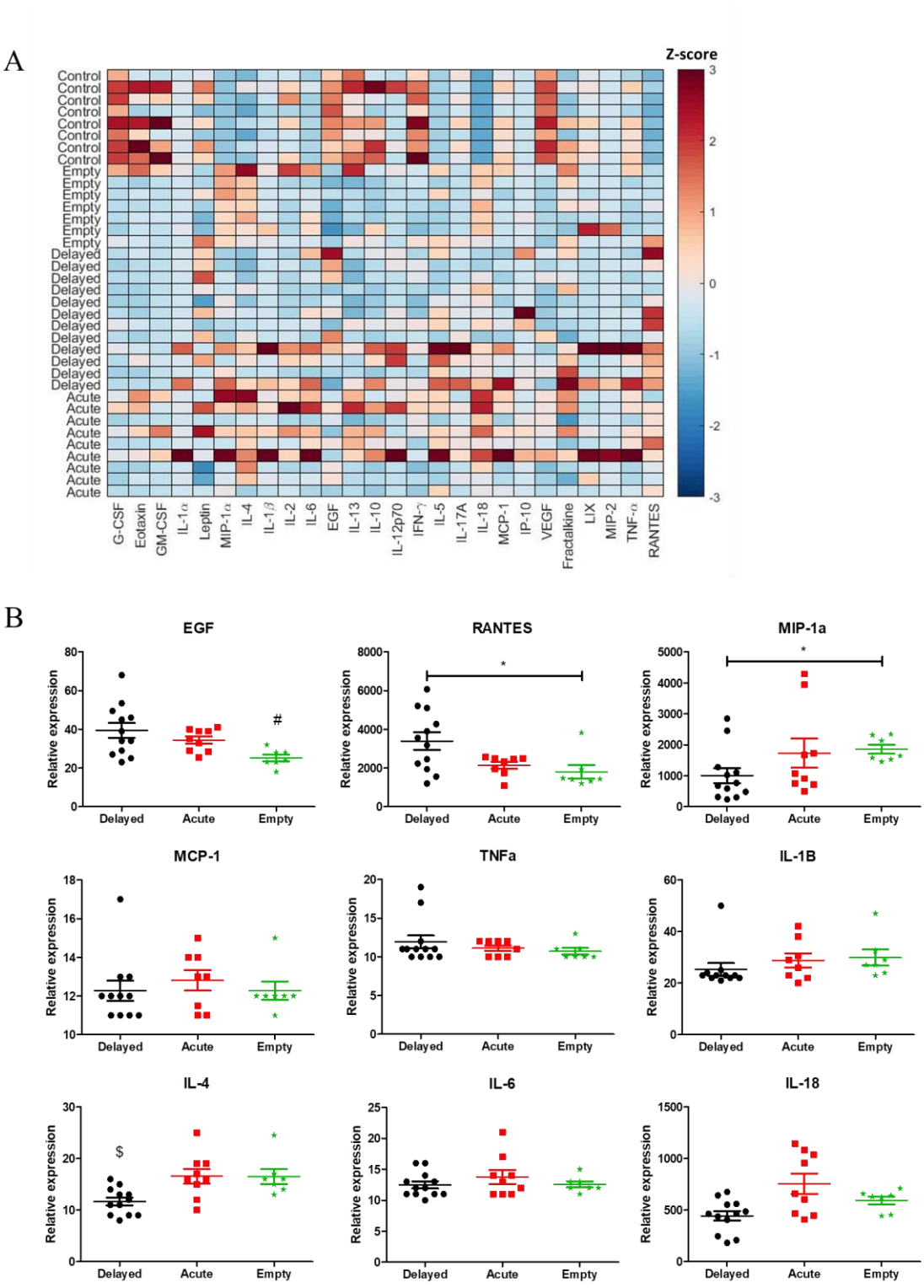

Figure 17 - Cytokine expression differences in local bone defect tissue at week 10. Cytokine expression profiles were quantified by multiplex array (A). Comparison of cytokine expression by 1-way ANOVA revealed several differences (B). Most notably,

the empty defect group demonstrated lower expression EGF compared to both delayed and acute treatment, while delayed treatment exhibited lower expression of the anti-inflammatory cytokine IL-4 compared to both acute treatment and empty. *$p<0.05$ as indicated, #$p<0.05$ vs Delayed and Acute, \$$p<0.05$ vs Acute and Empty, n = 7-12/group

To further evaluate the relationship between cytokine expression and healing response, a multivariate regression modelling approach was taken. Partial least squares discriminant analysis (PLSDA) of the regenerating bone defect tissue at 2 weeks post-treatment was able to separate treatment and control groups using model-generated latent variables (LV) (Figure 18A). LV1 demonstrated the greatest separation between delayed treatment and acute/empty treatment groups. The composition of LV1 indicates that delayed treatment is correlated with higher expression of EGF and RANTES and lower expression of anti- and pro-inflammatory cytokines IL-4, MIP-1α, IL-18 and IL-6 (Figure 18B). Intact control femurs were distinctly separated from all other groups using LV2. The composition of LV2 suggests that intact control samples were most highly correlated with expression of G-CSF, VEGF, and IFNγ, as well as most negatively correlated with expression of RANTES, IL-18, and MIP-1α (Figure 18B).

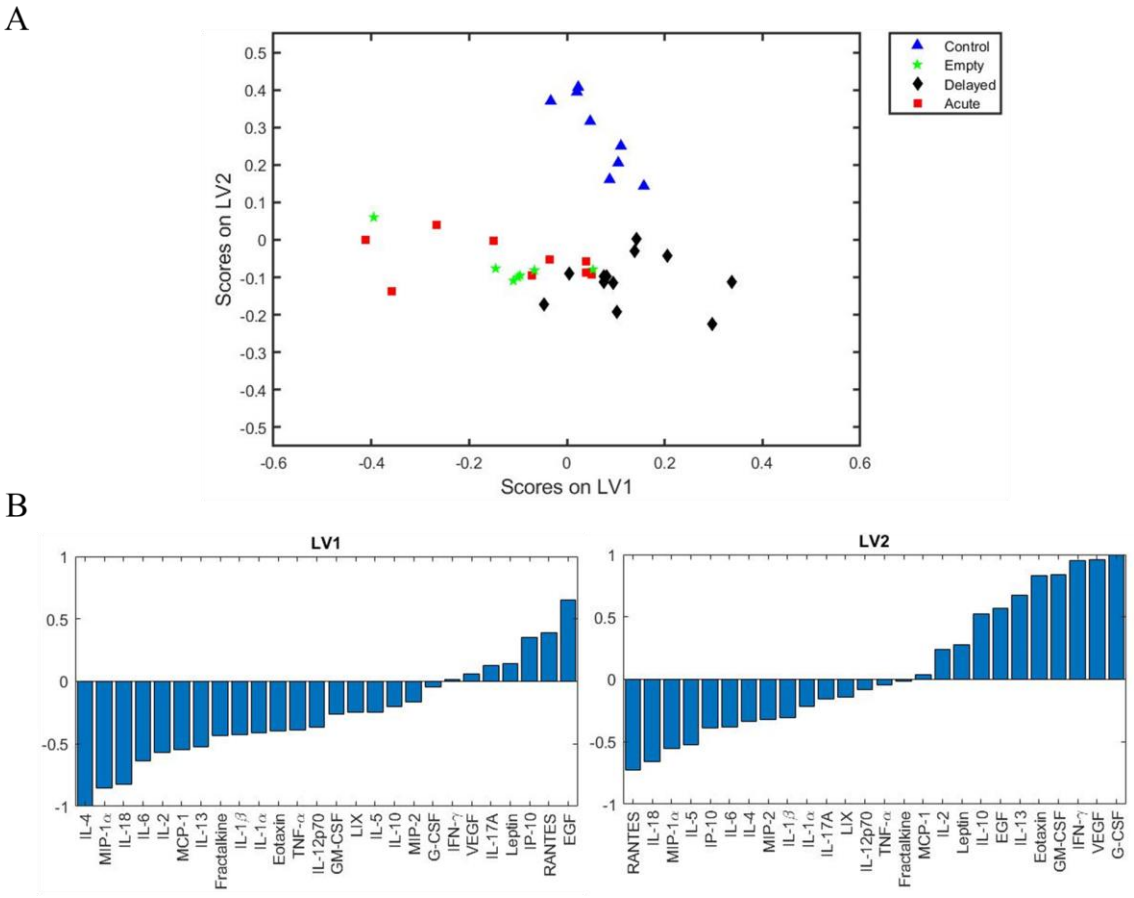

Figure 18 - Partial least squares discriminant analysis (PLSDA) of local bone defect cytokines. Computational regression analysis revealed separation between groups using latent variables (LV) (A). Cytokine composition and representation of their corresponding weights depict which cytokines are positively and negatively correlated with LV1 and LV2 (B).

5.4.2 Evaluation by μCT and biomechanical testing

Bone formation was quantified at weeks 14 and 20, corresponding to 6 and 12 weeks post-treatment, respectively. At both time points, acute treatment demonstrated higher bone volumes compared to delayed treatment (Figure 19A). No differences were observed in bone mineral density (Figure 19B). The biomechanical strengths of the

regenerated femurs were assessed at week 20 by torsion testing to failure. Bone defects given acute treatment exhibited increased max torque (Figure 19C) and torsional stiffness (Figure 19D) compared to delayed treatment. Interestingly, acute treatment samples demonstrated lower max torque but equivalent torsional stiffness when compared to intact control femurs.

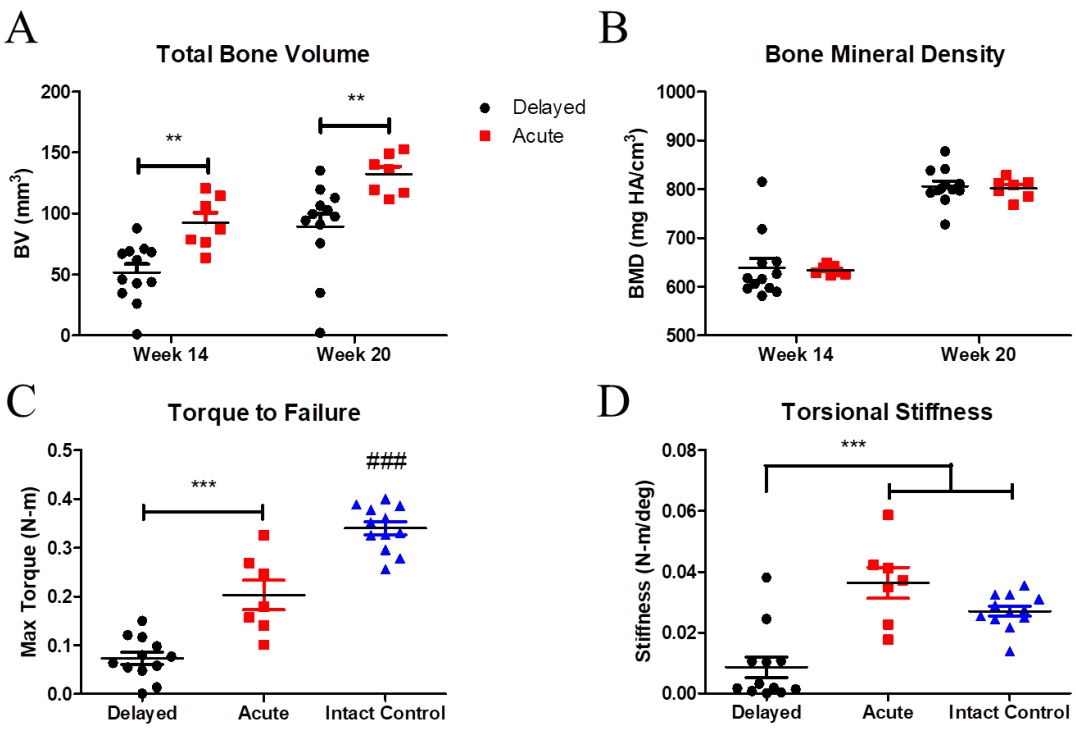

Figure 19 - MicroCT and biomechanical evaluation of regenerated femurs. Bone formation was assessed by μCT for total bone volume (A) and bone mineral density (B). Acutely-treated defects exhibited increased total bone volume at both weeks 14 and 20 compared to delayed treatment. No differences in bone mineral density were observed between treatment groups. The biomechanical strengths were determined at week 20 through torsional testing to failure. Acutely-treated defects demonstrated increased max torque (C) and torsional stiffness (D) compared to defects that received delayed treatment. **p<0.01, ***p<0.001 as indicated. ###p<0.001 vs Delayed and Acute. n=7-12/group

5.4.3 Longitudinal serum cytokine analyses

Serum collected at each time point was assessed for cytokine expression using multiplex array. As before, a multivariate regression analysis approach was taken to evaluate the relationship between cytokine profile and healing response. Here, partial least squares regression (PLSR) was performed and cytokine expression was correlated with a continuous variable (amount of bone formation at week 20) rather than correlation with a specific treatment group (delayed vs. acute). Using this approach, we observed very interesting separation using LV1 where this model-generated variable seems to match the continuum of healing responses quite well (Figure 20A). The cytokine composition of LV1 indicated that greater bone formation is positively correlated with certain inflammatory cytokines (IL-6, LIX, IL-13, RANTES) and negatively correlated with others (IP-10, IL-1β, IL-10) (Figure 20B).

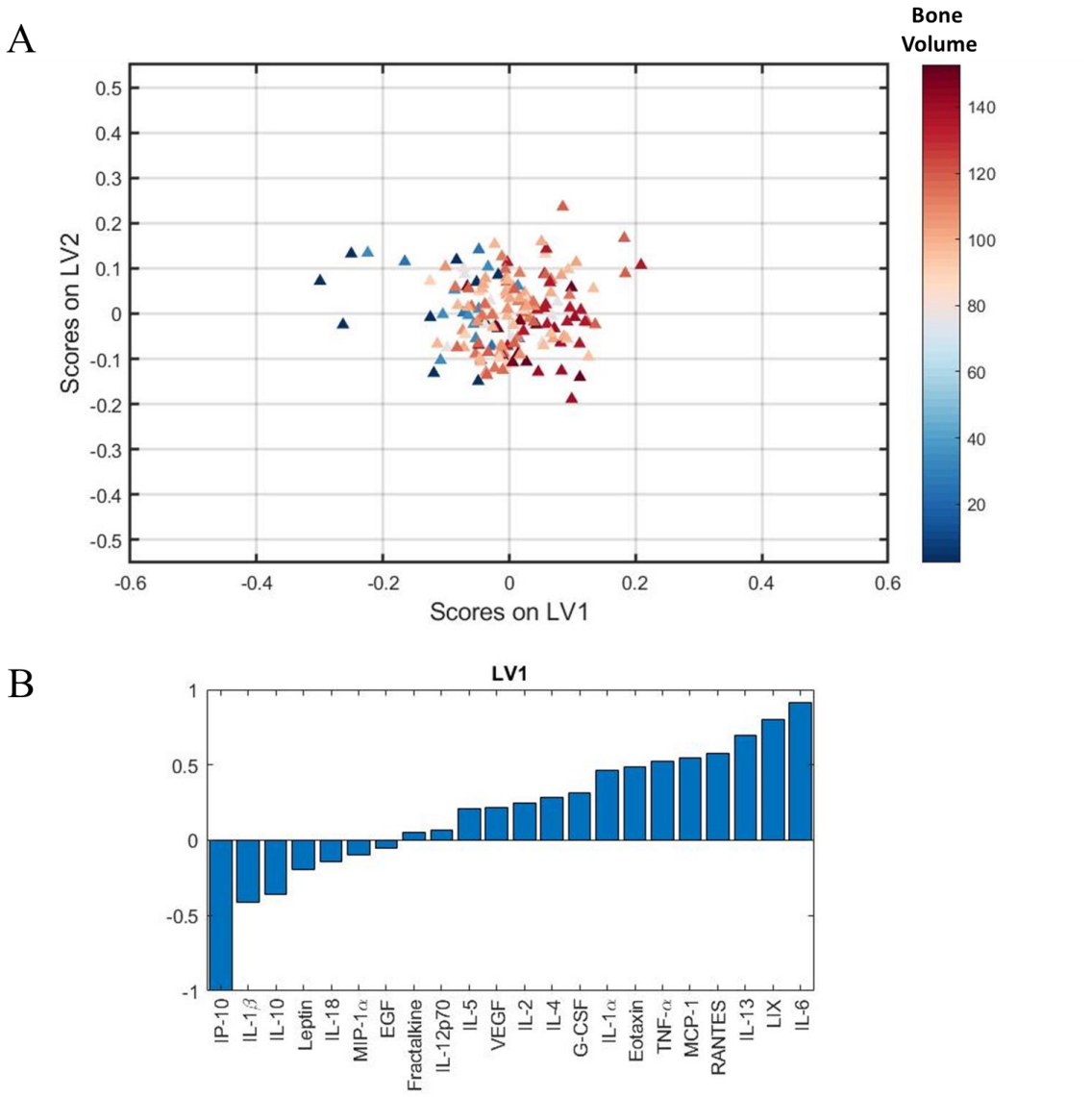

Figure 20 - Partial least squares regression (PLSR) analysis of serum cytokines. Computational regression of cytokine expression against bone formation at week 20 was able to delineate the continuum of healing responses using LV1 (A). The cytokine composition of LV1 suggests that greater bone formation is most strongly positively correlated with IL-6, LIX, IL-13, and RANTES, and most strongly negatively correlated with IP-10, IL-1β, and IL-10 (B).

5.4.4 Longitudinal circulating immune cell analyses

At the same time points that serum collection occurred, a separate fraction of whole blood was processed for evaluation of circulating immune cells by flow cytometry (Figure 21). No significant differences between delayed and acute treatment were observed in any of the immune cell populations at all of the time points tested. While not significant, CD3+ T cells and CD4+ T helper cells appeared elevated at weeks 12, 16, and 20 with acute treatment, whereas circulating MDSCs appeared elevated at weeks 12, 16, and 20 with delayed treatment.

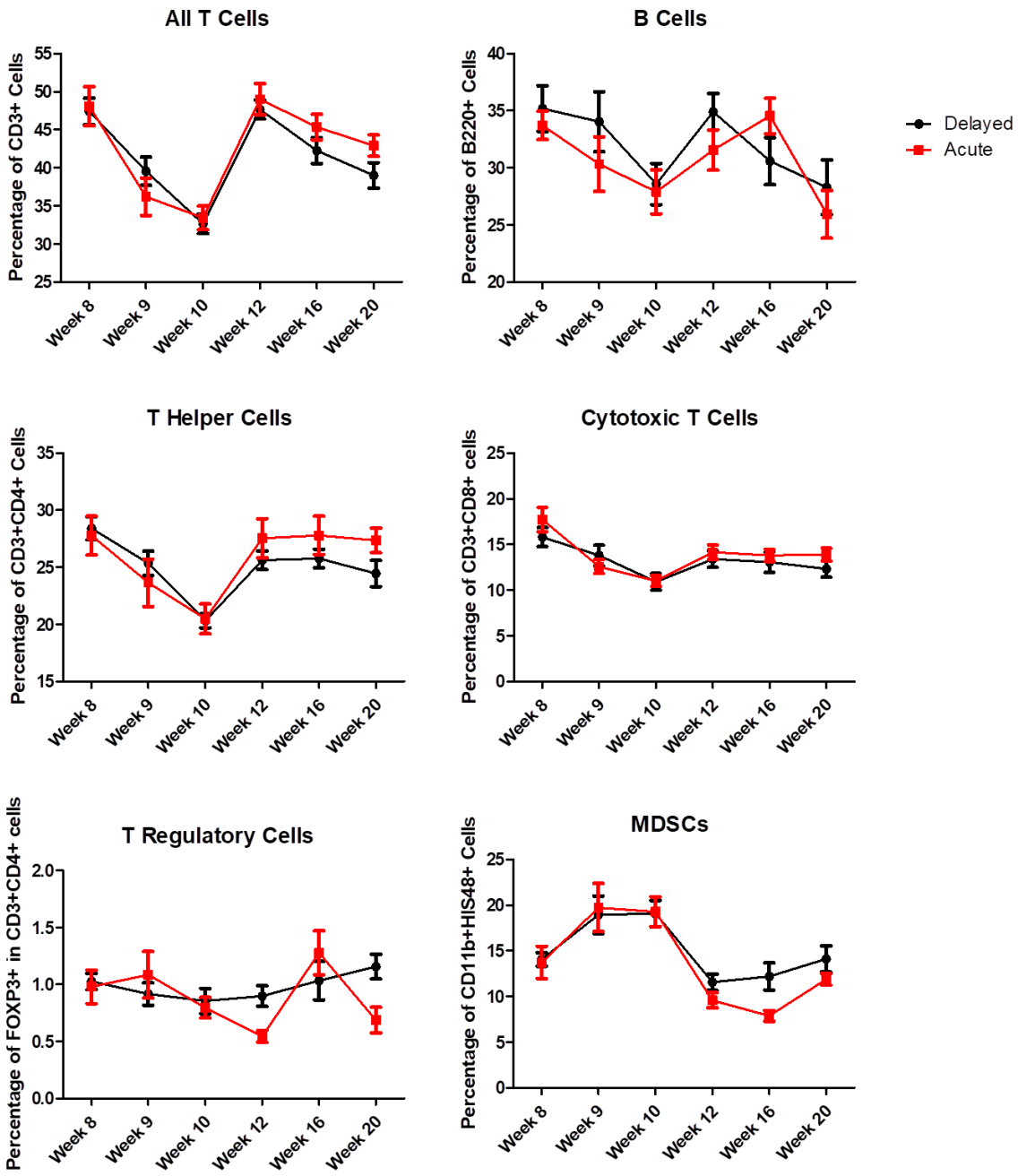

Figure 21 - Longitudinal assessment of circulating immune cells following treatment. Immune cell populations in blood were characterized by flow cytometry. No significant differences were observed between delayed and acute treatment. Week 8 corresponds to baseline levels before any treatment was administered. n=8-12/group for each time point.

5.4.5 Correlation of circulating immune cells to bone healing

To further investigate how circulating immune cells are related to the healing response, linear regression of the blood immune cell data was performed against bone formation. With this approach, we found several significant correlations. Most notably, there was a significant negative correlation between mean MDSC levels for each sample (calculated from all post-treatment time points combined) and bone formation (Figure 22A). Interestingly, the variability in MDSCs over all post-treatment time points for each sample (average standard deviation) was also significantly negatively correlated with bone formation (Figure 22A). Analysis at each individual time point revealed a significant negative correlation between MDSCs and bone formation at weeks 9, 10, and 20 (Figure 22B). Other significant correlations for individual time points include CD3+ T cells at week 20, CD4+ T helper cells at weeks 16 and 20, and B cells at (Supplemental?)

A

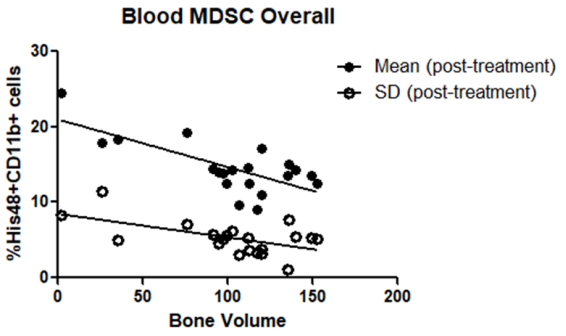

Linear Regression	Mean	SD
Slope	-0.06315 ± 0.01430	-0.03130 ± 0.01054
Y-intercept	20.97 ± 1.553	8.444 ± 1.145
Pearson r	-0.7213	-0.5734
p-value	0.0003	0.0082

B

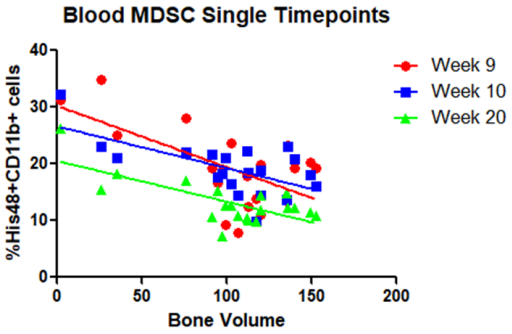

Linear Regression	Week 9	Week 10	Week 20
Slope	-0.1083 ± 0.03265	-0.07337 ± 0.02155	-0.07208 ± 0.01661
Y-intercept	30.23 ± 3.546	26.59 ± 2.341	20.52 ± 1.804
Pearson r	-0.6160	-0.6258	-0.7151
p-value	0.0038	0.0032	0.0004

Figure 22 - Correlation of circulating MDSC populations with bone formation using linear regression. Both the overall mean and standard deviation in MDSC levels (calculated for each individual sample from all post-treatment time points) were significantly negatively correlated with bone formation at week 20 (A). Following analysis of all individual time points, MDSC levels at weeks 9, 10, and 20 were also significantly negatively correlated with bone formation (B).

5.4.6 Analysis of additional tissues harvested at terminal time point

At week 20, spleen, bone marrow from ipsilateral tibia, and muscle tissue directly adjacent to the bone defect were collected and analysed by flow cytometry. Animals that received acute treatment demonstrated reduced levels of CD4+ T helper cells and MDSCs in bone marrow compared to animals that received delayed treatment (Figure 23). Levels of hematopoietic stem cells (HSCs) were also slightly elevated with acute

treatment, although not to a significant extent. No significant differences were observed in spleen and muscle tissues (not shown).

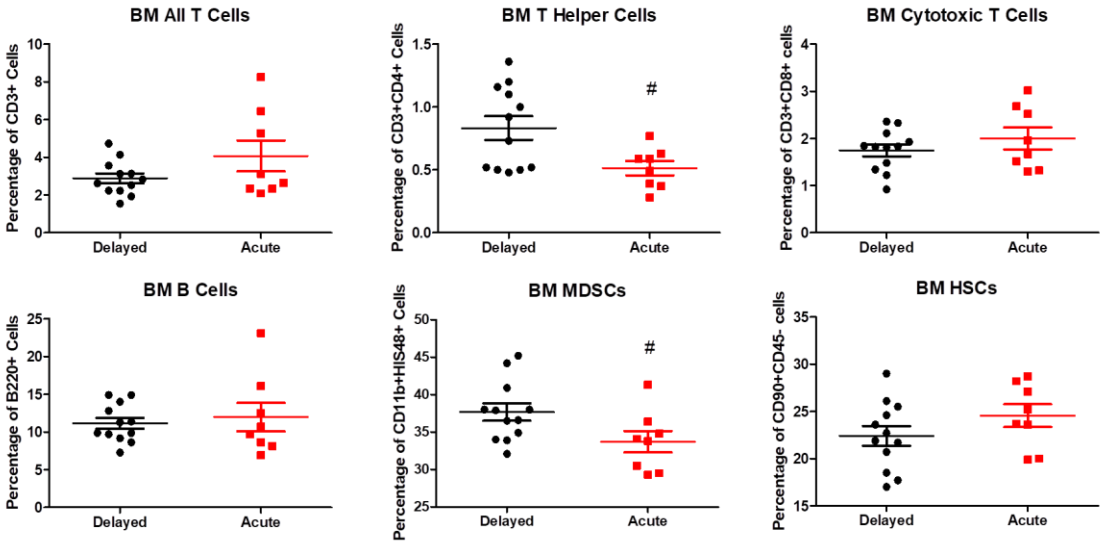

Figure 23 - Immune cell differences in bone marrow at week 20. Immune cell populations in bone marrow of ipsilateral tibia were analyzed by flow cytometry. Acute treatment exhibited reduced levels of T helper cells and MDSCs compared to delayed treatment. #p<0.05 vs Delayed by student's T test. n=8-12/group

5.5 Discussion

Immune dysfunction following severe trauma, unrelated to sepsis or multiple organ failure, has become fairly well-accepted by the clinical community in recent years as an important complication to be aware of. This has directly led to the creation of guidelines for the diagnosis of disorders like PICS [54]. However, this concept of persistent low-grade inflammation and immunosuppression that subtly impairs healing has yet to be explored much in the context of bone injuries, including nonunion.

To the best of our knowledge, this work represents the first of its kind to demonstrate long-term immune dysfunction in a preclinical model of chronic nonunion. We verified that acute treatment with BMP-2 results in better healing compared to equivalent delayed treatment after nonunion has already been established. Using multivariate regression analysis methods, we found that these two treatments exhibit distinct expression profiles both in local bone defect tissue and in systemic blood circulation. Delayed treatment resulted in significantly lower early expression of the major anti-inflammatory cytokine IL-4, which is widely known to induce a Th2 response [130] and promote M2 macrophage polarization [131]. This observation potentially indicates a diminished initial anti-inflammatory response with treatment following nonunion, which may foreshadow unsuccessful resolution of the acute inflammatory phase and consequently lead to persistent inflammation.

Computational regression analysis of serum cytokines implicated IL-6 and LIX as the cytokines most positively correlated with bone formation, whereas IP-10 was the cytokine that was most negatively correlated. These findings are consistent with those made by other groups, as IL-6 stimulates angiogenesis and promotes callus mineralization [132, 133] while LIX expression is necessary for IL-17-mediated protection from pathogenic bone destruction [134]. Interestingly, IP-10 (also called CXCL10) is one of the main pro-inflammatory cytokines secreted by MDSCs [135, 136].

Flow cytometry characterization of MDSCs in both blood and bone marrow tissues indicate that greater presence of MDSCs is associated with worse bone healing outcomes. Also, while not to a significant extent, we did observe slightly lower circulating levels of all T cells and CD4+ T helper cells with delayed treatment at weeks 16 and 20. Taken

together, these results suggest that impaired bone healing in this model involves a rise in MDSCs that subsequently leads to a long-term reduction in effector T cell populations, which fit the conventional profile of PICS and chronic immune dysregulation as described in detail above.

This study is not without limitations. For the systemic blood analyses in particular, the alterations observed in immune cell populations over time may be most influenced by changes due to aging rather than the response to trauma and subsequent treatment. In fact, immunosenescence with aging has been well-documented [137-139]. One of the hallmarks is an overall reduction in T and B lymphocytes as hematopoietic progenitors gradually favor a shift towards myeloid lineage cells, particularly pro-inflammatory monocytes and macrophages [140, 141]. However, many of these studies focus on age-related immune changes from childhood to old age. In this study, all rats were 13 weeks-old at the start and 33 weeks-old at the terminal time point, which falls well within early adulthood for rats and the 20 week duration of the study is relatively short considering the entire lifespan of rats (usually greater than 2 years). Consequently, we would expect age-related immune changes over the course of this study to be minimal. And yet, we still fully acknowledge that immune characterization of age-matched naïve animals over time would have been a valuable control group to confirm whether both delayed and acute treatment in this model actually exhibit abnormal immune variations. Despite this limitation, the results shown here still provide significant insight into long-term immune changes following treatment of nonunion and demonstrate a link between systemic immune health and bone healing.

In conclusion, this study investigated the role of immune dysregulation before and after treatment of nonunion. Delayed treatment was associated with changes in the local and systemic immune response compared to acute treatment, including lower early expression of anti-inflammatory cytokine IL-4 in the bone defect and higher systemic expression of IP-10, one of the main pro-inflammatory cytokines secreted by MDSCs. Additionally, increased presence of MDSCs was shown to correlate with poor bone healing outcomes. Further mechanistic studies are needed to validate that MDSCs are the main producers of the cytokines identified here, but it appears that overall, MDSCs and immune suppression do play a role in impaired healing after nonunion and could potentially be targeted in the future to improve treatment strategies.

CHAPTER 6. CONCLUSIONS AND FUTURE DIRECTIONS

6.1 Primary Conclusions

The first recorded bone grafting procedure was performed by Dr. Job van Meekeren in 1668, who transplanted a fragment of dog skull into the skull of a wounded solider [142]. In some ways, our treatment of bone injuries has not advanced much in the past few centuries as bone grafts, specifically autografts, remain the gold standard despite their known shortcomings. Bone repair involves a complex orchestration of biological events that is still not quite fully understood, but the influence of patient-specific factors has become more evident, and the need to account for these factors with more sophisticated treatment strategies has become increasingly apparent in recent years.

The work presented here represents a significant contribution to the field of bone research by helping elucidate several factors that impact bone healing. In Aim I, the roles of age and dose on BMP-2-mediated bone repair were investigated. Using the current clinical standard BMP-2 delivered in a collagen sponge, we found that young rats were more responsive to increases in BMP-2 dosing compared to adult rats, without experiencing more complications. This is a very notable observation as BMP-2 use clinically is a fairly contentious topic, as it has been linked to numerous adverse events and is currently contraindicated for skeletally immature patients. These results indicate that there is an age-related dose response that should be considered when administering BMP-2. Taking a more conservative dosing strategy is likely to be beneficial for young patients and less likely to encounter unwanted complications.

In Aim II, we established a novel model for studying chronic nonunion by delaying treatment to our standard femoral bone defect. We validated that delayed treatment of a nounion results in impaired bone healing compared to acute treatment of a freshly-made bone defect, and this deficit in healing could not be overcome with a modest increase in BMP-2 dose. Moreover, we showed potential evidence of long-term immune dysregulation with delayed treatment as the non-responders (samples that did not demonstrated radiographic bridging) exhibited significantly higher serum expression of TNFα and IL-1β compared to responders at week 20, suggestive of a prolonged inflammatory state.

Finally, in Aim III we performed much more in-depth characterization of the immune profiles in the chronic nonunion model. Early local defect tissue analysis revealed reduced local IL-4 expression with delayed treatment, possibly indicative of a diminished anti-inflammatory response after nonunion that will be insufficient to resolve acute inflammation. Furthermore, systemic evaluation of immune cells in blood and bone marrow established a link between increased MDSC presence and impaired bone healing. This observation was supported by serum cytokine analyses, which implicated a major cytokine produced by MDSCs, IP-10, as being strongly negatively correlated with bone formation. Overall, these results provide mounting evidence that long-term immune dysregulation is involved during nonunion, and that MDSCs may be one of the main drivers of chronic immune suppression that develops even after treatment. Both of these conclusions are novel contributions that motivate further research into the dynamics between immune dysfunction and nonunion.

6.2 Future Directions

The body of work shown here represents just one of many examples found throughout literature that support the importance of immune cells during normal bone repair. While prolonged inflammation is detrimental to healing, disrupting the initial acute inflammatory response by depleting certain immune cell populations can be equally as destructive. Seminal work by Godwin et al. demonstrated that knocking out macrophages completely abrogated normal limb regeneration in axolotls [143]. Nam et al. observed deficits in early osteogenic expression in a Rag1-/- murine model that lacks mature T and B cells compared to wild type mice [144]. Interestingly, a separate group utilizing the same Rag1-/- mouse actually found improved fracture healing compared to wild type mice [145]. This same group has since demonstrated inhibition of bone healing by a subset of CD8+ effector memory T cells [146]. These seemingly contradictory findings point to the complexity of the immune response during bone healing, and suggest that the roles that immune cells play are highly context and time-dependent. Regardless, all of these studies promote the idea that modulating the immune response can potentially enhance bone healing and lead to the discovery of new therapies.

Unfortunately, there have not been any documented successful therapies to combat long-term immune dysfunction such as in PICS, perhaps due in part to under-recognition of PICS as its own distinct phenotype from more well-established syndromes like MODS [53]. Nonetheless, chronic immune dysregulation remains an important concern for patients recovering from severe trauma, and certain immune cell populations, particularly Tregs and MDSCs, have drawn considerable interest from the scientific research community [135, 147]. Osteoimmunology is a rapidly emerging field that seems like the

prime candidate for tackling some of these challenges, yet it has primarily focused on the interactions between immune and skeletal systems in the context of diseases such as rheumatoid arthritis [148], cancer [149], osteoporosis [150], and certain autoimmune disorders [151]. Consequently, many questions remain about the interplay between these two complex systems following traumatic injury, and the importance of restoring long-term immune homeostasis on bone regeneration requires further investigation.

In that regard, the prospect of immunomodulation to improve bone repair remains an exciting possibility. Immunotherapies have been explored in recent years to treat a wide range of diseases including neurodegenerative disorders [152], HIV/AIDS [153], and most notably cancer [154]. The applications of immunomodulation to bone repair are not nearly as advanced comparatively, and have thus far mainly focused on the endogenous immunomodulatory capabilities of mesenchymal stem cells [155, 156] or the direct delivery of immunomodulatory cytokines [157, 158]. An idea that has gained traction within the orthopedic community is the importance of macrophages during bone repair. This is not surprising considering it is well-established that osteoclasts and macrophages share a common lineage, and it has even been shown that there are unique resident macrophages in bone [159]. A few groups have recently tried to promote osteogenesis by activating specific macrophage phenotypes [160, 161], but only *in vitro* or in heterotopic *in vivo* models. Nevertheless, these studies represent clear advancements in the field yet also demonstrate that there is much progress to be made in the development of more targeted immunomodulatory therapies for bone repair.

The results from this work, specifically the findings in Aim 3, motivate the targeting of certain immune cell types for bone repair. The Roy lab at Georgia Tech has

previously developed immunomodulating microparticles that can stimulate dendritic cells and alter their secretome [162]. Perhaps a similar approach could be taken to either inhibit immune suppressive cells such as MDSCs or augment positive immune effector cells as a means of improving healing in our model of chronic nonunion. Successful inhibition of MDSCs has actually been shown to enhance the effectiveness of cancer immunotherapies in treating tumors [77]. One could imagine that a combinatorial strategy that both rejuvenates the immune system to combat chronic immunosuppression as well as treats the primary traumatic injury will result in better regenerative outcomes than either single therapy alone. Another approach that could be taken would be to focus more broadly on the balance in overall Th1/Th2 response and the relative polarization of M1/M2 macrophages. Indeed, several groups have already started down this path and have demonstrated some promising results for repair of bone and other associated tissues [161, 163-167].

The major underlying theme of this thesis is that better understanding of patient-specific factors will potentially lead to better treatment strategies for bone repair. Many of these factors, such as age, gender, presence of co-morbidities, lifestyle choices, and diet are already widely accepted to have an impact on healing. Yet very rarely are these factors taken into account when implementing a bone healing treatment strategy. In Aim I, we demonstrated that adjusting something as simple as dose could be very beneficial for current BMP-2 therapies, particularly for the pediatric population for whom all BMP-2 use is contraindicated. Recently, technological advances have made genomic sequencing exponentially faster and much more affordable to the general public, and genetic testing has become much more widespread throughout all areas of healthcare. In

the context of bone injuries and diseases, there is some early evidence of a genetic predisposition towards poor healing outcomes such as nonunion [168-170].

Ultimately, the goal of characterizing the multifactorial problem that is bone repair would be to develop predictive models that can help guide the design of more personalized treatment strategies in order to achieve the best possible outcome for each patient. The results presented here demonstrate the potential value of monitoring specific noninvasive biomarkers following treatment, such as circulating cytokines and immune cells. Indeed, many groups have begun looking into various biomarkers and immune cell quantification as a means of predicting mortality, sepsis, and other complications following trauma and surgery [69, 171-173]. In the context of bone healing, Pountos et al. recently compiled a review of relevant biomarkers that have potential predictive power for fracture nonunion, including serum ALP and TGFβ1 levels [174]. For all of these predictive models though, it is important not to overstate the predictive power of biomarkers found in preclinical models and their applicability to human patients. This issue was highlighted recently in conflicting high impact publications that investigated the relevance and utility of murine models for the study of human inflammatory diseases [175, 176]. Nevertheless, our work provides substantial evidence of noninvasive biomarkers being highly correlated (both positively and negatively) with bone healing and motivates further efforts to develop potentially powerful tools for clinical prediction.

APPENDIX

A.1 CS-GAG SCAFFOLDS FOR CELL AND RECOMBINANT PROTEIN-BASED BONE REGENERATION[2]

Abstract

Bone morphogenetic protein 2 (BMP-2) loaded collagen sponges remain the clinical standard for treatment of large bone defects when there is insufficient autograft, despite associated complications. Recent efforts to negate co-morbidities have included biomaterials and gene therapy approaches to extend the duration of BMP-2 release and activity. In this study, we compared the collagen sponge clinical standard to chondroitin sulfate glycosaminoglycan (CS-GAG) scaffolds as a delivery vehicle for recombinant human BMP-2 (rhBMP-2) and rhBMP-2 expression via human BMP-2 gene inserted into mesenchymal stem cells (BMP-2 MSC). We demonstrated extended release of rhBMP-2 from CS-GAG scaffolds compared to their collagen sponge counterparts, and further extended release from CS-GAG gels seeded with BMP-2 MSC. When used to treat a challenging critically-sized femoral defect model in rats, both rhBMP-2 and BMP-2 MSC in CS-GAG induced comparable bone formation to the rhBMP-2 in collagen sponge, as measured by bone volume, strength, and stiffness. We conclude that CS-GAG scaffolds are a promising delivery vehicle for controlling the release of rhBMP-2 and to mediate the repair of critically-sized segmental bone defects.

[2]Portions of this chapter were adapted from S. Andrews*, A. Cheng*, H.Y. Stevens, M.T. Logun, R. Webb, E. Jordan, B. Xiao, L. Karumbaiah, R.E. Guldberg, S. Stice. CS-GAG scaffolds for cell and recombinant protein-based bone regeneration. Under review in Journal of Tissue Engineering and Regenerative Medicine (2017).

Introduction

Bone tissue is well known for its remarkable healing abilities, but there are instances in which these mechanisms are insufficient on their own. Large defects or gaps in bone are unable to be bridged without intervention. Allografts and autografts are popular bone grafting methods, accounting for over 2 million procedures per year [177]. However, these procedures are not devoid of complications. Autografts, which are derived from the patient themselves, are the current gold standard, but are the most difficult to obtain and have the risk of donor site morbidity [178, 179]. Allografts, from other individuals of the same species, are more likely to be rejected, require lifelong immunosuppression, and are potential sources of disease transmission [178, 180, 181]. Due to these issues, there have been numerous attempts to develop new synthetic bone graft substitutes to enhance bone healing.

Bone Morphogenetic Protein 2 (BMP-2) is an osteoinductive growth factor commonly used in bone substitute applications. It usually exists as a homodimer, binding to serine/threonine kinase receptors to initiate endocrine, paracrine, and autocrine effects [182, 183]. The recombinant human BMP-2 (rhBMP-2) is FDA-approved, and used clinically in combination with a collagen sponge. It has been shown to reduce the rate of secondary intervention and enhance fracture healing, and has shown additional benefits for many orthopedic applications [184, 185]. Thus any new modality for treating critically-sized bone defects should undergo a rigorous investigation with comparison to current FDA approved techniques, such as rhBMP-2 on collagen sponge.

Despite its well documented ability to induce bone formation, rhBMP-2 has a very short half-life, leading to the use of supraphysiological doses by clinicians [186, 187]. Complications associated with delivery of rhBMP-2 clinically have been reported to include ectopic bone formation, inflammation, and increased cancer rates among patients [11, 188]. Additionally, the large amount of recombinant protein required for this approach leads to increased costs compared to alternative treatments [189]. In rats, clinically relevant doses of rhBMP-2 have been shown to induce the formation of structurally abnormal bone, as well as inflammation [89]. These drawbacks could be addressed by using a delivery method with sustained release of a lower dose of BMP-2. One such delivery system could involve use of constitutive BMP-2 expression via genetically engineered mesenchymal stem cells (MSCs) for BMP-2 delivery (BMP-2 MSC) [190-193].

MSCs are multipotent stromal cells commonly studied and used for their ability to differentiate into bone, cartilage, and adipose tissue [194]. They are attractive as a delivery mechanism due to their ease of collection and expansion from bone marrow, adipose, and umbilical tissue, as well as their immune modulation capabilities and allogeneic tolerability. Osteogenic differentiation can be readily induced in MSCs, even in the absence of BMP-2 and transforming growth factor β1 (TGF-β1) signaling [195]. Our group has previously demonstrated success in creating ectopic bone, and regenerating critically-sized defects in rats using BMP-2-expressing MSCs encapsulated in poly-ethylene glycol (PEG) microspheres [196, 197]. However, these studies noted a sharp decrease in encapsulated cell viability after 4 days [196]. PEG has been shown to be safe for implantation but it is not inherently osteoconductive or biodegradable without

further modifications [198, 199]. In addition, PEG cell encapsulation procedures can be labor intensive, variable, and inefficient [200].

Chondroitin sulfate glycosaminoglycans (CS-GAGs) are found attached to CS proteoglycans in the extracellular matrix of cartilage, bone, and other tissues. They are O-linked glycans consisting of repeating glucuronic acid and N-acetylgalactosamine disaccharides. CS-GAGs are important for bone development as they can support osteogenesis and suppress bone resorption [195, 201-204]. Additionally, they regulate both TGF-β1 and BMP signaling in bone, and have been shown to retain TGF-β [195, 205]. In other studies, sulfated glycosaminoglycans assisted in BMP-2's interaction with its receptor, and oversulfated chondroitin sulfate enhanced osteoblast mineralization in the presence of BMP-4 [206, 207]. These qualities lend themselves to the use of CS-GAGs as a scaffold for the slow release of BMP-2.

In this study, we describe an injectable biologic therapy for large bone defect healing. It consists of human MSCs genetically engineered to overexpress BMP-2, which are then seeded in a CS-GAG gel. We demonstrated high levels of BMP-2 expression in BMP-2 MSCs, maintained viability post-seeding, and sustained *in vitro* BMP-2 release from this system compared to BMP-2 on collagen sponge. Additionally, we show the formation of comparable bone quantity and quality to the clinical standard in a rigorous rodent critically-sized segmental defect model. These results indicate the potential of this system to be a valuable therapeutic option for healing large bone defects.

Materials and Methods

Cell Culture and Transduction

Human umbilical (uMSC) or bone marrow MSCs (bmMSC), (Lifeline Cell Technology, Frederick MD, Sciencell, Carlsbad CA) were plated at 5000 cells/cm^2 on tissue culture flasks in complete media Alpha-Minimum Essential Medium (MEM-α), 10% defined fetal bovine serum (Hyclone, South Logan UT), 2 mM L-glutamine, 50 U/mL penicillin, 50 μg/mL streptomycin and allowed to grow to 80-90% confluency (20,000–25,000 cells/cm^2). To transduce, cells were harvested using 0.05% trypsin and plated at 26,000 cells/cm^2 in MEM-α, 10% defined fetal bovine serum, 5 μg/mL Polybrene (Sigma-Aldrich, St. Louis MO), and the appropriate MOI of prEF1a-BMP-2 or prEF1a-RFP lentivirus (Cellecta, Mountain View CA) on tissue culture flasks. The media was changed back to complete media 24 hours post-transduction. All cultures were maintained at 37°C and 5% CO_2, and used up to twenty passages. All materials were from Invitrogen (Carlsbad CA) unless otherwise stated.

In vitro RFP expression

Following transduction of uMSCs with the prEF1a-RFP vector in MOIs of 0, 1, 10, and 50 as described above, both phase contrast and fluorescent images were taken. Five images per well and three wells per condition were taken at 24, 48, and 72 hours post-transduction.

In vitro BMP-2 expression

Following transduction of uMSCs with the prEF1a-BMP-2 vector in MOIs of 10 and 50 as described above, 0.5 mL media samples were collected in triplicate from different sets of wells at 48, 72, 96 and 120 hours post-transduction. BMP-2 concentrations were determined via BMP-2 ELISA (R&D Systems, Minneapolis MN).

Hydrogel Preparation and Characterization

Rheological testing and Scanning Electron Microscopy (SEM) were used as previously described to characterize the CS-GAG hydrogels. Briefly, hydrogel mixture was prepared by reconstituting 3% w/v of lyophilized methacrylated chondroitin sulfate and 0.01% 2-hydroxy-4′-(2-hydroxyethoxy)-2-methylpropiophenone (Irgacure-2959, Sigma-Aldrich, St. Louis MO) in PBS.

Rheological testing of the hydrogel was performed as described previously [208]. Briefly, 500 µL of the hydrogel mixture was dispensed into a polydimethylsiloxane mold overlaid onto a glass slide, and exposed to 365 nm long-wavelength UV light (160 W BlakRay, UVP, Upland CA) for 3 min to yield hydrogel disks 1 in. in diameter and 6 mm thick. The hydrogels were then overlaid with 1 mL of PBS to swell overnight before rheological testing, which was performed on an ARES rheometer (TA Instruments, New Castle DE), using a parallel plate geometry. Frequency sweep experiments from 0.1 to 100 Hz were performed at 5% strain at 25°C.

Morphology of gold coated lyophilized hydrogel samples was examined as described previously using a Zeiss 1450EP SEM scanning electron microscope (Carl Zeiss, Oberkochen Germany) [208]. Briefly, hydrogels were flash frozen in liquid nitrogen and lyophilized. They were then mounted on 10 mm SEM stubs and sputter coated (Structure Probe Inc., West Chester PA) with gold for 30 s, and imaged under an accelerated voltage of 5 kV. Images were acquired at 165x and 500x to observe the porosity and microstructure of the hydrogels.

Cell Seeding

Following casting as described above, 500 µL gels were frozen overnight at -80°C, after which they were lyophilized for 24 hours (Fig. 3A). To rehydrate them, the lyophilized hydrogels were overlaid with either a $6.66x10^6$/mL cell suspension (GAG+MSC or GAG+BMP-2 MSC) or 33.3 µg/mL rhBMP-2 (GAG+rhBMP-2) of equal volume to the gel in MEM-α and allowed to incubate at 37°C and 5 % CO_2 until all free liquid was absorbed into the gel. The hydrogel was then transferred to a sterile 1cc syringe, pulse centrifuged to remove air pockets and injected/ejected with a sterile 22G needle.

Viability and Distribution

24 hours after transduction with the prEF1a-RFP vector at MOI 10, uMSCs were seeded in CS-GAG hydrogels and overlaid with 2 µM Calcein in PBS. Cells were imaged using FITC and TRITC fluorescent filters 3 hours after seeding. Viability of transduced cells was determined by quantifying the degree of fluorescence overlap of RFP and Calcein using the Mander's overlap co-efficient parameters in Volocity (PerkinElmer, Waltham MA) as described previously.

Nanofiber mesh fabrication

Perforated nanofiber mesh tubes were fabricated as described previously [98]. A 12% (w/v) solution of poly(ε-caprolactone) (PCL) was made by dissolving PCL (Sigma-Aldrich, St. Louis MO) in a 90:10 mixture of hexafluoro-2-propanol:dimethylformamide (Sigma-Aldrich, St. Louis MO). The solution (~4mL) was electrospun onto a static collector plate to obtain PCL sheets. Rectangular sections (12x19 mm) containing twenty three 1-mm-diameter circular holes were then cut using a VLS3.50 laser cutter (Universal

Laser Systems, Scottsdale AZ). Each rectangular piece was then rolled up into a cylindrical tube (5 mm diameter, 12 mm in length) and glued using medical grade UV-curable adhesive (Dymax, Torrington CT). Meshes were sterilized by ethanol evaporation, washed and stored in PBS, and then transferred to MEM-α and stored at 4°C prior to use.

Preparation of GAG treatment groups

One day prior to surgery/experiment, uMSCs were either left non-transduced or transduced at 10 MOI and seeded in CS-GAG hydrogels 24 hours after transduction as described above. On the day of surgery/experiment, rhBMP-2 (R&D Systems, Minneapolis MN) was reconstituted according to the manufacturer's instructions, diluted to 33.3 ug/mL in MEM-α, and used to rehydrate lyophilized CS-GAG hydrogel as described above.

Collagen sponge preparation

The day before each surgery/experiment, rhBMP-2 (Pfizer Inc., New York, NY) in 0.1% rat serum albumin (Sigma-Aldrich, St. Louis MO) in 4 mM HCL solution was made up to a concentration of 33.3 ug/mL and then stored at 4°C overnight. Collagen sponge cylinders ~5mm in diameter and 10mm in length were created by biopsy punching out from a sheet of bovine collagen sponge (Kensey Nash/DSM, Exton PA). All collagen sponge cylinders were sterilized by ethylene oxide. Prior to the start of the surgery/experiment, the collagen sponge cylinders were transferred to a 24-well plate, and then 150 μl of the rhBMP-2 solution was slowly loaded onto each cylinder. The sponges were left to sit for ~10 minutes to soak up any residual rhBMP-2 solution in the

well before being carefully transferred to another well plate for *in vitro* release characterization or press-fit into the bone defect for *in vivo* studies

Hydrogel BMP-2 Release

Experimental groups were prepared as follows: CS-GAG hydrogels were rehydrated with $6.67x10^6$ cells/mL non-transduced uMSCs (GAG+MSC), transduced uMSCs (GAG+BMP-2 MSC), or 3.33 μg/mL rhBMP-2 (GAG+rhBMP-2), and 150 μL of each rehydrated gel was injected into polycaprolactone (PCL) nanofiber meshes and placed into individual wells of an ultra-low adhesion 24-well plate (Nunclon Sphera, ThermoFisher, Waltham MA). For the collagen sponge group (Col+rhBMP-2), 150 μL of 3.33μg/mL rhBMP-2 solution was loaded onto each sponge and each sponge was then placed into an individual well of the 24-well plate (without any PCL mesh).

For the release experiment, 1 mL of MEM-α only were added to each well. All scaffolds were then allowed to incubate at 37°C and 5 % CO_2. At 3 h, 12 h, 1, 2, 3, 5, 7, 9, 11, and 13 days, the overlaid media were collected and immediately stored at -80°C, and the extracted media was replaced with 1 ml of fresh media. On day 15, media were collected and then replaced with 1 ml of digest solution. The CS-GAG hydrogels were digested with 1 ml media containing 20 mU of chondroitinase ABC (Sigma-Aldrich, St. Louis MO) while the collagen sponges were digested with 1 mg/ml collagenase type I (Sigma-Aldrich, St. Louis MO). Digestion occurred for 24 hours at 37°C before collection and storage at -80°C as before. BMP-2 ELISA was performed on the collected media to determine the amount of BMP-2 released from the scaffolds at each timepoint.

Segmental defect surgery

The surgical procedure has been described previously [96]. Briefly, an anterolateral skin incision was made in the leg, and then blunt dissection was performed to allow for placement of a polysulfone fixation plate. Critically-sized 8 mm defects were created in the mid-diaphysis of the femur using an oscillating saw. The desired therapeutic was then delivered to the defect site, and finally the muscle and skin were closed using 4-0 vicryl suture (Ethicon, Somerville NJ) and wound clips, respectively. Prior to surgery, all animals were given a subcutaneous injection of slow-release buprenorphine for analgesia and anesthesia was induced using isoflurane. For all experiments, 14-week-old female RNU Nude rats (Charles River Laboratories, Wilmington MA) were used.

Radiography and microcomputed tomography

To qualitatively assess longitudinal bone regeneration, 2D in vivo radiographs were taken using the MX-20 digital machine (Faxitron X-ray Corp, Tucson AZ) at 2, 4, 8, and 12 weeks post-surgery. Radiographs were acquired using an exposure time of 15 seconds and energy at 25 kV. Bridging scores were assigned to each radiograph by two blinded investigators where bridging was defined as contiguous bone spanning the entire defect space (from bone end to bone end). In instances of disagreement, a third blinded investigator served as tiebreaker.

New bone formation was quantitatively evaluated using 3D microcomputed tomography (μCT) at 12 weeks post-surgery. Scans were performed using the vivaCT40 (Scanco Medical, Brüttisellen Switzerland). Ex vivo scans were performed at a 21 μm voxel size, 55 kVp voltage, and a 145 μA current. The volume of interest (VOI) consisted of the

central 6.36 mm (303 slices) of the defect. A threshold corresponding to 50% of native cortical bone density was applied to segment bone mineral [209].

Mechanical testing

Torsional testing to failure was performed as previously described [96]. Femurs were excised at 12 weeks post-surgery, wrapped in PBS-soaked gauze, and stored at -20°C until testing could be performed. On the day of testing, samples were thawed in a beaker of tap water, the surrounding soft tissues were excised, and the fixation plate was removed so that the native bone ends could be potted in Wood's metal (Alfa Aesar, Haverhill MA). Potted femurs were then rotated at a rate of 3 degrees per second until failure using the EnduraTEC ELF3200 axial/torsion testing system (Bose, Framingham MA). Failure strength was determined by locating the failure (peak) torque within the first 60° of rotation. Torsional stiffness was calculated by finding the slope of the linear region before failure in the torque-rotation plot.

Statistical Analysis

Unless otherwise noted, all data were analyzed via nonparametric Kruskal-Wallis test with multiple comparisons made by Dunn's post-tests as appropriate using GraphPad Prism software. Significance was determined as $p < 0.05$.

Results

MSC transduction

Fluorescence microscopy of pr-EF1a-RFP lentivirus transduced uMSCs qualitatively showed transduction efficiency at 24, 48, and 72 hours post-transduction.

Visual transduction efficiency approached 100% at 10 and 50 MOI (Fig. 1A). BMP-2 ELISA of media collected from pr-EF1a-BMP2 lentivirus transduced MSCs at 48, 72, 96, and 120 hours post-transduction assessed rhBMP-2 production in both uMSCs and bmMSCs at 10 and 50 MOI (Fig. 1B). Non-transduced MSCs expressed BMP-2 below the detection threshold of the ELISA kit used and are not shown. All transductions resulted in greater amounts of rhBMP-2 released over time. By 96 and 120 hours post-transduction, significantly more BMP-2/cell was produced at both 10 and 50 MOI in uMSC than bmMSC. However, there was no significant difference between 10 and 50 MOI for either cell type.

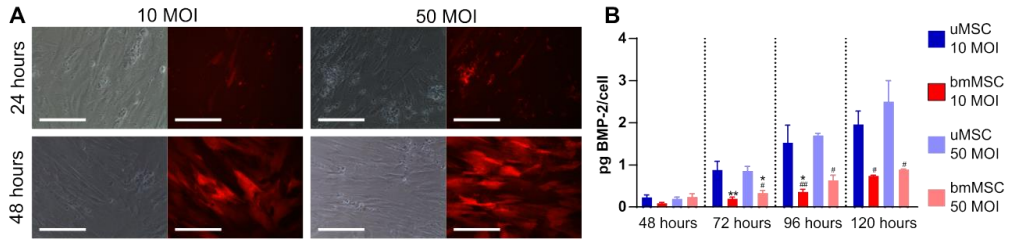

Figure 24 - Efficient transduction of uMSCs with a lentiviral vector at 10 MOI. (A) Images of uMSC over 72 hours after transducing with prEF1a-RFP at 10 and 50 MOI under phase contrast and RFP filter to evaluate transduction efficiency. Scale bars indicate 200 µm. N = 15. (B) Mean BMP-2 expression in uMSCs and bmMSCs at 48, 72, 96, and 120 hours after transducing with prEF1a-BMP2 at 10, and 50 MOI, comparing expression over cell type and MOI within each time point. Transductions at 0 MOI did not result in BMP-2 expression detectable by BMP-2 ELISA. Significant differences from uMSC 10 MOI (*,**) and 50 MOI (#,##) at $p<0.05$ and 0.01 respectively. Error bars indicate standard error. Two-way ANOVA with Tukey's multiple comparison test (n=5-6).

CS hydrogel characterization

The 3% CS hydrogels were transparent and porous (Fig. 2A), with pores ranging between 20-100 μm in diameter. The hydrogel storage modulus ranged between 350 and 450 Pa, increased at higher frequencies indicating strain hardening, and demonstrated nonlinear elasticity that is typical of biological materials (Fig. 2B) (6).

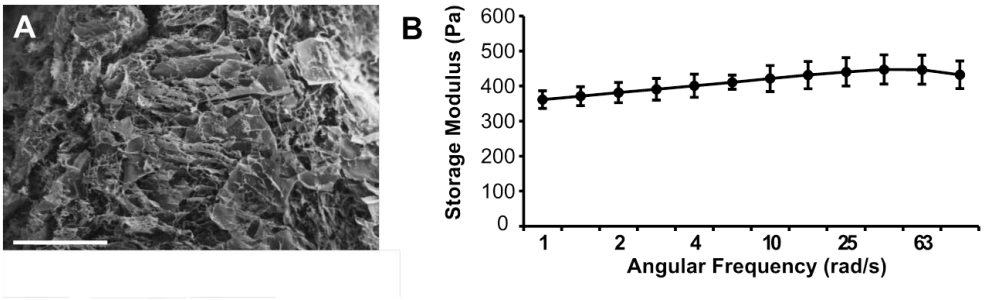

Figure 25 - CS-GAG hydrogel is porous with stable rheology. (A) Scanning electron microscopy of CS gel surface at 165x magnification. Pore sizes are about 20-100 μm. Scale bars indicate 500 μm and 100 μm respectively. (B) Rheology of CS-GAG gel. Data indicate stable rheological properties across a range of frequencies. Error bars indicate standard error (n=5).

Transduced MSC Viability and Distribution in CS hydrogels

Viable transduced MSCs were identified via colocalization of RFP and Calcein AM. Seeded MSCs were distributed homogeneously, and showed colocalization of RFP and Calcein in the cytoplasm. Mean values and standard error of Pearson's Correlation and Colocalization Coefficients M1 and M2 were 0.88± 0.01, 0.94 ± 0.01, and 0.85 ± 0.02, respectively, indicating approximately 85-88% viability in seeded cells (Fig 3B).

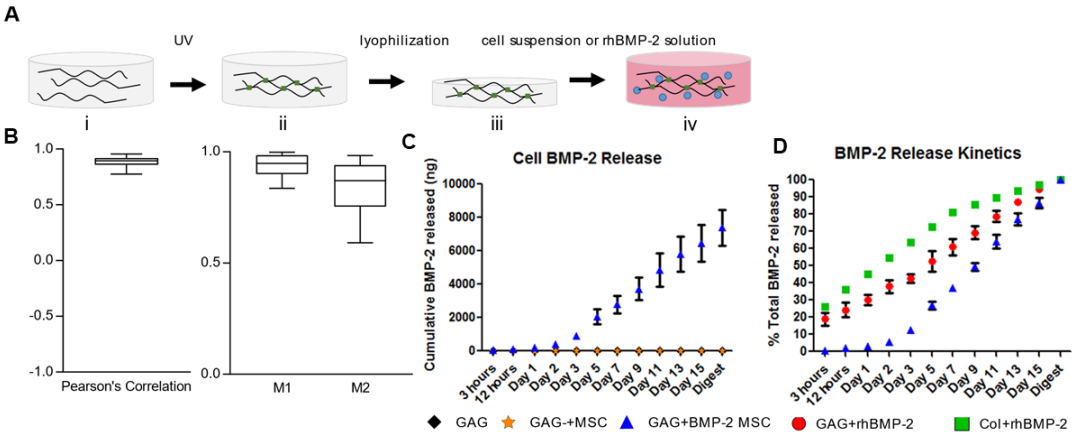

Figure 26 - Preparation of CS-GAG hydrogel and interactions with transduced MSCs. (A) Casting of 3% GAG hydrogel (i) followed by photo crosslinking under UV light (ii). The hydrogel is lyophilized for 24 hours (iii) before it is rehydrated with a cell suspension in basal media (iv). (B) Measures of colocalization for calcein and RFP: Pearsons Correlation, describing the extent of overlap between RFP and calcein images, and Colocalization Coefficients M1/M2, describing the fraction of RFP colocalizing with calcein, and the fraction of calcein localizing with RFP, respectively (n=5). (C) Cumulative BMP-2 release over 15 days from empty GAG gels, GAG gels loaded with 1 million non-transduced MSCs, and GAG gels loaded with 1 million BMP-2 MSCs (n=3-4). (D) BMP-2 release kinetics shown as percentage of the total amount released for GAG gels loaded with BMP-2 MSCs, as well as GAG gels and collagen sponges loaded with rhBMP-2 (n=3-4).

Quantification of BMP-2 release

BMP-2 MSC in GAG hydrogel secreted over 7 µg of BMP-2 cumulatively over the course of 16 days *in vitro*, which was over 1000x higher than the release from non-transduced MSCs in GAG in the same time period (Fig. 3C). Furthermore, comparison of the release kinetics to exogenous delivery of rhBMP-2 revealed that Col+rhBMP-2 had the highest initial burst release of BMP-2, followed by GAG+rhBMP-2, and GAG+BMP-

2 MSC having the slowest BMP-2 release profile (Fig. 3D). The time taken to release 50% of the total BMP-2, was approximately Day 1.5, Day 5, and Day 9 for Col+rhBMP-2, GAG+rhBMP-2, and GAG+BMP-2 MSC, respectively.

Bone defect bridging

Radiographs qualitatively showed progressive mineralization from 4 to 12 weeks in the GAG+BMP-2 MSC, GAG+rhBMP-2, and Col+rhBMP-2 groups (Fig. 4B). Defect bridging was determined from the radiographs after 12 weeks, and the bridging scores for each group were 0/7 for GAG+MSC, 4/7 for GAG+BMP-2 MSC, 6/8 for GAG+rhBMP-2, and 7/8 for Col+rhBMP-2. These two-dimensional assessments of defect bridging were verified using three-dimensional μCT reconstructions as well (Fig. 4C).

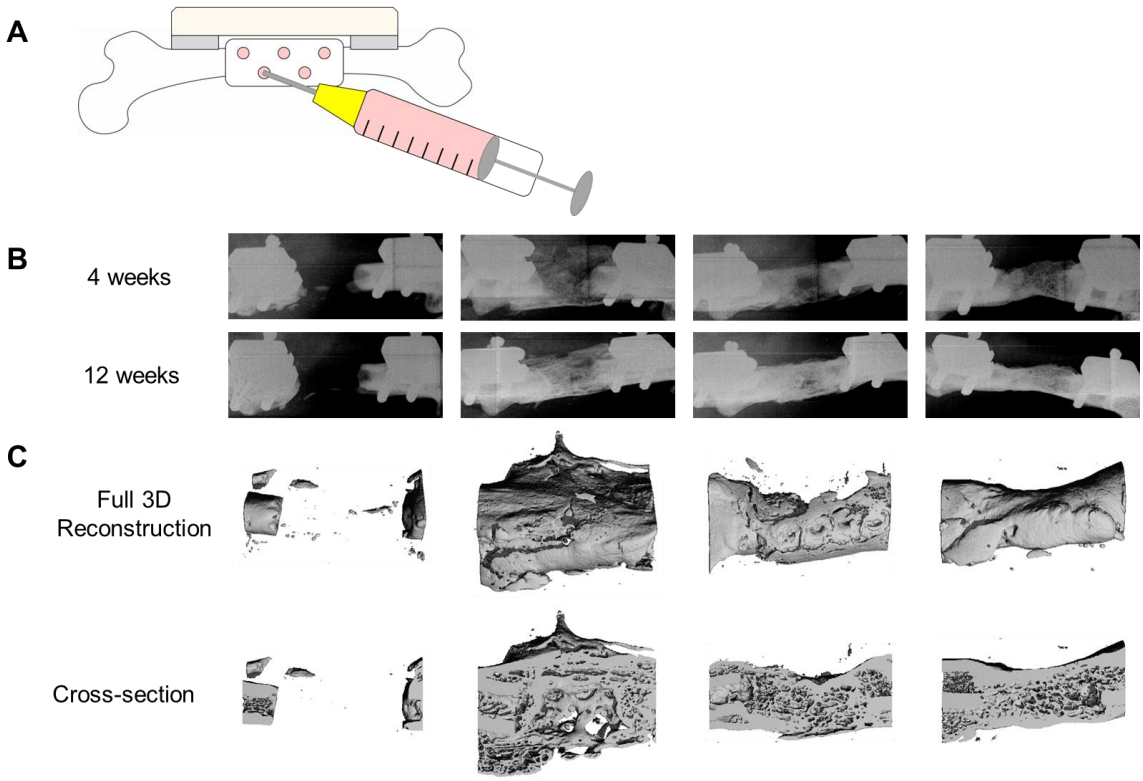

Figure 27 - Bone defects bridge when treated with rhBMP-2 or BMP-2 MSCs. (A) Illustration of rat femoral defect model with an internal fixation plate and delivery of gel into the perforated holes of the PCL nanofiber mesh. (B) Representative longitudinal radiographs at 4 and 12 weeks post-surgery. Defects were treated with 1 million non-transduced uMSCs in 150 µLCS-GAG gel, 1 million BMP-2 uMSCs in 150 µLCS-GAG gel, 150 µL CS-GAG hydrogel loaded with 5 µg rhBMP-2, or 150 µL collagen sponge loaded with 5 µg rhBMP-2. (C) 12-week µCT reconstructions of the same bone defects shown in the radiographs.

Bone formation quantification

µCT analysis showed mean total bone volumes of 2.81, 42.91, 44.52 and 39.70 mm^3, respectively, in the GAG+MSC, GAG+BMP-2 MSC, GAG+rhBMP-2, and Col+rhBMP-2 groups at 12 weeks (Fig. 5A). Bone volumes in the GAG+MSC group were significantly lower than that of the other three groups. There were no significant

differences in bone volume among GAG+BMP-2 MSC, GAG+rhBMP-2, and Col+rhBMP-2. Interestingly, when polar moment of inertia (pMOI) was calculated to assess the spatial distribution of the newly formed bone (Fig. 5B), both GAG+BMP-2 MSC and GAG+rhBMP-2 groups had significantly higher average pMOI compared to GAG+MSC, while Col+rhBMP-2 did not.

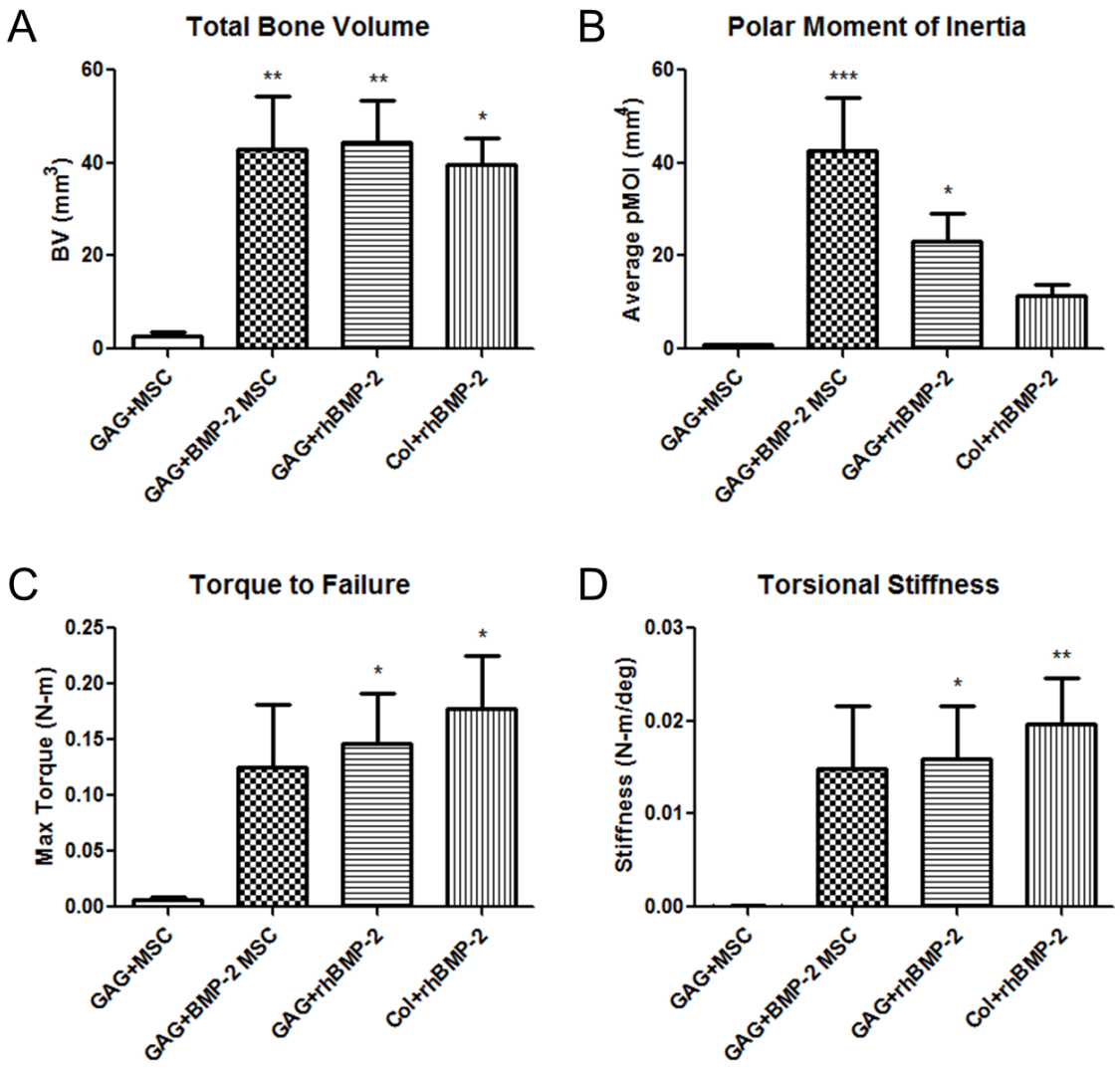

Figure 28 - Newly-formed bone similar between rhBMP-2 and BMP-2 MSC groups. µCT characterization and mechanical testing of regenerated femurs at 12 weeks. (A) Quantification of new bone revealed GAG+BMP-2 MSC, GAG+rhBMP-2, and Col+rhBMP-2 all demonstrated greater total bone volumes than GAG+MSC. (B)

Calculated average polar moment of inertia (pMOI) showed both GAG+BMP-2 MSC and GAG+rhBMP-2 groups had significantly higher pMOI compared to GAG+MSC. (C) Torque to failure and (D) torsional stiffness measured from testing regenerated femurs to failure at 12 weeks. Both GAG+rhBMP-2 and Col+rhBMP-2 groups had significantly higher torque to failure and torsional stiffness compared to GAG+MSC. There were no significant differences between GAG+BMP-2 MSC, GAG+rhBMP-2, and Col+rhBMP-2 for any of these metrics. Error bars indicate standard error (n=7-8/group).

Biomechanical testing

The mean failure torques were 0.0066, 0.1250, 0.1465 and 0.1774 N-m, respectively, in the GAG+MSC, GAG+BMP-2 MSC, GAG+rhBMP-2, and Col+rhBMP-2 groups at 12 weeks (Fig. 5C). The mean torsional stiffnesses were 0.00009, 0.0149, 0.0159 and 0.0197 N-m/deg, respectively, in the GAG+MSC, GAG+BMP-2 MSC, GAG+rhBMP-2, and Col+rhBMP-2 groups (Fig. 5D). For both parameters, only the GAG+rhBMP-2 and Col+rhBMP-2 groups had significantly higher values compared to GAG+MSC. However, there were no significant differences among GAG+BMP-2 MSC, GAG+rhBMP-2, and Col+rhBMP-2 groups.

Histology

H&E staining demonstrated clear morphological differences between the three BMP-2 groups and the GAG+MSC group (Fig. 6). In the GAG+MSC samples, there was very little new bone formation and instead, the defect was filled with mostly soft, fibrous-like tissue with extensive cell infiltrate. In contrast, the GAG+BMP-2 MSC, GAG+rhBMP-2, and Col+rhBMP-2 groups all showed distinct islands of new bone formation that were surrounded by marrow-like material. In the Col+rhBMP-2 group in particular, this marrow-like material appeared less dense and much more disperse. When

viewed under polarized light, the collagen of the new bone in the Col+rhBMP-2 group appeared much more aligned (bright pink), indicative of lamellar structure, whereas the new bone in both GAG+BMP-2 MSC and GAG+rhBMP-2 groups had more disorganized collagen, suggestive of woven bone morphology.

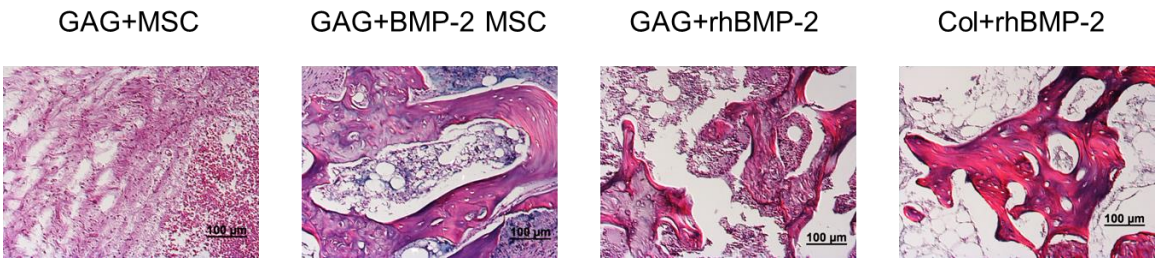

Figure 29 - Histology reveals qualitative differences in bone maturity. H&E staining of defect tissue viewed under polarized light. All BMP-2 groups exhibited islands of new bone formation while GAG+MSC did not. Furthermore, upon inspection under polarized light to assess collagen alignment, the bone in the Col+rhBMP-2 group appeared to be predominantly lamellar in structure whereas both GAG+BMP-2 MSC and GAG+rhBMP-2 had material resembling woven bone.

Discussion

The complex milieu of cells, soluble factors and extracellular matrix at the bone defect site is largely unexplored. However, treatment with substantial doses of rhBMP-2 at orthotopic sites can lead to robust bone healing. Given the complications that can arise from high dose bolus rhBMP-2 treatment, alternative controlled delivery strategies have been sought, comprising cell and gene-based therapies within biomaterial carriers. Indeed rhBMP-2 genetically-engineered MSCs have been shown to promote bone regeneration in a rat calvarial bone defect [210] and in mandible distraction surgery in dogs [211]. In previous studies, polymer scaffolds coated with adeno-associated viral vector encoding

rhBMP-2 successfully bridged about 50% of rat femoral defects at 12 weeks without ectopic bone formation [212], and low dose sustained rhBMP-2 expression was achieved by PEG-encapsulated rhBMP-2 expressing MSCs [197]. In the latter case, the use of a CS-GAG hydrogel could present additional advantages with sulfated CS-GAGs promoting rhBMP-2 stabilization as demonstrated previously [206], and as discussed in our findings here.

In this study, we compared the collagen sponge clinical standard to CS-GAG as a delivery vehicle for recombinant human BMP-2 (rhBMP-2) and rhBMP-2 expression via rhBMP-2 gene inserted into mesenchymal stem cells (BMP-2 MSC). Since the lentiviral system is able to integrate into the host cell genome, MSCs were transduced with a lentiviral vector to express high levels of rhBMP-2, with MSCs sourced from umbilical tissue expressing at a higher level than those from bone marrow. Most previous studies have used bone marrow MSCs, but Mizrahi et al showed similar efficiency of BMP overexpression between bone and adipose-derived MSCs [192, 213-215]. Compared to previous studies using adenovirus or nucleofection, lentiviral transduction induced a higher expression of BMP, and greater bone formation *in vivo* [197, 216, 217]. Our comparisons between adeno- and lentiviral transduction within the same MSC population (not shown) corroborate these findings, prompting us to implant far fewer cells (only 1 million BMP-2 MSCs per defect) than similar studies.

The characterization of the *in vitro* rhBMP-2 release profiles permitted greater insights into the potential differences in bone regeneration *in vivo*. Of the three rhBMP-2 treatment groups tested (GAG+BMP-2 MSC, GAG+rhBMP-2, and Col+rhBMP-2), Col+rhBMP-2 demonstrated the fastest initial burst release while GAG+BMP-2 MSC

exhibited the slowest, most sustained release. These *in vitro* observations were partially reflected in the spatial distribution of newly formed bone *in vivo,* as the GAG+BMP-2 MSC group had the highest average pMOI, indicative of bone formation that is more disperse and peripheral. These results are in-line with findings from other groups, which have shown that the timing of rhBMP-2 expression/release greatly influences the distribution and quality of new bone formation. In particular, Koh et al. demonstrated that using a rapamycin-inducible system to generate more sustained rhBMP-2 release from delivered fibroblasts results in better mineralization compared to uncontrolled constitutive expression of rhBMP-2 [218]. Furthermore, histological characterization in our study revealed that the new bone formed in the Col+rhBMP-2 group had a lamellar-like structure, indicative of mature bone. This may suggest that the bone observed in the histological sections from the other two rhBMP-2 groups (GAG+BMP-2 MSC and GAG+rhBMP-2) had been deposited more recently and was possibly still actively (re)modeling at the 12-week time point. Interestingly, these observed differences in bone maturity and spatial distribution did not translate into functional differences between the three groups, in terms of the mechanical strength and stiffness of the regenerated femurs. A longer-term study may enable newly formed bone in all groups to progress to a similar stage of maturation and consequently result in quantifiable mechanical differences. Overall, these results suggest that GAG+BMP-2 MSC delivery remains a viable treatment strategy which is comparable to delivery of rhBMP-2 in collagen sponge in this pre-clinical model.

Although GAG+BMP-2 MSC did not perform significantly better than Col+rhBMP-2 in this study, it is still remarkable that sufficient rhBMP-2 was released to

induce healing that was comparable to the 5 μg rhBMP-2 delivered on collagen sponge. The 5 μg dose was chosen because previous work from our group has demonstrated this to be the optimal healing dose in this rat segmental defect model [219]. However, we should acknowledge that this level of dosing is not reflective of clinical doses, which is often orders of magnitude higher (even after accounting for dose per weight) [220]. Recent work has shown that using higher doses of rhBMP-2 on collagen sponge in this model results in substantial ectopic bone formation [88], recapitulating one of the main adverse events associated with high dose rhBMP-2 use clinically. It remains to be seen whether this GAG gel system, which we demonstrated here to exhibit more sustained release compared to collagen sponge, would perform better at higher, more clinically-relevant doses of rhBMP-2.

These results add to a growing body of evidence concerning the importance of CS-GAG to bone formation and BMP-2 signaling. While there has been some disagreement on the role of glycosaminoglycans in BMP-2 release, the sustained BMP-2 release profile from CS-GAG as compared to collagen may be explained by CS-GAG sulfation [221, 222]. Wang et al. found that CS-modified collagen scaffolds were more hydrophilic and had greater surface energy than their unmodified counterparts, which they postulated contributed to higher initial release of rhBMP-2 in the first 8 hours [223]. This contrasts somewhat with the *in vitro* release we observed, but may indicate that sulfated GAGs play a role in rhBMP-2 stabilization. The importance of GAG sulfation is further reinforced by Hintze et al, who showed that CS with a higher degree of sulfation interacted with rhBMP-2 more strongly than their less sulfated counterparts for the same concentration [206], indicating that GAGs contributed to conformational and

thermodynamic stabilization of rhBMP-2 and as a result, enhanced rhBMP-2 signaling. This enhanced rhBMP-2 stabilization and signaling could help explain the presence of woven bone in defects treated with either CS-GAG group in our study.

To our knowledge, this is the first study to investigate the suitability of CS-GAG hydrogels for rhBMP-2 delivery, and to mediate the regeneration of a critically-sized bone defect. Beyond the collagen scaffolds used clinically, there are a host of scaffold materials under development for BMP delivery [224]. Members of our group have previously demonstrated similar success in this same model with an alginate hydrogel [81]. In a study comparing rhBMP-2 delivery by chitosan and hyaluronic acid hydrogels, Luca et al showed greater bone formation by volume using hyaluronic acid, while the chitosan scaffold led to more mature bone [225]. While both materials are polysaccharides, chitosan is positively charged and hyaluronic acid is negatively charged – likely influencing their interactions with the positively charged rhBMP-2. Of these materials, hyaluronic acid is the most chemically similar to CS-GAG, with one of its key differences being a lack of sulfation. In a study examining rhBMP-2 release kinetics from hyaluronic acid, 100% of the protein was eluted within 1 week from a relatively slowly degrading gel [226], which reinforces CS-GAG's advantages as scaffold for slow release of rhBMP-2.

Our *in vitro* results demonstrated that the GAG+BMP-2 MSC system resulted in slower release compared to Col+rhBMP-2. Future studies could assess cumulative release at higher rhBMP-2 doses and more importantly, whether sustained release at higher doses is actually beneficial. In addition, one of the main concerns associated with rhBMP-2 use clinically is a heightened and uncontrolled inflammatory response [11, 90]. While this

was not directly investigated in this study, MSC delivery may mitigate these risks, given MSCs have extensive immunomodulatory capabilities and can influence multiple immune cell types [227-230]. Future work exploring how MSC therapy may improve rhBMP-2-mediated bone healing by limiting adverse effects could be impactful for clinicians.

Finally, this GAG+BMP-2 MSC system could potentially be enhanced further through incorporation of cell-adhesive ligands. In the context of bone repair, the fibronectin motif RGD [98] and the collagen-mimetic peptide GFOGER [231] have been shown to be effective in promoting new bone formation. These studies have demonstrated that including cell adhesion ligands in the biomaterial scaffold can improve healing for both rhBMP-2 delivery as well as cell delivery approaches. Shekaran et al. showed that GFOGER delivered with a low dose of rhBMP-2 actually increased recruitment of CD45-/CD90+ osteoprogenitor cells to a radial defect compared to collagen sponge with rhBMP-2 [232]. In addition, Moshaverinia et al. demonstrated that osteogenic differentiation of multiple types of MSCs was enhanced when the cells were encapsulated in RGD alginate microspheres compared to non-functionalized alginate [233]. For our study, we tested both rhBMP-2 and MSC delivery approaches with a non-functionalized GAG gel and observed comparable healing to collagen sponge with rhBMP-2. Based on these findings from other labs, it seems plausible that functionalizing our GAG gel with RGD or GFOGER in the future could potentially result in even better outcomes.

A.2 ASSESSING STATE STEM CELL PROGRAMS IN THE UNITED STATES: HOW HAS STATE FUNDING AFFECTED PUBLICATION TRENDS?[3]

[3]Portions of this chapter were adapted from H. Alberta, A. Cheng, E.L. Jackson, M. Pjecha, A.D. Levine. Assessing State Stem Cell Programs in the United States: How Has State Funding Affected Publication Trends? *Cell Stem Cell* (2015).

Abstract

This article examines publication trends in four states – California, Connecticut, Maryland and New York – with state stem cell funding programs and finds that both California and Connecticut account for a greater share of pluripotent stem cell related publications than they do in comparison fields not targeted by specific state policies.

Introduction

The isolation of human embryonic stem cells (hESCs) in 1998 intensified discussions about ethical issues associated with stem cell research and inspired a still-ongoing global policy debate over the acceptability of and funding for various types of stem cell research [234]. In the U.S., three distinct federal funding policies – corresponding to the Clinton, Bush and Obama Administrations – have been adopted [234] and the policy environment has been further complicated by uncertainty associated with congressional action and litigation [235].

Extensive policy action has also occurred at the state level in the U.S., with states both supporting and restricting stem cell research and related areas of scientific inquiry [236]. Six states—California, Connecticut, Illinois, Maryland, New Jersey, and New York—took the unusual step of dedicating state funding to support basic and translational

stem cell research (including research using hESCs) [237]. These state policies had several goals encompassing the advancement of science (including hESC research that could not be conducted with federal funding during the Bush Administration) and economic development priorities. Although stem cell funding programs in Illinois and New Jersey have ceased operations, funding programs of various sizes – ranging up to California's $3 billion program – continue in the other four states (see Table 3 for details on these programs and data on their size relative to NIH funding in each state).

Table 3 - Overview of four major state stem cell research funding programs.

		California	Connecticut	Maryland	New York
First grants awarded		2006	2006	2007	2008
Initial funding / Time period		$3B / 10 years	$100M / 10 years	N/A	$600M / 11 years
Approximate annual funding		$300M	$10M	$14M	$55M
NIH Funding (FY13)	hESC	$36M (28.8%)	$4.4M (3.5%)	$2.4M (2.0%)	$7.9M (6.4%)
	SC	$222M (20.3%)	$21M (1.9%)	$41M (3.8%)	$108M (9.8%)
	All	$3.3B (14.8%)	$445M (2.0%)	$1.6B (7.1%)	$1.9B (8.6%)

Notes: Approximate annual funding was calculated by dividing total commitment by time period of commitment for CA, CT and NY. Maryland's approximate annual funding was calculated by dividing its total funding through July 2014 by its years of operation. For comparison, NIH funding received by each state for hESC, all stem cell (SC) and all extramural research is shown. The total dollar value of NIH funding was extracted from the NIH RePORT system (http://report.nih.gov/) and the share of all NIH extramural funding in that category was calculated from these data.

Despite the scale of these programs, relatively little is known about their impact on the field. One exception is a 2010 assessment that found that between December 2005 and the end of 2009, the programs collectively awarded approximately 750 grants totaling US$1.25 billion in state funding [237]. This assessment found wide variation (ranging from 21% in New York and New Jersey to 97% in Connecticut) among the states in the extent to which their grants focused on hESC research and suggested that one key success of the programs had been drawing new scientists into the field of stem cell research [237].

As some of these state programs are nearing the final years of their initial funding commitments, understanding their effects on the scientific enterprise is an increasingly important policy question. In this paper, we contribute to this effort by examining publications in stem cell related fields in the four states with sustained stem cell funding programs and comparing the share of hESC- and induced pluripotent stem cell (iPSC)-related publications with the share of publications in other areas of biomedical research (RNAi- and cancer-related research) presumed to be less affected by state policies. In addition, we examine the funding sources acknowledged in both hESC- and RNAi-related publications to assess how state funding contributed to the differences we observe. This analysis builds on a series of studies looking at the international distribution of stem cell publications generally [238-240] and the publication performance of the United States following the adoption of the restrictive funding policy in the Bush Administration more specifically [241, 242]. (See Supplemental Experimental Procedures for more information about our data collection and analysis strategies.)

Publications Trends Vary by State

Figure 30 shows the share of U.S. hESC-, iPSC-, RNAi- and cancer-related publications with at least one author from California, Connecticut, Maryland or New York as well as the share of hESC-related publications acknowledging funding from each state. Table S1 shows the difference between each state's share of hESC- and iPSC-related publications and its share of cancer-related publications broken into three timeframes. These timeframes were selected to represent the period when hESCs were under investigation but state policies had not yet been adopted (early hESC: 1998-2004), the period during which most state stem cell funding policies were adopted and awarded their initial grants (adoption: 2005-2008), and the period when these programs were up and running and, given time lags between funding and publication, their effects could plausibly be seen in the publication record (implementation: 2009-2013).

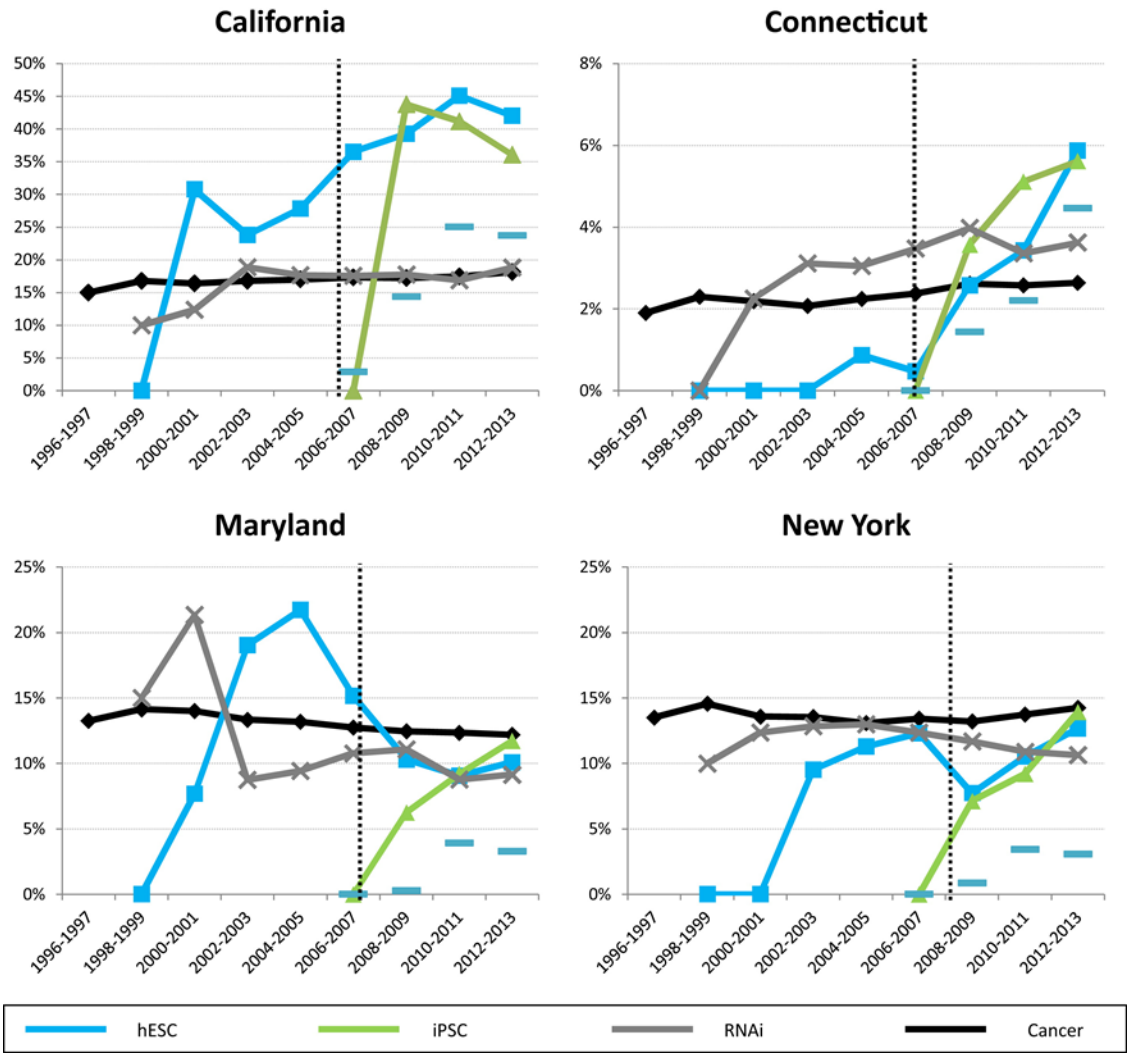

Figure 30 - Trends in state publication percentages for hESC, iPSC, RNAi and cancer-related research.

California's share of publications in the two comparison groups was quite consistent. Between 15% and 18% of U.S. cancer-related publications had at least one author from the state in each two-year period assessed between 1996 and 2013 and, following an initial period of growth, the state's share of RNAi-related publications remained between 17% and 19% from 2002 through 2013. The state's share of hESC- and iPSC-related research differed markedly from its share of these comparison groups. Its share of hESC-related research exceeded its share of the comparison groups as early

as 2000-2001 and this difference continued to grow in future years, reaching a high of 45% in 2010-2011. California's share of iPSC-related research has been high since shortly after the technology's discovery, with the state accounting for 44% of U.S. publications in 2008-2009. These differences are statistically significant in both the adoption and implementation time periods for hESC-related research and during the implementation period for iPSC-related research ($P<0.01$ for each test, see Table S1). After the California Institute for Regenerative Medicine (CIRM) issued its first grants in April 2006, the share of articles acknowledging California funding increased rapidly from approximately 3% in 2006-07 to more than 20% in 2010-11 and 2012-13. Overall, California state funding was acknowledged in nearly 19% of all hESC-related articles in our dataset published between 2006 and 2013, compared with 1.8% of articles in a comparable set of RNAi-related research (t-test, $P<0.01$). 45% of the hESC-related articles published between 2006 and 2013 in our dataset with at least one author from California acknowledged funding from the state.

Similar trends were seen in Connecticut. The state's share of cancer-related publications was relatively consistent, ranging from 2% to 3% throughout the time period studied, while the state's share of hESC-related research grew from 0% in 2002-2003 to 6% in 2012-13. Similar to California, Connecticut's share of iPSC-related research publications exceeded its share of cancer-related research as early as 2008-2009 and, in Connecticut's case, this difference continued to grow through 2012-2013. Overall, Connecticut state funding was acknowledged in 2.4% of all hESC-related articles published between 2006 and 2013 in our dataset, compared with 0.2% of articles in the comparable set of RNAi-related research (t-test, $P<0.01$). 67% of the hESC-related

articles published between 2006 and 2013 in our dataset with at least one author from Connecticut acknowledged funding from the state.

For Maryland and New York, in contrast, the share of hESC- and iPSC- related research in recent years was similar to the share of the two comparison groups. Maryland's share of hESC-related research declined from a high of 22% in 2004-2005 to 10% in 2008-2009 before leveling off. State funding from Maryland was acknowledged in 2.2% of the hESC-related articles published between 2006 and 2013 in our dataset, with most of these state-supported articles published between 2010 and 2013. In New York, the share of hESC-related research publications grew from a low of 8% in 2008-2009 to 13% in 2012-2013 but, even following this growth, remained similar to the state's share of publications in the two comparison groups. Funding from New York was also acknowledged in 2.2% of the hESC-related articles published between 2006 and 2013 in our dataset and most of these articles were published between 2010 and 2013.

Policy Considerations

Our comparative analysis provides some of the first evidence that the distribution of stem cell related publications in the United States differs from the distribution of publications in fields not targeted by specific state funding policies, and our analysis of the funding sources acknowledged in many of these articles strongly suggests that state funding is responsible, in part, for these differences. The share of hESC- and iPSC-related publications produced in each of the four states examined depends on a variety of considerations including the size, strengths, and interests of the scientific community and the specifics of the policy itself (i.e. its timing, its size, and its focus). In addition, it

depends on the competitive environment within the United States, as over-performance in one state must be balanced by under-performance in others.

In both California and Connecticut, state funding programs appear to have contributed to over-performance in the field. In California's case, the state was already a strong performer in hESC-related research before its state funding policy was adopted in 2004 and funding began flowing in 2006. This may reflect a generally supportive state environment or a first-mover advantage, as Geron Corporation, a key funder of early hESC research, is based in the state. Following passage of Proposition 71 in November 2004 and the creation of CIRM in the ensuing years, the state's share of hESC-related research grew from approximately 25% in 2002-2003 to more than 40% and the state maintained this position of strength in both hESC- and iPSC-related research from 2008 through the end of our data in 2013. Between 2010 and 2013, approximately 55% of hESC-related articles published with at least one California author acknowledged state funding, suggesting that this funding program played an important role as California maintained and built upon its early leadership in the field. The Connecticut case is even more suggestive of a policy impact, as the state showed very little hESC-related research activity through 2004-2005, and then showed steady growth in publication share following adoption of its funding policy in 2005, with approximately 67% of these articles acknowledging state funding. These findings align well with previous work [237] indicating that California and Connecticut, at least in the early years of their funding programs, focused more of their grants on hESC research than did other states. Given the close relationship between hESC and iPSC research [243], it is not surprising that, although iPSC cells were not explicitly prioritized by these state programs, these states

also produced a higher share of iPSC-related research than they did in the comparison fields.

In contrast to California and Connecticut, over-performance in pluripotent stem cell research was not seen in Maryland and New York. Our analysis shows, however, that state funding from each of these states contributed to approximately 3% of the hESC-related publications in our dataset between 2010 and 2013. This funding appears to have helped these states maintain a share of hESC-related research similar to their share in the comparison fields and, given the competitive environment with other states investing heavily in stem cell research, this may well be a successful policy outcome.

This analysis illustrating the relative performance of states in the production of stem cell related research publications provides a useful starting point for policymakers and, potentially, voters considering the future of state stem cell funding efforts as well as others interested in state science and technology policy more generally. We focused our analysis on hESC-related research as this field was a key motivation for some state stem cell funding programs [237], but future work could examine the effects of state stem cell programs on the broader fields of stem cell research and regenerative medicine. In addition, while we analyzed hESC-and iPSC-related research separately, these fields are closely intertwined [243] (see Supplemental Experimental Procedures for discussion) and future work could examine how state programs reacted to the development of iPSCs and prioritized their funding among these two related but distinct forms of pluripotent stem cell research. In addition, publications are only one measure of the impact of state science funding programs and examining other outcomes (e.g. patents awarded, clinical trials initiated, etc.) is an important topic for future research. Indeed more thorough efforts to

evaluate these state stem cell programs, ideally drawing on the initial goals of the programs and a wide range of relevant outcomes, would be an important step to help assess their impact on the field and the value of field-specific state science funding programs more generally.

Author Contributions

HBA, AC, ELJ and MP collected data, designed and conducted initial analyses and wrote an initial draft of the manuscript. ADL collected additional data, revised the analyses and prepared the final manuscript. All authors approved the final version of the manuscript.

Acknowledgements

The initial analysis for this manuscript was conducted in a class developed as part of the NSF Stem Cell Biomanufacturing IGERT program (DGE 0965945), which supported AC and ELJ, and revised as part of an NSF CAREER award (DRL 1150114) which supported HBA, MP and ADL. The authors acknowledge research assistance from Georgia Tech undergraduate students Arush Lal and Sana Surani.

REFERENCES

1. Ud-Din, S., S.W. Volk, and A. Bayat, *Regenerative healing, scar-free healing and scar formation across the species: current concepts and future perspectives.* Exp Dermatol, 2014. **23**(9): p. 615-9.

2. Schmidmaier, G., et al., *Bone morphogenetic proteins in critical-size bone defects: what are the options?* Injury, 2009. **40 Suppl 3**: p. S39-43.

3. Obremskey, W., et al., *Current Practice in the Management of Open Fractures Among Orthopaedic Trauma Surgeons. Part B: Management of Segmental Long Bone Defects. A Survey of Orthopaedic Trauma Association Members.* J Orthop Trauma, 2014. **28**(8): p. e203-7.

4. Bahney, C.S., et al., *Stem cell-derived endochondral cartilage stimulates bone healing by tissue transformation.* J Bone Miner Res, 2014. **29**(5): p. 1269-82.

5. Kretlow, J.D. and A.G. Mikos, *Review: mineralization of synthetic polymer scaffolds for bone tissue engineering.* Tissue Eng, 2007. **13**(5): p. 927-38.

6. Greenwald, A.S., et al., *Bone-graft substitutes: facts, fictions, and applications.* J Bone Joint Surg Am, 2001. **83-A Suppl 2 Pt 2**: p. 98-103.

7. Laurencin, C., Y. Khan, and S.F. El-Amin, *Bone graft substitutes.* Expert Rev Med Devices, 2006. **3**(1): p. 49-57.

8. Cahill, K.S., et al., *Prevalence, complications, and hospital charges associated with use of bone-morphogenetic proteins in spinal fusion procedures.* JAMA, 2009. **302**(1): p. 58-66.

9. Cahill, K.S., P.C. McCormick, and A.D. Levi, *A comprehensive assessment of the risk of bone morphogenetic protein use in spinal fusion surgery and postoperative cancer diagnosis.* J Neurosurg Spine, 2015. **23**(1): p. 86-93.

10. Epstein, N.E., *Complications due to the use of BMP/INFUSE in spine surgery: The evidence continues to mount.* Surg Neurol Int, 2013. **4**(Suppl 5): p. S343-52.

11. Tannoury, C.A. and H.S. An, *Complications with the use of bone morphogenetic protein 2 (BMP-2) in spine surgery.* Spine J, 2014. **14**(3): p. 552-9.

12. Gruber, R., et al., *Fracture healing in the elderly patient.* Exp Gerontol, 2006. **41**(11): p. 1080-93.

13. Lindaman, L.M., *Bone healing in children.* Clin Podiatr Med Surg, 2001. **18**(1): p. 97-108.

14. Lu, C., et al., *Effect of age on vascularization during fracture repair.* J Orthop Res, 2008. **26**(10): p. 1384-9.

15. Lu, C., et al., *Cellular basis for age-related changes in fracture repair.* J Orthop Res, 2005. **23**(6): p. 1300-7.

16. Meyer, R.A., Jr., et al., *Age and ovariectomy impair both the normalization of mechanical properties and the accretion of mineral by the fracture callus in rats.* J Orthop Res, 2001. **19**(3): p. 428-35.

17. Gaston, M.S. and A.H. Simpson, *Inhibition of fracture healing.* J Bone Joint Surg Br, 2007. **89**(12): p. 1553-60.

18. Giannoudis, P., et al., *Fracture healing in osteoporotic fractures: is it really different? A basic science perspective.* Injury, 2007. **38 Suppl 1**: p. S90-9.

19. Birkhold, A.I., et al., *The influence of age on adaptive bone formation and bone resorption.* Biomaterials, 2014. **35**(34): p. 9290-301.

20. Meyer, R.A., Jr., et al., *Young, adult, and old rats have similar changes in mRNA expression of many skeletal genes after fracture despite delayed healing with age.* J Orthop Res, 2006. **24**(10): p. 1933-44.

21. Boden, S.D., *Overview of the biology of lumbar spine fusion and principles for selecting a bone graft substitute.* Spine (Phila Pa 1976), 2002. **27**(16 Suppl 1): p. S26-31.

22. Green, E., J.D. Lubahn, and J. Evans, *Risk factors, treatment, and outcomes associated with nonunion of the midshaft humerus fracture.* J Surg Orthop Adv, 2005. **14**(2): p. 64-72.

23. Tzioupis, C. and P.V. Giannoudis, *Prevalence of long-bone non-unions.* Injury, 2007. **38 Suppl 2**: p. S3-9.

24. Goel, A., et al., *Percutaneous bone marrow grafting for the treatment of tibial non-union.* Injury, 2005. **36**(1): p. 203-6.

25. Hernigou, P., et al., *Percutaneous autologous bone-marrow grafting for nonunions. Influence of the number and concentration of progenitor cells.* J Bone Joint Surg Am, 2005. **87**(7): p. 1430-7.

26. Kokubu, T., et al., *Development of an atrophic nonunion model and comparison to a closed healing fracture in rat femur.* J Orthop Res, 2003. **21**(3): p. 503-10.

27. Megas, P., *Classification of non-union.* Injury, 2005. **36 Suppl 4**: p. S30-7.

28. Iwakura, T., et al., *Human hypertrophic nonunion tissue contains mesenchymal progenitor cells with multilineage capacity in vitro.* J Orthop Res, 2009. **27**(2): p. 208-15.

29. Giannoudis, P.V., et al., *The synergistic effect of autograft and BMP-7 in the treatment of atrophic nonunions.* Clin Orthop Relat Res, 2009. **467**(12): p. 3239-48.

30. Giannoudis, P.V., et al., *Masquelet technique for the treatment of bone defects: tips-tricks and future directions.* Injury, 2011. **42**(6): p. 591-8.

31. Masquelet, A.C. and T. Begue, *The concept of induced membrane for reconstruction of long bone defects.* Orthop Clin North Am, 2010. **41**(1): p. 27-37; table of contents.

32. Pelissier, P., et al., *Induced membranes secrete growth factors including vascular and osteoinductive factors and could stimulate bone regeneration.* J Orthop Res, 2004. **22**(1): p. 73-9.

33. Christou, C., et al., *The Masquelet technique for membrane induction and the healing of ovine critical sized segmental defects.* PLoS One, 2014. **9**(12): p. e114122.

34. Schaefer, L., *Complexity of danger: the diverse nature of damage-associated molecular patterns.* J Biol Chem, 2014. **289**(51): p. 35237-45.

35. Maslanik, T., et al., *The inflammasome and danger associated molecular patterns (DAMPs) are implicated in cytokine and chemokine responses following stressor exposure.* Brain Behav Immun, 2013. **28**: p. 54-62.

36. Bianchi, M.E., *DAMPs, PAMPs and alarmins: all we need to know about danger.* J Leukoc Biol, 2007. **81**(1): p. 1-5.

37. Piccinini, A.M. and K.S. Midwood, *DAMPening inflammation by modulating TLR signalling.* Mediators Inflamm, 2010. **2010**.

38. Klune, J.R., et al., *HMGB1: endogenous danger signaling.* Mol Med, 2008. **14**(7-8): p. 476-84.

39. Park, J.S., et al., *High mobility group box 1 protein interacts with multiple Toll-like receptors.* Am J Physiol Cell Physiol, 2006. **290**(3): p. C917-24.

40. Suda, K., et al., *Anti-high-mobility group box chromosomal protein 1 antibodies improve survival of rats with sepsis.* World J Surg, 2006. **30**(9): p. 1755-62.

41. Yang, H., et al., *Reversing established sepsis with antagonists of endogenous high-mobility group box 1.* Proc Natl Acad Sci U S A, 2004. **101**(1): p. 296-301.

42. Ulloa, L., et al., *High mobility group box chromosomal protein 1 as a nuclear protein, cytokine, and potential therapeutic target in arthritis.* Arthritis Rheum, 2003. **48**(4): p. 876-81.

43. Rock, K.L. and H. Kono, *The inflammatory response to cell death.* Annu Rev Pathol, 2008. **3**: p. 99-126.

44. Binkowska, A.M., G. Michalak, and R. Slotwinski, *Current views on the mechanisms of immune responses to trauma and infection.* Cent Eur J Immunol, 2015. **40**(2): p. 206-16.

45. National Trauma Institute (CDC). *Trauma Statistics*. 2015 [cited 2016 10 Jan]; Available from: http://www.nationaltraumainstitute.org/home/trauma_statistics.html.

46. Anke, A.G., et al., *Long-term prevalence of impairments and disabilities after multiple trauma.* J Trauma, 1997. **42**(1): p. 54-61.

47. Flohe, S., et al., *Immune response of severely injured patients--influence of surgical intervention and therapeutic impact.* Langenbecks Arch Surg, 2007. **392**(5): p. 639-48.

48. Kimura, F., et al., *Immunosuppression following surgical and traumatic injury.* Surg Today, 2010. **40**(9): p. 793-808.

49. Tschoeke, S.K. and W. Ertel, *Immunoparalysis after multiple trauma.* Injury, 2007. **38**(12): p. 1346-57.

50. Lord, J.M., et al., *The systemic immune response to trauma: an overview of pathophysiology and treatment.* Lancet, 2014. **384**(9952): p. 1455-65.

51. Rosenthal, M.D. and F.A. Moore, *Persistent Inflammation, Immunosuppression, and Catabolism: Evolution of Multiple Organ Dysfunction.* Surg Infect (Larchmt), 2016. **17**(2): p. 167-72.

52. Xiao, W., et al., *A genomic storm in critically injured humans.* J Exp Med, 2011. **208**(13): p. 2581-90.

53. Rosenthal, M.D. and F.A. Moore, *Persistent inflammatory, immunosuppressed, catabolic syndrome (PICS): A new phenotype of multiple organ failure.* J Adv Nutr Hum Metab, 2015. **1**(1).

54. Gentile, L.F., et al., *Persistent inflammation and immunosuppression: a common syndrome and new horizon for surgical intensive care.* J Trauma Acute Care Surg, 2012. **72**(6): p. 1491-501.

55. Vanzant, E.L., et al., *Persistent inflammation, immunosuppression, and catabolism syndrome after severe blunt trauma.* J Trauma Acute Care Surg, 2014. **76**(1): p. 21-9; discussion 29-30.

56. Brochner, A.C. and P. Toft, *Pathophysiology of the systemic inflammatory response after major accidental trauma.* Scand J Trauma Resusc Emerg Med, 2009. **17**: p. 43.

57. Albertsmeier, M., et al., *Major surgical trauma differentially affects T-cells and APC.* Innate Immun, 2015. **21**(1): p. 55-64.

58. Makarenkova, V.P., et al., *CD11b+/Gr-1+ myeloid suppressor cells cause T cell dysfunction after traumatic stress.* J Immunol, 2006. **176**(4): p. 2085-94.

59. Mathias, B., et al., *Human Myeloid-derived Suppressor Cells are Associated With Chronic Immune Suppression After Severe Sepsis/Septic Shock.* Ann Surg, 2017. **265**(4): p. 827-834.

60. MacConmara, M.P., et al., *Increased CD4+ CD25+ T regulatory cell activity in trauma patients depresses protective Th1 immunity.* Ann Surg, 2006. **244**(4): p. 514-23.

61. Venet, F., et al., *Regulatory T cell populations in sepsis and trauma.* J Leukoc Biol, 2008. **83**(3): p. 523-35.

62. Sakaguchi, S., et al., *Foxp3+ CD25+ CD4+ natural regulatory T cells in dominant self-tolerance and autoimmune disease.* Immunol Rev, 2006. **212**: p. 8-27.

63. Elpek, K.G., et al., *CD4+CD25+ T regulatory cells dominate multiple immune evasion mechanisms in early but not late phases of tumor development in a B cell lymphoma model.* J Immunol, 2007. **178**(11): p. 6840-8.

64. Liu, V.C., et al., *Tumor evasion of the immune system by converting CD4+CD25- T cells into CD4+CD25+ T regulatory cells: role of tumor-derived TGF-beta.* J Immunol, 2007. **178**(5): p. 2883-92.

65. Venet, F., et al., *Increased circulating regulatory T cells (CD4(+)CD25 (+)CD127 (-)) contribute to lymphocyte anergy in septic shock patients.* Intensive Care Med, 2009. **35**(4): p. 678-86.

66. Ni Choileain, N., et al., *Enhanced regulatory T cell activity is an element of the host response to injury.* J Immunol, 2006. **176**(1): p. 225-36.

67. von Boehmer, H., *Mechanisms of suppression by suppressor T cells.* Nature Immunology, 2005. **6**: p. 338.

68. Venet, F., et al., *Human CD4+CD25+ regulatory T lymphocytes inhibit lipopolysaccharide-induced monocyte survival through a Fas/Fas ligand-dependent mechanism.* J Immunol, 2006. **177**(9): p. 6540-7.

69. Huang, L.F., et al., *Association between regulatory T cell activity and sepsis and outcome of severely burned patients: a prospective, observational study.* Crit Care, 2010. **14**(1): p. R3.

70. Gabrilovich, D.I. and S. Nagaraj, *Myeloid-derived suppressor cells as regulators of the immune system.* Nat Rev Immunol, 2009. **9**(3): p. 162-74.

71. Jia, W., C. Jackson-Cook, and M.R. Graf, *Tumor-infiltrating, myeloid-derived suppressor cells inhibit T cell activity by nitric oxide production in an intracranial rat glioma + vaccination model.* J Neuroimmunol, 2010. **223**(1-2): p. 20-30.

72. Zhang, C., et al., *Accumulation of myeloid-derived suppressor cells in the lungs during Pneumocystis pneumonia.* Infect Immun, 2012. **80**(10): p. 3634-41.

73. Raber, P., A.C. Ochoa, and P.C. Rodriguez, *Metabolism of L-arginine by myeloid-derived suppressor cells in cancer: mechanisms of T cell suppression and therapeutic perspectives.* Immunol Invest, 2012. **41**(6-7): p. 614-34.

74. Geiger, R., et al., *L-Arginine Modulates T Cell Metabolism and Enhances Survival and Anti-tumor Activity.* Cell, 2016. **167**(3): p. 829-842 e13.

75. Li, H., et al., *Cancer-expanded myeloid-derived suppressor cells induce anergy of NK cells through membrane-bound TGF-beta 1.* J Immunol, 2009. **182**(1): p. 240-9.

76. Condamine, T. and D.I. Gabrilovich, *Molecular mechanisms regulating myeloid-derived suppressor cell differentiation and function.* Trends Immunol, 2011. **32**(1): p. 19-25.

77. Veltman, J.D., et al., *COX-2 inhibition improves immunotherapy and is associated with decreased numbers of myeloid-derived suppressor cells in mesothelioma. Celecoxib influences MDSC function.* BMC Cancer, 2010. **10**: p. 464.

78. Oryan, A., et al., *Bone regenerative medicine: classic options, novel strategies, and future directions.* J Orthop Surg Res, 2014. **9**(1): p. 18.

79. Mehta, M., et al., *Biomaterial delivery of morphogens to mimic the natural healing cascade in bone.* Adv Drug Deliv Rev, 2012. **64**(12): p. 1257-76.

80. Jones, C.B., et al., *Improved healing efficacy in canine ulnar segmental defects with increasing recombinant human bone morphogenetic protein-2/allograft ratios.* J Orthop Trauma, 2008. **22**(8): p. 550-9.

81. Krishnan, L., et al., *Hydrogel-based Delivery of rhBMP-2 Improves Healing of Large Bone Defects Compared With Autograft.* Clin Orthop Relat Res, 2015. **473**(9): p. 2885-97.

82. Mehta, M., et al., *Influences of age and mechanical stability on volume, microstructure, and mineralization of the fracture callus during bone healing: is osteoclast activity the key to age-related impaired healing?* Bone, 2010. **47**(2): p. 219-28.

83. Strube, P., et al., *Influence of age and mechanical stability on bone defect healing: age reverses mechanical effects.* Bone, 2008. **42**(4): p. 758-64.

84. Ekeland, A., L.B. Engesoeter, and N. Langeland, *Influence of age on mechanical properties of healing fractures and intact bones in rats.* Acta Orthop Scand, 1982. **53**(4): p. 527-34.

85. Osyczka, A.M., et al., *Age and skeletal sites affect BMP-2 responsiveness of human bone marrow stromal cells.* Connect Tissue Res, 2009. **50**(4): p. 270-7.

86. Lee, K.B., et al., *The efficacy of rhBMP-2 versus autograft for posterolateral lumbar spine fusion in elderly patients.* Eur Spine J, 2010. **19**(6): p. 924-30.

87. Yamaji, K., et al., *Effects of dose of recombinant human BMP-2 on bone formation at palatal sites in young and old rats.* Dent Mater J, 2007. **26**(4): p. 481-6.

88. Krishnan, L., et al., *Delivery vehicle effects on bone regeneration and heterotopic ossification induced by high dose BMP-2.* Acta Biomater, 2017. **49**: p. 101-112.

89. Zara, J.N., et al., *High doses of bone morphogenetic protein 2 induce structurally abnormal bone and inflammation in vivo.* Tissue Eng Part A, 2011. **17**(9-10): p. 1389-99.

90. Ritting, A.W., E.W. Weber, and M.C. Lee, *Exaggerated inflammatory response and bony resorption from BMP-2 use in a pediatric forearm nonunion.* J Hand Surg Am, 2012. **37**(2): p. 316-21.

91. MacDonald, K.M., et al., *Exaggerated inflammatory response after use of recombinant bone morphogenetic protein in recurrent unicameral bone cysts.* J Pediatr Orthop, 2010. **30**(2): p. 199-205.

92. Oetgen, M.E. and B.S. Richards, *Complications associated with the use of bone morphogenetic protein in pediatric patients.* J Pediatr Orthop, 2010. **30**(2): p. 192-8.

93. Papanna, M.C., et al., *The use of recombinant morphogenic protein-2(rhBMP-2) in children undergoing revision surgery for persistent non-union.* Strategies Trauma Limb Reconstr, 2016. **11**(1): p. 53-8.

94. Molinari, R.W. and C. Molinari, *The Use of Bone Morphogenetic Protein in Pediatric Cervical Spine Fusion Surgery: Case Reports and Review of the Literature.* Global Spine J, 2016. **6**(1): p. e41-6.

95. Mladenov, K.V., P. Kunkel, and R. Stuecker, *The use of recombinant human BMP-2 as a salvage procedure in the pediatric spine: a report on 3 cases.* Eur Spine J, 2010. **19 Suppl 2**: p. S135-9.

96. Oest, M.E., et al., *Quantitative assessment of scaffold and growth factor-mediated repair of critically sized bone defects.* J Orthop Res, 2007. **25**(7): p. 941-50.

97. Boerckel, J.D., et al., *Effects of protein dose and delivery system on BMP-mediated bone regeneration.* Biomaterials, 2011. **32**(22): p. 5241-51.

98. Kolambkar, Y.M., et al., *An alginate-based hybrid system for growth factor delivery in the functional repair of large bone defects.* Biomaterials, 2011. **32**(1): p. 65-74.

99. Spurgeon, S.L., R.C. Jones, and R. Ramakrishnan, *High throughput gene expression measurement with real time PCR in a microfluidic dynamic array.* PLoS One, 2008. **3**(2): p. e1662.

100. Vandesompele, J., et al., *Accurate normalization of real-time quantitative RT-PCR data by geometric averaging of multiple internal control genes.* Genome Biol, 2002. **3**(7): p. RESEARCH0034.

101. Wolfinger, R.D., et al., *Assessing gene significance from cDNA microarray expression data via mixed models.* J Comput Biol, 2001. **8**(6): p. 625-37.

102. Hettiaratchi, M.H., et al., *Competitive Protein Binding Influences Heparin-Based Modulation of Spatial Growth Factor Delivery for Bone Regeneration.* Tissue Eng Part A, 2017.

103. James, A.W., et al., *A Review of the Clinical Side Effects of Bone Morphogenetic Protein-2.* Tissue Eng Part B Rev, 2016. **22**(4): p. 284-97.

104. Carragee, E.J., E.L. Hurwitz, and B.K. Weiner, *A critical review of recombinant human bone morphogenetic protein-2 trials in spinal surgery: emerging safety concerns and lessons learned.* Spine J, 2011. **11**(6): p. 471-91.

105. McKay, W.F., S.M. Peckham, and J.M. Badura, *A comprehensive clinical review of recombinant human bone morphogenetic protein-2 (INFUSE Bone Graft).* Int Orthop, 2007. **31**(6): p. 729-34.

106. Woo, E.J., *Adverse events reported after the use of recombinant human bone morphogenetic protein 2.* J Oral Maxillofac Surg, 2012. **70**(4): p. 765-7.

107. Woo, E.J., *Adverse events after recombinant human BMP2 in nonspinal orthopaedic procedures.* Clin Orthop Relat Res, 2013. **471**(5): p. 1707-11.

108. Desai, B.J., et al., *The effect of age on gene expression in adult and juvenile rats following femoral fracture.* J Orthop Trauma, 2003. **17**(10): p. 689-98.

109. Sinder, B.P., A.R. Pettit, and L.K. McCauley, *Macrophages: Their Emerging Roles in Bone.* J Bone Miner Res, 2015. **30**(12): p. 2140-9.

110. Rundle, C.H., et al., *Microarray analysis of gene expression during the inflammation and endochondral bone formation stages of rat femur fracture repair.* Bone, 2006. **38**(4): p. 521-9.

111. Wang, X., et al., *MMP9 regulates the cellular response to inflammation after skeletal injury.* Bone, 2013. **52**(1): p. 111-9.

112. Dupont, K.M., et al., *Human stem cell delivery for treatment of large segmental bone defects.* Proc Natl Acad Sci U S A, 2010. **107**(8): p. 3305-10.

113. Hussein, K.A., et al., *Difference in soft tissue response between immediate and delayed delivery suggests a new mechanism for recombinant human bone morphogenetic protein 2 action in large segmental bone defects.* Tissue Eng Part A, 2012. **18**(5-6): p. 665-75.

114. Lopas, L.A., et al., *Fractures in geriatric mice show decreased callus expansion and bone volume.* Clin Orthop Relat Res, 2014. **472**(11): p. 3523-32.

115. Nishida, S., et al., *Number of osteoprogenitor cells in human bone marrow markedly decreases after skeletal maturation.* J Bone Miner Metab, 1999. **17**(3): p. 171-7.

116. Fan, W., R. Crawford, and Y. Xiao, *Structural and cellular differences between metaphyseal and diaphyseal periosteum in different aged rats.* Bone, 2008. **42**(1): p. 81-9.

117. Mills, L., et al., *The multifactorial aetiology of fracture nonunion and the importance of searching for latent infection.* Bone Joint Res, 2016. **5**(10): p. 512-519.

118. Santolini, E., R. West, and P.V. Giannoudis, *Risk factors for long bone fracture non-union: a stratification approach based on the level of the existing scientific evidence.* Injury, 2015. **46 Suppl 8**: p. S8-S19.

119. Kratzel, C., et al., *Characterization of a rat osteotomy model with impaired healing.* BMC Musculoskelet Disord, 2008. **9**: p. 135.

120. Kwong, F.N., et al., *Altered relative expression of BMPs and BMP inhibitors in cartilaginous areas of human fractures progressing towards nonunion.* J Orthop Res, 2009. **27**(6): p. 752-7.

121. Kloen, P., D. Lauzier, and R.C. Hamdy, *Co-expression of BMPs and BMP-inhibitors in human fractures and non-unions.* Bone, 2012. **51**(1): p. 59-68.

122. Fajardo, M., et al., *Matrix metalloproteinases that associate with and cleave bone morphogenetic protein-2 in vitro are elevated in hypertrophic fracture nonunion tissue.* J Orthop Trauma, 2010. **24**(9): p. 557-63.

123. Bajada, S., et al., *Decreased osteogenesis, increased cell senescence and elevated Dickkopf-1 secretion in human fracture non union stromal cells.* Bone, 2009. **45**(4): p. 726-35.

124. Tawonsawatruk, T., M. Kelly, and H. Simpson, *Evaluation of native mesenchymal stem cells from bone marrow and local tissue in an atrophic nonunion model.* Tissue Eng Part C Methods, 2014. **20**(6): p. 524-32.

125. Hofmann, A., et al., *Cell viability, osteoblast differentiation, and gene expression are altered in human osteoblasts from hypertrophic fracture non-unions.* Bone, 2008. **42**(5): p. 894-906.

126. Noel, J.G., et al., *Thermal injury elevates the inflammatory monocyte subpopulation in multiple compartments.* Shock, 2007. **28**(6): p. 684-93.

127. Delano, M.J., et al., *MyD88-dependent expansion of an immature GR-1(+)CD11b(+) population induces T cell suppression and Th2 polarization in sepsis.* J Exp Med, 2007. **204**(6): p. 1463-74.

128. Dougherty, A.L., et al., *Battlefield extremity injuries in Operation Iraqi Freedom.* Injury, 2009. **40**(7): p. 772-7.

129. Banerjee, M., et al., *Epidemiology of extremity injuries in multiple trauma patients.* Injury, 2013. **44**(8): p. 1015-21.

130. Swain, S.L., et al., *IL-4 directs the development of Th2-like helper effectors.* J Immunol, 1990. **145**(11): p. 3796-806.

131. Stein, M., et al., *Interleukin 4 potently enhances murine macrophage mannose receptor activity: a marker of alternative immunologic macrophage activation.* J Exp Med, 1992. **176**(1): p. 287-92.

132. Marsell, R. and T.A. Einhorn, *The biology of fracture healing.* Injury, 2011. **42**(6): p. 551-5.

133. Yang, X., et al., *Callus mineralization and maturation are delayed during fracture healing in interleukin-6 knockout mice.* Bone, 2007. **41**(6): p. 928-36.

134. Yu, J.J., et al., *An essential role for IL-17 in preventing pathogen-initiated bone destruction: recruitment of neutrophils to inflamed bone requires IL-17 receptor-dependent signals.* Blood, 2007. **109**(9): p. 3794-802.

135. Cuenca, A.G., et al., *A paradoxical role for myeloid-derived suppressor cells in sepsis and trauma.* Mol Med, 2011. **17**(3-4): p. 281-92.

136. Dross, S.E., et al., *Kinetics of Myeloid-Derived Suppressor Cell Frequency and Function during Simian Immunodeficiency Virus Infection, Combination Antiretroviral Therapy, and Treatment Interruption.* J Immunol, 2017. **198**(2): p. 757-766.

137. Dorshkind, K., E. Montecino-Rodriguez, and R.A. Signer, *The ageing immune system: is it ever too old to become young again?* Nat Rev Immunol, 2009. **9**(1): p. 57-62.

138. Montecino-Rodriguez, E., B. Berent-Maoz, and K. Dorshkind, *Causes, consequences, and reversal of immune system aging.* J Clin Invest, 2013. **123**(3): p. 958-65.

139. Weiskopf, D., B. Weinberger, and B. Grubeck-Loebenstein, *The aging of the immune system.* Transpl Int, 2009. **22**(11): p. 1041-50.

140. Linton, P.J. and K. Dorshkind, *Age-related changes in lymphocyte development and function.* Nat Immunol, 2004. **5**(2): p. 133-9.

141. Shaw, A.C., et al., *Aging of the innate immune system.* Curr Opin Immunol, 2010. **22**(4): p. 507-13.

142. Donati, D., et al., *Bone grafting: historical and conceptual review, starting with an old manuscript by Vittorio Putti.* Acta Orthop, 2007. **78**(1): p. 19-25.

143. Godwin, J.W., A.R. Pinto, and N.A. Rosenthal, *Macrophages are required for adult salamander limb regeneration.* Proc Natl Acad Sci U S A, 2013. **110**(23): p. 9415-20.

144. Nam, D., et al., *T-lymphocytes enable osteoblast maturation via IL-17F during the early phase of fracture repair.* PLoS One, 2012. **7**(6): p. e40044.

145. Toben, D., et al., *Fracture healing is accelerated in the absence of the adaptive immune system.* J Bone Miner Res, 2011. **26**(1): p. 113-24.

146. Reinke, S., et al., *Terminally differentiated CD8(+) T cells negatively affect bone regeneration in humans.* Sci Transl Med, 2013. **5**(177): p. 177ra36.

147. Nascimento, D.C., et al., *Role of regulatory T cells in long-term immune dysfunction associated with severe sepsis.* Crit Care Med, 2010. **38**(8): p. 1718-25.

148. Takayanagi, H., *Osteoimmunology: shared mechanisms and crosstalk between the immune and bone systems.* Nat Rev Immunol, 2007. **7**(4): p. 292-304.

149. Jones, D.H., et al., *Regulation of cancer cell migration and bone metastasis by RANKL.* Nature, 2006. **440**(7084): p. 692-6.

150. Jones, D., L.H. Glimcher, and A.O. Aliprantis, *Osteoimmunology at the nexus of arthritis, osteoporosis, cancer, and infection.* J Clin Invest, 2011. **121**(7): p. 2534-42.

151. Takayanagi, H., *New developments in osteoimmunology.* Nat Rev Rheumatol, 2012. **8**(11): p. 684-9.

152. Monsonego, A. and H.L. Weiner, *Immunotherapeutic approaches to Alzheimer's disease.* Science, 2003. **302**(5646): p. 834-8.

153. Lam, S., et al., *Broadly-specific cytotoxic T cells targeting multiple HIV antigens are expanded from HIV+ patients: implications for immunotherapy.* Mol Ther, 2015. **23**(2): p. 387-95.

154. Kalos, M. and C.H. June, *Adoptive T cell transfer for cancer immunotherapy in the era of synthetic biology.* Immunity, 2013. **39**(1): p. 49-60.

155. Kikuiri, T., et al., *Cell-based immunotherapy with mesenchymal stem cells cures bisphosphonate-related osteonecrosis of the jaw-like disease in mice.* J Bone Miner Res, 2010. **25**(7): p. 1668-79.

156. Kode, J.A., et al., *Mesenchymal stem cells: immunobiology and role in immunomodulation and tissue regeneration.* Cytotherapy, 2009. **11**(4): p. 377-91.

157. Kim, Y.H., H. Furuya, and Y. Tabata, *Enhancement of bone regeneration by dual release of a macrophage recruitment agent and platelet-rich plasma from gelatin hydrogels.* Biomaterials, 2014. **35**(1): p. 214-24.

158. Dimitriou, R., E. Tsiridis, and P.V. Giannoudis, *Current concepts of molecular aspects of bone healing.* Injury, 2005. **36**(12): p. 1392-404.

159. Chang, M.K., et al., *Osteal tissue macrophages are intercalated throughout human and mouse bone lining tissues and regulate osteoblast function in vitro and in vivo.* J Immunol, 2008. **181**(2): p. 1232-44.

160. Loi, F., et al., *The effects of immunomodulation by macrophage subsets on osteogenesis in vitro.* Stem Cell Res Ther, 2016. **7**(1): p. 15.

161. Spiller, K.L., et al., *Sequential delivery of immunomodulatory cytokines to facilitate the M1-to-M2 transition of macrophages and enhance vascularization of bone scaffolds.* Biomaterials, 2015. **37**: p. 194-207.

162. Pradhan, P., et al., *The effect of combined IL10 siRNA and CpG ODN as pathogen-mimicking microparticles on Th1/Th2 cytokine balance in dendritic cells and protective immunity against B cell lymphoma.* Biomaterials, 2014. **35**(21): p. 5491-504.

163. Lu, L.Y., et al., *Pro-inflammatory M1 macrophages promote Osteogenesis by mesenchymal stem cells via the COX-2-prostaglandin E2 pathway.* J Orthop Res, 2017. **35**(11): p. 2378-2385.

164. Pacifici, R., *The Role of IL-17 and TH17 Cells in the Bone Catabolic Activity of PTH.* Front Immunol, 2016. **7**: p. 57.

165. Sato, K., et al., *Th17 functions as an osteoclastogenic helper T cell subset that links T cell activation and bone destruction.* J Exp Med, 2006. **203**(12): p. 2673-82.

166. Schlundt, C., et al., *Immune modulation as a therapeutic strategy in bone regeneration.* J Exp Orthop, 2015. **2**(1): p. 1.

167. Mountziaris, P.M., et al., *Harnessing and modulating inflammation in strategies for bone regeneration.* Tissue Eng Part B Rev, 2011. **17**(6): p. 393-402.

168. Dimitriou, R., et al., *Genetic predisposition to fracture non-union: a case control study of a preliminary single nucleotide polymorphisms analysis of the BMP pathway.* BMC Musculoskelet Disord, 2011. **12**: p. 44.

169. Dimitriou, R., et al., *Genetic predisposition to non-union: evidence today.* Injury, 2013. **44 Suppl 1**: p. S50-3.

170. Zeckey, C., et al., *Are polymorphisms of molecules involved in bone healing correlated to aseptic femoral and tibial shaft non-unions?* J Orthop Res, 2011. **29**(11): p. 1724-31.

171. Cuenca, A.G., et al., *Development of a genomic metric that can be rapidly used to predict clinical outcome in severely injured trauma patients.* Crit Care Med, 2013. **41**(5): p. 1175-85.

172. Rosenberger, P.H., et al., *Surgical stress-induced immune cell redistribution profiles predict short-term and long-term postsurgical recovery. A prospective study.* J Bone Joint Surg Am, 2009. **91**(12): p. 2783-94.

173. Forsberg, J.A., et al., *Do inflammatory markers portend heterotopic ossification and wound failure in combat wounds?* Clin Orthop Relat Res, 2014. **472**(9): p. 2845-54.

174. Pountos, I., et al., *Fracture non-union: Can biomarkers predict outcome?* Injury, 2013. **44**(12): p. 1725-32.

175. Seok, J., et al., *Genomic responses in mouse models poorly mimic human inflammatory diseases.* Proc Natl Acad Sci U S A, 2013. **110**(9): p. 3507-12.

176. Takao, K. and T. Miyakawa, *Genomic responses in mouse models greatly mimic human inflammatory diseases.* Proc Natl Acad Sci U S A, 2015. **112**(4): p. 1167-72.

177. Greenwald, A.S., et al., *Bone-graft substitutes: facts, fictions, and applications.* (0021-9355 (Print)).

178. Toolan, B.C., *Current Concepts Review: Orthobiologics.* Foot and ankle international, 2006. **27**(7).

179. De Long WG, E.T., Koval K, *Current concepts review: Bone grafts and bone graft substitutes in orthopaedic trauma surgery.* Journal of Bone and Joint Surgery American Edition, 2007. **89**: p. 649-658.

180. Laurencin, C., Y. Khan, and S.F. El-Amin, *Bone graft substitutes.* Expert Review of Medical Devices, 2006. **3**(1): p. 49-57.

181. Desai, B.M., *Osteobiologics.* (1078-4519 (Print)).

182. Rahman, M.S., et al., *TGF-beta/BMP signaling and other molecular events: regulation of osteoblastogenesis and bone formation.* Bone Res, 2015. **3**: p. 15005.

183. Balboni, A.L., et al., *ΔNp63α-Mediated Activation of Bone Morphogenetic Protein Signaling Governs Stem Cell Activity and Plasticity in Normal and Malignant Mammary Epithelial Cells.* Cancer Research, 2013. **73**: p. 1020-1030.

184. Govender S, C.C., Genant HK, Valentin-Opran A, Amit Y, Arbel R, Aro H, Atar D, Bishay M, Borner MG, Chiron P, Choong P, Cinats J, Courtenay B, Feibel R, Geulette B, Gravel C, Haas N, Raschke M, Hammacher E, van der Velde D, Hardy P, Holt M, Josten C, Ketterl RL, Lindeque B, Lob G, Mathevon H, McCoy G, Marsh D, Miller R, Munting E, Oevre S, Nordsletten L, Patel A, Pohl A, Rennie W, Reynders P, Rommens PM, Rondia J, Rossouw WC, Daneel PJ, Ruff S, Ruter A, Santavirta S, Schildhauer TA, Gekle C, Schnettler R, Segal D, Seiler H, Snowdowne RB, Stapert J, Taglang G, Verdonk R, Vogels L, Weckbach A, Wentzensen A, Wisniewski T, *Recombinant human bone morphogenetic protein-2 for treatment of open tibial fractures: a prospective, controlled, randomized study of four hundred and fifty patients.* Journal of Bone and Joint Surgery American Edition, 2002. **84**: p. 2123-2134.

185. D. Gothard, E.L.S., J.M. Kanczler, H. Rashidi, O. Qutachi, J. Henstock, M. Rotherham, A. El Haj, K.M. Shakesheff, R.O.C. Oreffo, *Tissue engineered bone using select growth factors: A comprehensive review of animal studies and clinical translation studies in man.* European Cells and Materials, 2014. **28**: p. 166-208.

186. Jones AL, B.R., Bosse MJ, Mirza SK, Lyon TR, Webb LX, Pollak AN, Golden JD, Valentin-Opran A, *Recombinant human BMP-2 and allograft compared with autogenous bone graft for reconstruction of diaphyseal tibial fractures with cortical defects.* Journal of Bone and Joint Surgery American Edition, 2006. **88**: p. 1431-1441.

187. Zhao B, K.T., Toyoda H, Takada T, Yanai T, Fukuda T, Chung UI, Koike T, Takaoka K, Kamijo R, *Heparin potentiates the in vivo ectopic bone formation induced by bone morphogenetic protein-2.* J Biol Chem, 2006. **281**(32): p. 23246-23253.

188. Valdes, M.A., et al., *Recombinant bone morphogenic protein-2 in orthopaedic surgery: a review.* Arch Orthop Trauma Surg, 2009. **129**(12): p. 1651-7.

189. Daniel S. Mulconrey, M., Keith H. Bridwell, MD, Jennifer Flynn, BS, Geoffrey A. Cronen, MD, and Peter S. Rose, MD, *Bone Morphogenetic Protein (RhBMP-2) as a Substitute for Iliac Crest Bone Graft in Multilevel Adult Spinal Deformity Surgery.* Spine J, 2008. **33**(20): p. 2153-2159.

190. K. D. Riew, N.M.W., S.-L. Cheng, L. V. Avioli, J. Lou, *Induction of Bone Formation Using a Recombinant Adenoviral Vector Carrying the Human BMP-2 Gene in a Rabbit Spinal Fusion Model.* Calcified Tissue International, 1998. **63**: p. 357-360.

191. Jay Lieberman, A.D., Sharon Stevenson, Lily Wu, Paula McAllister, Yu Po Lee, Michael Kabo, Gerald Finerman, Arnold Berk, Owen Wite, *The effect of regional gene therapy with bone morphogenetic protein-2-producing bone-marrow cells on the repair of segmental femoral defects in rats.* Journal of Bone and Joint Surgery, 1999. **81-A**(7).

192. S-L Cheng, J.L., N. M. Wright, C.-F. Lai, L. V. Avioli, K. D. Riew, *In Vitro and In Vivo Induction of Bone Formation Using a Recombinant Adenoviral Vector Carrying the Human BMP-2 Gene.* Calcified Tissue International, 2001. **68**: p. 87-94.

193. Hiroyuki Tsuchida, J.H., Eric Crawford, Paul Manske, Jueren Lou, *Engineered allogeneic mesenchymal stem cells repair femoral segmental defect in rats.* Journal of Orthopaedic Research, 2003. **21**: p. 44-53.

194. Campana, V., et al., *Bone substitutes in orthopaedic surgery: from basic science to clinical practice.* J Mater Sci Mater Med, 2014. **25**(10): p. 2445-61.

195. Buttner, M., et al., *Over-sulfated chondroitin sulfate derivatives induce osteogenic differentiation of hMSC independent of BMP-2 and TGF-beta1 signalling.* J Cell Physiol, 2013. **228**(2): p. 330-40.

196. Mumaw, J., et al., *Rapid Heterotrophic Ossification with Cryopreserved Poly(ethylene glycol-) Microencapsulated BMP2-Expressing MSCs.* Int J Biomater, 2012. **2012**: p. 861794.

197. Sonnet, C., et al., *Rapid healing of femoral defects in rats with low dose sustained BMP2 expression from PEGDA hydrogel microspheres.* J Orthop Res, 2013. **31**(10): p. 1597-604.

198. Nuttelman, C.R., M.C. Tripodi, and K.S. Anseth, *Synthetic hydrogel niches that promote hMSC viability.* Matrix Biol, 2005. **24**(3): p. 208-18.

199. Lutolf, M.P., et al., *Synthetic matrix metalloproteinase-sensitive hydrogels for the conduction of tissue regeneration: engineering cell-invasion characteristics.* Proc Natl Acad Sci U S A, 2003. **100**(9): p. 5413-8.

200. Olabisi, R.M., *Cell microencapsulation with synthetic polymers.* Journal of Biomedical Materials Research. Part a, 2015. **103**(2): p. 846-859.

201. Salbach-Hirsch, J., et al., *Sulfated glycosaminoglycans support osteoblast functions and concurrently suppress osteoclasts.* J Cell Biochem, 2014. **115**(6): p. 1101-11.

202. Koike, T., et al., *Chondroitin sulfate-E fine-tunes osteoblast differentiation via ERK1/2, Smad3 and Smad1/5/8 signaling by binding to N-cadherin and cadherin-11.* Biochem Biophys Res Commun, 2012. **420**(3): p. 523-9.

203. Gualeni, B., et al., *Alteration of proteoglycan sulfation affects bone growth and remodeling.* Bone, 2013. **54**(1): p. 83-91.

204. Cortes, M., A.T. Baria, and N.B. Schwartz, *Sulfation of chondroitin sulfate proteoglycans is necessary for proper Indian hedgehog signaling in the developing growth plate.* Development, 2009. **136**(10): p. 1697-706.

205. Lim, J.J. and J.S. Temenoff, *The effect of desulfation of chondroitin sulfate on interactions with positively charged growth factors and upregulation of cartilaginous markers in encapsulated MSCs.* Biomaterials, 2013. **34**(21): p. 5007-18.

206. Hintze, V., et al., *Sulfated Glycosaminoglycans Exploit the Conformational Plasticity of Bone Morphogenetic Protein-2 (BMP-2) and Alter the Interaction Profile with Its Receptor.* Biomacromolecules, 2014. **15**(8): p. 3083-3092.

207. Miyazaki, T., et al., *Oversulfated chondroitin sulfate-E binds to BMP-4 and enhances osteoblast differentiation.* Journal of Cellular Physiology, 2008. **217**(3): p. 769-777.

208. Karumbaiah, L., et al., *Chondroitin Sulfate Glycosaminoglycan Hydrogels Create Endogenous Niches for Neural Stem Cells.* Bioconjug Chem, 2015. **26**(12): p. 2336-49.

209. Duvall, C.L., et al., *Impaired angiogenesis, early callus formation, and late stage remodeling in fracture healing of osteopontin-deficient mice.* J Bone Miner Res, 2007. **22**(2): p. 286-97.

210. He, X., et al., *BMP2 genetically engineered MSCs and EPCs promote vascularized bone regeneration in rat critical-sized calvarial bone defects.* PLoS One, 2013. **8**(4): p. e60473.

211. Castro-Govea, Y., et al., *Human bone morphogenetic protein 2-transduced mesenchymal stem cells improve bone regeneration in a model of mandible distraction surgery.* J Craniofac Surg, 2012. **23**(2): p. 392-6.

212. Dupont, K.M., et al., *Synthetic scaffold coating with adeno-associated virus encoding BMP2 to promote endogenous bone repair.* Cell Tissue Res, 2012. **347**(3): p. 575-88.

213. Mizrahi, O., et al., *BMP-6 is more efficient in bone formation than BMP-2 when overexpressed in mesenchymal stem cells.* Gene Ther, 2013. **20**(4): p. 370-7.

214. Lieberman JR, D.A., Stevenson S, Wu L, McAllister P, Lee YP, Kabo JM, Finerman GAM, Berk A, Witte ON, *The effect of regional gene therapy with bone morphogenetic protein-2-producing bone-marrow cells on the repair of segmental femoral defects in rats.* Journal of Bone and Joint Surgery, 1999. **81**(7): p. 905.

215. Chang, S.C., et al., *Repair of large cranial defects by hBMP-2 expressing bone marrow stromal cells: comparison between alginate and collagen type I systems.* J Biomed Mater Res A, 2010. **94**(2): p. 433-41.

216. Pelled, G., et al., *BMP6-Engineered MSCs Induce Vertebral Bone Repair in a Pig Model: A Pilot Study.* Stem Cells Int, 2016. **2016**: p. 6530624.

217. Miyazaki, T., et al., *Oversulfated chondroitin sulfate-E binds to BMP-4 and enhances osteoblast differentiation.* J Cell Physiol, 2008. **217**(3): p. 769-77.

218. Koh, J.T., et al., *Use of a stringent dimerizer-regulated gene expression system for controlled BMP2 delivery.* Mol Ther, 2006. **14**(5): p. 684-91.

219. Kolambkar, Y.M., et al., *Spatiotemporal delivery of bone morphogenetic protein enhances functional repair of segmental bone defects.* Bone, 2011. **49**(3): p. 485-92.

220. Fu, R., et al., *Effectiveness and harms of recombinant human bone morphogenetic protein-2 in spine fusion: a systematic review and meta-analysis.* Ann Intern Med, 2013. **158**(12): p. 890-902.

221. Jiao, X., et al., *Heparan sulfate proteoglycans (HSPGs) modulate BMP2 osteogenic bioactivity in C2C12 cells.* J Biol Chem, 2007. **282**(2): p. 1080-6.

222. Takada, T., et al., *Sulfated polysaccharides enhance the biological activities of bone morphogenetic proteins*. Vol. 278. 2003.

223. Wang, Y., et al., *Effect of chondroitin sulfate modification on rhBMP-2 release kinetics from collagen delivery system*.

224. Blackwood, K.A., et al., *Scaffolds for Growth Factor Delivery as Applied to Bone Tissue Engineering.* International Journal of Polymer Science, 2012. **2012**: p. 1-25.

225. Luca, L., et al., *The effects of carrier nature and pH on rhBMP-2-induced ectopic bone formation.* J Control Release, 2010. **147**(1): p. 38-44.

226. Patterson, J., et al., *Hyaluronic acid hydrogels with controlled degradation properties for oriented bone regeneration.* Biomaterials, 2010. **31**(26): p. 6772-81.

227. Chiesa, S., et al., *Mesenchymal stem cells impair in vivo T-cell priming by dendritic cells.* Proc Natl Acad Sci U S A, 2011. **108**(42): p. 17384-9.

228. Corcione, A., et al., *Human mesenchymal stem cells modulate B-cell functions.* Blood, 2006. **107**(1): p. 367-72.

229. English, K., *Mechanisms of mesenchymal stromal cell immunomodulation.* Immunol Cell Biol, 2013. **91**(1): p. 19-26.

230. Maggini, J., et al., *Mouse bone marrow-derived mesenchymal stromal cells turn activated macrophages into a regulatory-like profile.* PLoS One, 2010. **5**(2): p. e9252.

231. Wojtowicz, A.M., et al., *Coating of biomaterial scaffolds with the collagen-mimetic peptide GFOGER for bone defect repair.* Biomaterials, 2010. **31**(9): p. 2574-82.

232. Shekaran, A., et al., *Bone regeneration using an alpha 2 beta 1 integrin-specific hydrogel as a BMP-2 delivery vehicle.* Biomaterials, 2014. **35**(21): p. 5453-61.

233. Moshaverinia, A., et al., *Bone regeneration potential of stem cells derived from periodontal ligament or gingival tissue sources encapsulated in RGD-modified alginate scaffold.* Tissue Eng Part A, 2014. **20**(3-4): p. 611-21.

234. Gottweis, H., *The endless hESC controversy in the United States: history, context, and prospects.* Cell Stem Cell, 2010. **7**(5): p. 555-8.

235. Levine, A.D., *Policy Uncertainty and the Conduct of Stem Cell Research.* Cell Stem Cell, 2011. **8**(2): p. 132-135.

236. Levine, A.D., T.A. Lacy, and J.C. Hearn, *The origins of human embryonic stem cell research policies in the US states.* Science and Public Policy, 2013. **40**(4): p. 544-558.

237. Karmali, R.N., N.M. Jones, and A.D. Levine, *Tracking and assessing the rise of state-funded stem cell research.* Nature Biotechnology, 2010. **28**(12): p. 1246-8.

238. Guhr, A., et al., *Current state of human embryonic stem cell research: An overview of cell lines and their use in experimental work.* Stem Cells, 2006. **24**(10): p. 2187-2191.

239. Levine, A.D., *Trends in the geographic distribution of human embryonic stem cell research.* Politics and the Life Sciences, 2005. **23**(2): p. 40-45.

240. Levine, A.D., *Identifying Under- and Overperforming Countries in Research Related to Human Embryonic Stem Cells.* Cell Stem Cell, 2008. **2**(6): p. 521-524.

241. Furman, J.L., F. Murray, and S. Stern, *Growing Stem Cells: The Impact of Federal Funding Policy on the U.S. Scientific Frontier.* Journal of Policy Analysis and Management, 2012. **31**(3): p. 661-705.

242. Owen-Smith, J. and J. McCormick, *An international gap in human ES cell research.* Nature Biotechnology, 2006. **24**: p. 391-392.

243. Scott, C.T., et al., *Democracy Derived? New Trajectories in Pluripotent Stem Cell Research.* Cell, 2011. **145**(6): p. 820-6.